MICROCOPY RESOLUTION TEST CHART

NAVAL POSTGRADUATE SCHOOL
Monterey, California

DTIC

S ELECTE D

MAY 3 1 1988

H

THESIS

USE OF A COHERENT SQUARE WAVE REFERENCE
TO DEMODULATE
BPSK CARRIERS AND A VISUAL INDICATOR OF
THE QUALITY
OF RECEIVED QPSK CARRIERS

by

Mehmet Kubilay Tok

December 1987

Thesis Advisor   Glenn A. Myers

REPORT DOCUMENTATION PAGE

1a REPORT SECURITY CLASSIFICATION	1b RESTRICTIVE MARKINGS
UNCLASSIFIED	

2a. SECURITY CLASSIFICATION AUTHORITY	3 DISTRIBUTION/AVAILABILITY OF REPORT
2b DECLASSIFICATION/DOWNGRADING SCHEDULE	Approved for public release; distribution is unlimited

4. PERFORMING ORGANIZATION REPORT NUMBER(S)	5 MONITORING ORGANIZATION REPORT NUMBER(S)

6a. NAME OF PERFORMING ORGANIZATION	6b OFFICE SYMBOL (If applicable)	7a NAME OF MONITORING ORGANIZATION
Naval Postgraduate School	62	Naval Postgraduate School

6c. ADDRESS (City, State, and ZIP Code)	7b. ADDRESS (City, State, and ZIP Code)
Monterey, California 93943-5000	Monterey, California 93943-5000

8a. NAME OF FUNDING SPONSORING ORGANIZATION	8b OFFICE SYMBOL (If applicable)	9 PROCUREMENT INSTRUMENT IDENTIFICATION NUMBER

8c. ADDRESS (City, State, and ZIP Code)	10 SOURCE OF FUNDING NUMBERS			
	PROGRAM ELEMENT NO.	PROJECT NO	TASK NO	WORK UNIT ACCESSION NO

11 TITLE (Include Security Classification)
USE OF A COHERENT SQUARE WAVE REFERENCE TO DEMODULATE BPSK CARRIERS AND A VISUAL INDICATOR OF THE QUALITY OF RECEIVED QPSK CARRIERS (U)

12 PERSONAL AUTHOR(S)
TOK, Mehmet Kubilay

13a. TYPE OF REPORT	13b TIME COVERED	14 DATE OF REPORT (Year, Month, Day)	15 PAGE COUNT
Master's Thesis	FROM _____ TO _____	1987 December	130

16 SUPPLEMENTARY NOTATION

17 COSATI CODES			18 SUBJECT TERMS (Continue on reverse if necessary and identify by block number)
FIELD	GROUP	SUB-GROUP	BPSK, QPSK, Digital Communication, Constellation Diagrams, Modulation, Demodulation, Multipath, ISI

19 ABSTRACT (Continue on reverse if necessary and identify by block number)

This report consists of two parts. Part 1 compares the noise performance of a coherent phase demodulator when using as a carrier reference a square wave signal versus using a sinusoidal signal. Analyses for both signal references are included for the cases of allpass noise and of bandpass noise at the demodulator input. The theory indicates the demodulator operating with either the square wave signal or the sinusoidal signal as a carrier will result in identical noise performance for the theoretical case of bandpass noise. However, experimental results demonstrate that the demodulator operating with the square wave signal reference has a 0.4 db. performance advantage for digital data transmission using binary phase shift keying, when compared under similar conditions to operations with the sinusoidal reference signal.

20 DISTRIBUTION/AVAILABILITY OF ABSTRACT	21 ABSTRACT SECURITY CLASSIFICATION
☒ UNCLASSIFIED/UNLIMITED ☐ SAME AS RPT ☐ DTIC USERS	UNCLASSIFIED

22a NAME OF RESPONSIBLE INDIVIDUAL	22b TELEPHONE (Include Area Code)	22c OFFICE SYMBOL
G. A. Myers	(408) 646-2325	62Mv

DD FORM 1473, 84 MAR — 83 APR edition may be used until exhausted — All other editions are obsolete

SECURITY CLASSIFICATION OF THIS PAGE

☆ U.S. Government Printing Office: 1986—606-24.

1

UNCLASSIFIED

19.   Abstract (continued)

      Part 2 investigates the features of a visual indicator (x-y oscilliscope display) depicting the quality of received quadrature phase shift keyed carriers. Such a display allows for visualization of the signal degrading effects due to noise, channel bandlimiting induced ISI, and multipath propagation. The observed pattern formed by the visual indicator allows an operator to determine these channel impairments. With experience, an operator can assess the system probability of a bit error under a variety of operating conditions.

Accession For

NTIS GRA&I	☑
DTIC TAB	☐
Unannounced	☐
Justification	

By
Distribution/
Availability Codes

| Dist | Avail and/or Special |
| A-1 | |

**Use of a Coherent Square Wave Reference to Demodulate
BPSK Carriers and a Visual Indicator of
the Quality of Received QPSK Carriers**

by

Mehmet Kubilay Tok
Lieutenant Junior Grade, Turkish Navy
B.S., Turkish Naval Academy, 1980

Submitted in partial fulfillment of the
requirements for the degree of

MASTER OF SCIENCE IN
ELECTRICAL ENGINEERING

from the
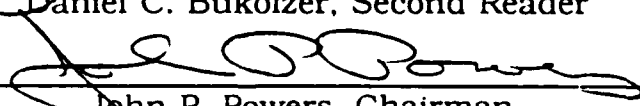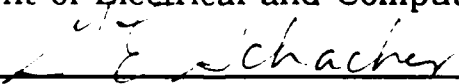
NAVAL POSTGRADUATE SCHOOL
December 1987

Author: _____
Mehmet Kubilay Tok

Approved by: _____
Glen A. Myers, Thesis Advisor

_____
Daniel C. Bukofzer, Second Reader

_____
John P. Powers, Chairman,
Department of Electrical and Computer Engineering

_____
Gordon E. Schacher, Dean,
Science and Engineering

3

ABSTRACT

This report consists of two parts. Part 1 compares the noise performance of a coherent phase demodulator when using as a carrier reference a square-wave signal versus a sinusoidal signal. Analyses for both signal references are included for the cases of allpass noise and of bandpass noise at the demodulator input. The theory indicates the demodulator operating with either the square-wave signal or the sinusoidal signal as a carrier will result in identical noise performance for the theoretical case of bandpass noise. However, experimental results demonstrate that the demodulator operating with the square-wave signal has a 0.4 dB performance advantage for digital data transmission using binary phase shift keying, when compared under similar conditions to operations with the sinusoidal reference signal.

Part 2 investigates the features of a visual indicator (x-y oscilloscope display) depicting the quality of received quadrature phase shift keyed carriers. Such a display allows for visualization of the signal-degrading effects due to noise, channel bandlimiting induced ISI, and multipath propagation. The observed pattern formed by the visual indicator allows an operator to determine these channel impairments. With experience, an operator can assess the system probability of a bit error under a variety of operating conditions.

INTRODUCTION

This research consists of two parts. Both parts are concerned with the transmission of digital data using phase shift keying. Part 1 considers the noise performance of a coherent receiver which uses a square-wave reference instead of the usual sinusoidal reference. Binary phase shift keying is used as carrier modulation. In Part 2, a visual indication of the quality of the communication link is achieved using an x-y oscilloscope for the case of quadrature phase shift keying. Both of these parts are reported on separately.

TABLE OF CONTENTS—PART 1

6

TABLE OF CONTENTS—PART 2

LIST OF SYMBOLS AND ABBREVIATIONS

A	Amplitude of the transmitted signal s(t)
AM	Amplitude modulation
DSBSC	Double sideband suppressed carrier
A_0	Amplitude of a carrier wave c(t)
A_v	Amplitude of polar pseudo random data d(t)
AVM	Analog voltage multiplier
AWGN	Additive white Gaussian noise
BER	Bit error ratio
BPSK	Binary phase shift keying
c(t)	carrier oscillator
d(t)	Polar pseudo random data
$\hat{d}(t)$	Estimate of the original polar pseudo random data
$d_1(t)$	I–channel transmitted pseudo random data
$d_2(t)$	Q–channel transmitted pseudo random data
$\hat{d}_1(t)$	Analog estimate of the original polar data $d_1(t)$ at the lowpass filter output
$\hat{d}_2(t)$	Analog estimate of the original polar data $d_2(t)$ at the lowpass filter output
FSR	Feedback shift register

ISI	Intersymbol interference
$l(T)$	Random variable at the output of a system model of BPSK receiver for BER analysis
$n(t)$	Bandpass Gaussian noise
$n_d(t)$	Noise (random) portion of the demodulator output $v_d(t)$
$n_0(T)$	Noise (random) portion of the integrate and dump circuit output $v_{ID}(t)$
pdf	Probability density function
P_e	Probability of error
PM	Phase modulation
QPSK	Quadrature phase shift keying
$R_n(t - \tau)$	Autocorrelation function of the Gaussian noise
$s(t)$	Transmitted signal
$s_0(t)$	Transmitted signal corresponding to the "0" sent
$s_1(t)$	Transmitted signal corresponding to the "1" sent
$s_{00}(t)$	Transmitted signal corresponding to the "00" sent
$s_{10}(t)$	Transmitted signal corresponding to the "10" sent
$s_{11}(t)$	Transmitted signal corresponding to the "11" sent
$s_{01}(t)$	Transmitted signal corresponding to the "01" sent
$S_B(f)$	Baseband power spectral density of $n(t)$

$[s(t) + n(t)]_{RMS}$	RMS value of signal plus noise at the input to the demodulator
$S_n(f)$	Bandpass power spectral density of n(t)
SNR	Signal-to-noise ratio at the input to the demodulator
$s_r(t)$	Signal plus noise at the QPSK receiver input
T	Bit interval (1 msec) in BPSK transmitter
T_s	Symbol interval (1 msec) in QPSK transmitter
τ	Relative time difference
TTL	Transistor-transistor logic
V	Signal portion of the matched filter output random variable $l(T)$ in BER analysis model for BPSK receiver
$v_d(t)$	Demodulated signal plus noise at the demodulator output
$v_{d_1}(t)$	Demodulated signal when using sinusoidal reference voltage in BPSK receiver
$v_{d_2}(t)$	Demodulated signal when using square-wave reference voltage in BPSK receiver
$\overline{v_{d_1}(t)}$	Average value of $v_{d_1}(t)$
$\overline{v_{d_2}(t)}$	Average value of $v_{d_2}(t)$
v_I	I-channel output voltage in QPSK receiver
$v_{ID}(t)$	Integrate and dump circuit output in BPSK receiver

10

$v_{in}(t)$	Signal plus noise at the input to the matched filter in BER analysis model for BPSK receiver
$v_L(t)$	Local reference voltage in BER analysis model for BPSK receiver
$v_{SH}(t)$	Sample and hold circuit output in BPSK receiver
v_Q	Q–channel output voltage in QPSK receiver
WGN	White Gaussian noise
$z(t)$	A special rectangular window pulse defined in the interval of $0 < t < T$ only
σ_0^2	Output noise power at the output of the matched filter in BER analysis model (for BPSK receiver)
σ^2	Noise power at the output of the IF amplifier (input to the demodulator)

PART I
I. <u>INTRODUCTION</u>

A variety of digital communication systems with military and commercial applications have emerged in recent years. Performance of those digital communication systems has been analyzed and largely documented. Operating systems are subject to limiting factors such as characteristics of the communication channel, data rate, modulation and demodulation techniques used, etc.

In certain applications, a small increase in performance can enhance the communication capability. This research is concerned with use of a square wave local reference voltage instead of a sinusoid with coherent demodulators. This technique may provide hardware and design advantages in some applications. Experimental results show that the square wave reference voltage has better noise performance.

A binary phase shift keyed (BPSK) system was designed, constructed, and tested utilizing, separately, the coherent sine wave and coherent square wave for demodulation of the BPSK carrier. In each case, the bit error ratio (BER) is obtained as a function of demodulator input signal-to-noise ratio (SNR).

Chapter II presents the motivation for this research and discusses the demodulation of BPSK signals with a coherent square wave reference voltage and a sine wave reference voltage. The associated SNR and BER analyses are given in this chapter. Chapter III describes the experimental system and its operation, explains and discusses the test

12

procedures, and presents the experimental results. Chapter IV contains conclusions and recommendations. Analytical BER calculations are presented in Appendix 1A. Circuit diagrams are given in Appendix 1B.

II. DESCRIPTION OF THE RESEARCH

A. OBJECTIVE

The objective of this research is to determine the noise performance of a BPSK receiver which uses a square wave as a coherent reference signal.

Results (analytical and experimental) are presented as a graph of BER as a function of demodulator input SNR. Since the performance of a demodulator using a square wave reference voltage is undocumented, an analysis is also an objective of this project.

B. SYSTEM DESCRIPTION

In BPSK, the phase of a carrier is switched between two values according to the two possible inputs "0" and "1." The two phases are separated by π radians, so BPSK consists of the two possible transmitter waveforms

$$s(t) = \begin{cases} s_0(t) = -A\cos(\omega_0 t + \varnothing_0) & 0 \le t \le T \\ s_1(t) = +A\cos(\omega_0 t + \varnothing_0) & 0 \le t \le T \end{cases} \qquad (1.1)$$

where T is the duration of each data bit.

The transmitted signal is equivalent to double sideband suppressed-carrier amplitude-modulated (AM-DSBSC) where the message is a digital waveform having values $+A_v$ or $-A_v$ volts [Ref. 1:p. 252]. Figure 1.1 illustrates the block diagram of the BPSK transmitter.

Polar data, d(t), phase modulates a sinusoidal carrier and s(t) becomes the transmitted signal. Figure 1.2 pictorially presents the
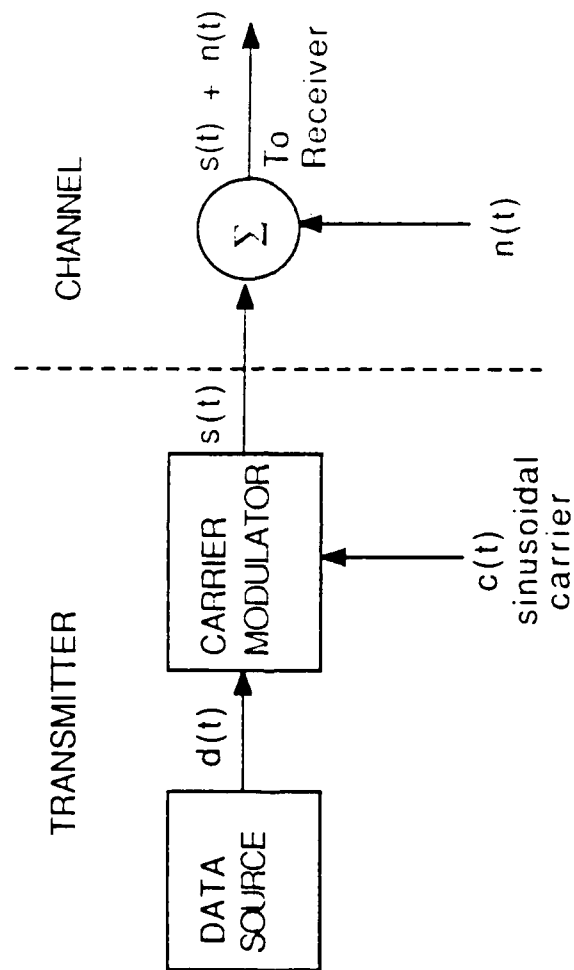
14

Figure 1.1

Block Diagram of the BPSK Transmitter and Channel

polar data d(t), sinusoidal carrier c(t), and corresponding phase modulated carrier s(t), respectively. Modulation is accomplished in practice by forming the product of d(t) of amplitude $\pm A_v$ volts and c(t) of amplitude A_0 volts. This gives $A = A_0 \cdot A_v$.
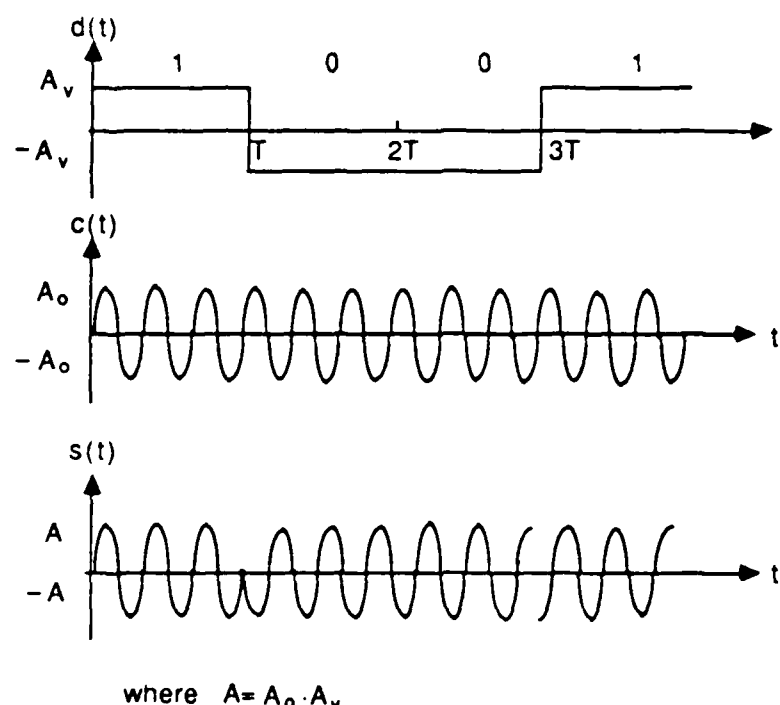

where $A = A_0 \cdot A_v$

Figure 1.2

Transmitter Signals

In this project, the RF stages of the transmitter and receiver are not considered. White Gaussian noise (WGN) n(t) is added to the transmitted signal in the system channel. The modulated carrier s(t) plus noise n(t) is amplified and filtered by the receiver front end. Figure 1.3 shows the BPSK receiver block diagram. In the receiver, the
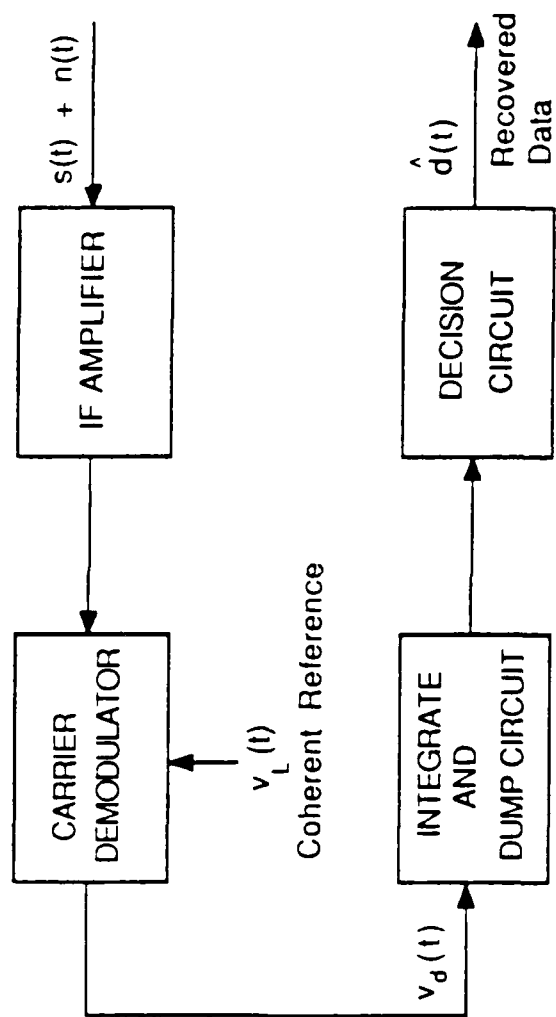
16

Figure 1.3

Block Diagram of the BPSK Receiver

carrier demodulator produces an output voltage $v_d(t)$ which is the product of $[s(t) + n(t)]$ and a local reference signal $v_L(t)$. For BPSK , $v_L(t)$ must be phase coherent with $s(t)$. The product $v_d(t)$ is processed by an integrate and dump circuit which is an equivalent form of a matched filter for a rectangular pulse [Ref. 2:p. 324]. This coherent multiplication and integration process are the important parts of the receiver and determine the ability of the receiver to recover the transmitted data. In fact, the motivation of this research is to investigate this process using a square ware reference voltage instead of a sinusoid and to compare the receiver performance for each case. After demodulation and when there is no noise, the demodulator output voltages $v_{d_1}(t)$ and $v_{d_2}(t)$ are as follows for each case.

a. Sinusoidal reference voltage: $v_L(t) = \cos\omega_0 t$

$$v_{d_1}(t) = s(t)\ v_L(t)$$

$$= \pm A\ \cos^2\omega_0 t \qquad\qquad 0 \le t \le T \qquad\qquad (1.2)$$

b. Square wave reference voltage: $v_L(t)$ = square wave of amplitude ± 1 volt

$$v_{d_2}(t) = \pm A\ |\cos\omega_0 t| \qquad\qquad 0 \le t \le T \qquad\qquad (1.3)$$

Averaging $v_d(t)$ over one bit interval is equivalent, in practice, to averaging one cycle of $v_d(t)$. Therefore,

$$\overline{v_{d_1}(t)} = \frac{1}{\pi} \int_0^\pi v_{d_1}(t)dt = \pm \frac{A}{2} \qquad\qquad (1.4)$$

18

and

$$\overline{v_{d_2}(t)} = \frac{1}{\pi} \int\limits_{0}^{\pi} v_{d_2}(t)dt = \pm \frac{2A}{\pi} \tag{1.5}$$

where the overbar denotes averaging.

The integrate and dump circuit output is $\int\limits_{0}^{T} v_d(t)dt = s(t)$ which is, then, $\pm\frac{AT}{2}$ for the sinusoidal reference and $\frac{2AT}{\pi}$ for the square-wave reference. These are signal voltage levels. Comparing these values shows the level is larger by a factor of $\frac{4}{\pi}$ (2db) when using the square-wave reference. This increase in signal voltage may result in improved BER performance of the BPSK receiver.

A decision circuit is necessary to derive a binary representation of the original data from the integrate and dump circuit output. Once this recovered data $\hat{d}(t)$ has been obtained, a comparison with d(t) is made to obtain the BER.

C. BIT ERROR RATIO ANALYSIS

BER is a measure of quality of a digital communication system. Consequently, BER is used to compare the performance of the BPSK receiver when using a sinusoidal reference voltage and when using a square-wave reference voltage. The BER analysis problem associated with the communication system (BPSK) can be modeled as shown in Figure 1.4, where V is the signal portion (constant) of the output $l(T)$ and $n_0(T)$ is the noise portion (random) of the output.
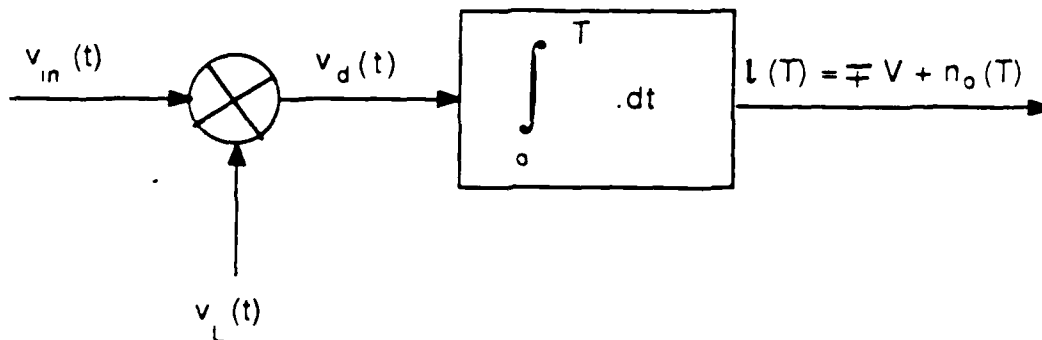
19

Figure 1.4

BPSK Receiver Model for BER Analysis

We are interested in BER vs. SNR when $v_L(t)$ (local reference voltage) is a sinusoidal and $v_L(t)$ is a square wave. The probability of bit error is the average of the shaded area of the output probability density functions (pdfs) shown in Figure 1.5 when the bits are equiprobable [Ref. 1:p. 152]. In most textbooks, the associated BER analysis is given when considering allpass white noise in the channel. In this research, both allpass and bandpass noise cases are analyzed.

The detailed BER analysis is given in Appendix 1A. The BER analysis procedure follows.

There are three parameters which determine the associated BER analysis: (1) V, the output signal, (2) σ_0^2, the output noise power, and (3) the pdfs given a "1" and given a "0."

From before (following equations 1.4 and 1.5), the signal voltage V at the sample time is $\frac{AT}{2}$ for the sinusoidal reference and $\frac{2AT}{\pi}$ for the square-wave reference.
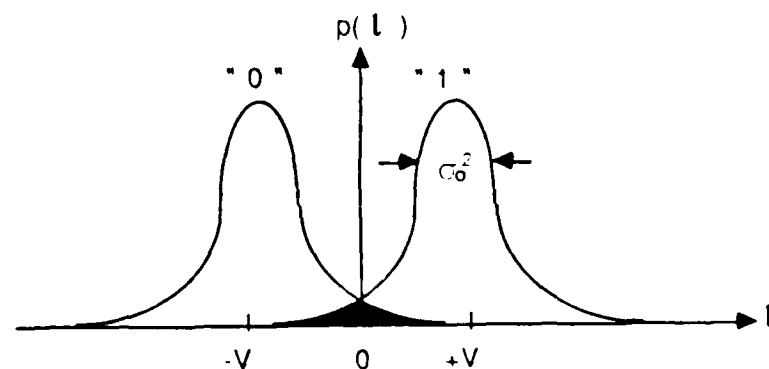
20

Figure 1.5

**Indication of the pdfs of a BPSK Receiver Output
When the Bits are Equiprobable**

From equation 1-A.8, the output noise power σ_0^2 is

$$\sigma_0^2 = \int_0^T \int_0^T R_n(t - \tau) \, v_L(t) \, v_L(\tau) \, dtd\tau \qquad (1-A.8)$$

where $R_n(t - \tau)$ is the autocorrelation function of the noise $n(t)$. Alternatively, from equation 1-A.16, we can write

$$\sigma_0^2 = \int_{-\infty}^{\infty} S_n(f) \, |V_L(f)|^2 \, df \qquad (1-A.16)$$

where $S_n(f)$ is the power spectrum of $n(t)$ and

$$V_L(f) = \mathcal{F} \left\{ v_L(t) \cdot z(t) \right\}$$

21

where

$$z(t) = \begin{cases} 1 & 0 < t < T \\ 0 & \text{elsewhere} \end{cases}$$

and

$$S_n(f) = S_B (f - f_0) + S_B (f + f_0)$$

$$S_B(f) = \frac{N_0}{2} |H(f)|^2$$

where $H(f)$ is the IF amplifier transfer function and $\frac{N_0}{2}$ is the noise power spectral density level.

Now, when $n(t)$ is white with constant two-sided power spectral density function of value equal to $\frac{N_0}{2}$, then

$$R_n (t - \tau) = \frac{N_0}{2} \delta (t - \tau)$$

and so

$$\sigma_0^2 = \frac{N_0}{2} \int_0^T v_L^2(t) \, dt$$

A sinusoidal $v_L(t) = \cos \omega_{IF} t$ gives $\sigma_0^2 = \frac{N_0 T}{4}$ and a square-wave $v_L(t)$ with values ± 1 volt gives $\sigma_0^2 = \frac{N_0 T}{2}$.

A conclusion is, then, that when the input noise is white the noise power out of the detector is doubled when using a square-wave reference as compared to a sinusoidal reference.

If n(t) is bandpass, then, in general, numerical integration must be used to evaluate σ_0^2. For example, when the IF amplifier is ideal (rectangular form for $|H(f)|$) then $\sigma_0^2 = \dfrac{1.4181 \; T \; N_0}{2\pi}$ for a sinusoidal reference and $\sigma_0^2 = \dfrac{1.4181 \; T \; N_0}{2\pi} \times \left(\dfrac{4}{\pi}\right)^2$ for a square-wave reference. This increase in noise power is identical to the increase in signal power for the square-wave reference.

To obtain BER (bit error probability), we need the pdfs of $l(T)$. Using the noise model of Rice [Ref. 3:pp. 46–157],

$$n(t) = x(t) \cos\omega_0 t - y(t) \sin\omega_0 t = \text{bandpass noise} \tag{1.6}$$

where s(t) and y(t) are lowpass and uncorrelated voltages with mean zero and variance σ^2. With a sinusoidal reference, the lowpass noise term out of the voltage multiplier is $x(t)/2$. Since the integrator is a linear system, then $n_0(T)$ is also Gaussian. So, the pdfs of Figure 1.5 are $N\left(\pm\dfrac{AT}{2}, \dfrac{1.4181 \; T \; N_0}{2\pi}\right)$ when the reference is a sinusoid.

For the square-wave reference voltage, express $v_L(t)$ as a Fourier series. Then,

$$v_L(t) = \frac{4}{\pi} \cos\omega_0 t + \frac{4}{3\pi} \cos3\omega_0 t + \frac{4}{5\pi} \cos5\omega_0 t + \dots \tag{1.7}$$

and so the noise (random) portion of the demodulator output is

$$n_0(T) = \int_0^T n(t) \; v_L(t) \; dt \tag{1.8}$$

23

Use of equations 1.6 and 1.7 in equation 1.8 gives $n_0(T) = x(t)/2$, since the cross terms integrate to zero. Therefore, the output pdfs of Figure 1.5 are again $N\left[\pm\dfrac{2AT}{\pi}, \dfrac{1.4181\,T\,N_0}{2\pi}\cdot\left(\dfrac{4}{\pi}\right)^2\right]$. Since the form of the pdfs of $l(T)$ are Gaussian, then the shaded areas of Figure 1.5 are erfc (V/σ_0), which is P_e = BER. We can now tabulate an expression for the four cases analyzed as shown in Table 1.

TABLE 1

BER EXPRESSIONS FOR THE FOUR CASES ANALYZED

	sinusoidal reference	square-wave reference
bandpass noise	$\text{erfc}\left(\sqrt{\dfrac{2\,Eb}{N_0}}\times 1.1\right)$	$\text{erfc}\left(\sqrt{\dfrac{2\,Eb}{N_0}}\times 1.1\right)$
white noise	$\text{erfc}\left(\sqrt{\dfrac{2\,Eb}{N_0}}\right)$	$\text{erfc}\left(\sqrt{\dfrac{2\,Eb}{N_0}}\times 0.81\right)$

This BER analysis shows that the performance of the BPSK receiver is the same for a coherent sine wave and a coherent square-wave reference for the bandpass noise case. But the square wave is worse when considering white noise (impractical case) because of additional lowpass noise power due to the odd harmonics of the square wave. Therefore, in practice, a coherent square-wave

24

reference voltage can be used to demodulate the BPSK signals without degrading receiver performance. Associated BER curves are shown in Figure 1.6. An important part of this research is the measurement of BER vs. SNR for the case of a sinusoidal reference and a square-wave reference. This is done to verify analytical results. The system used to obtain these measurements is described in the next chapter.
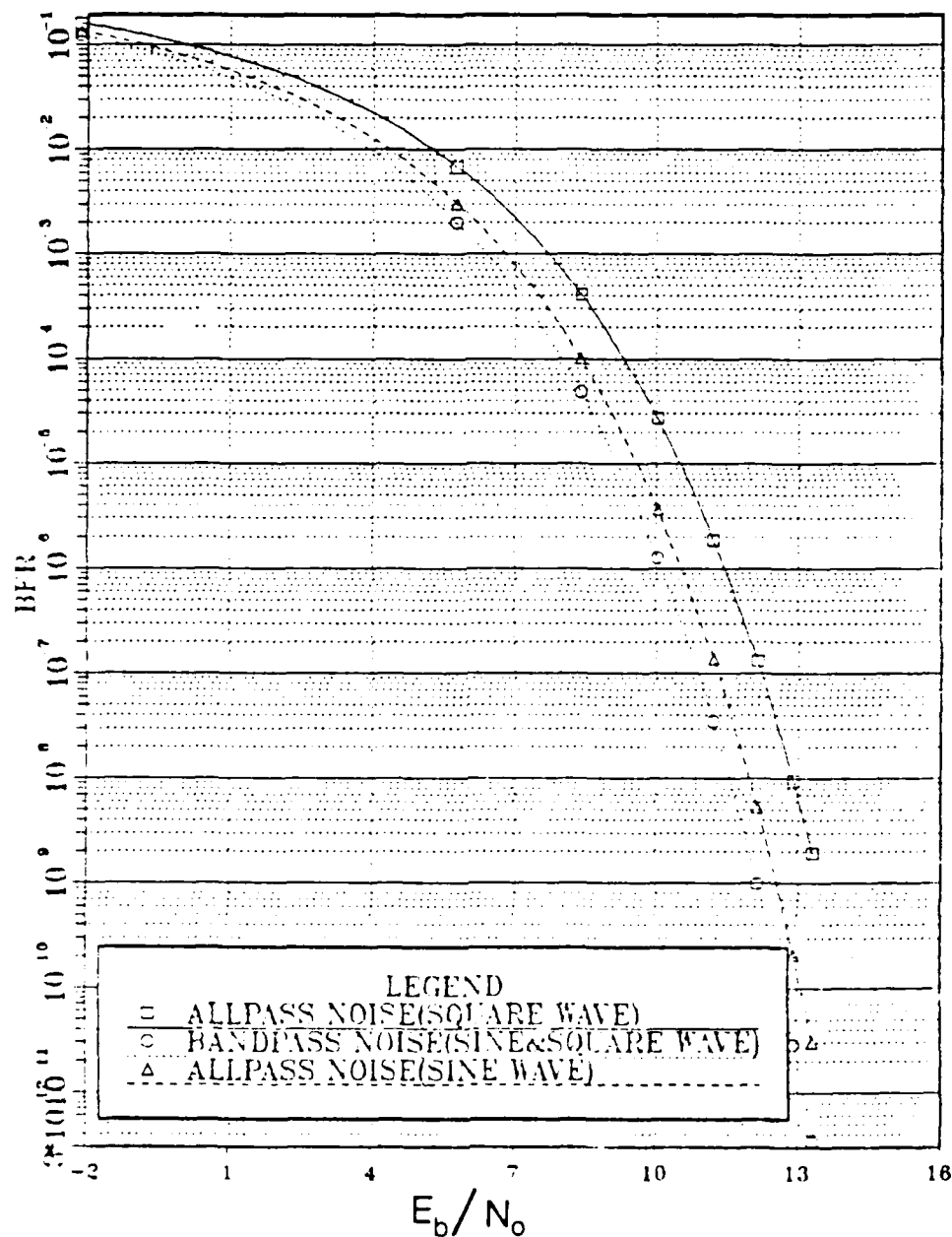
BPSK BER CURVE FOR MF DETECTION

Figure 1.6

BPSK BER Curves (Analytical Results)

26

III. THE EXPERIMENTAL SYSTEM

The experimental system consists of a transmitter, channel, and receiver. Block diagrams of the experimental BPSK transmitter, channel, and receiver are shown in Figures 1.7 and 1.8, respectively. The transmitter employs a feedback shift register (FSR) to simulate the random data, $d(t)$. Polar data $d(t)$ phase modulates a sinusoidal carrier and so the transmitter output $s(t)$ is a BPSK carrier. Narrow band Gaussian noise is added to $s(t)$ to represent a typical system channel. The white noise is band-limited to represent the type of noise which would be passed through the tuned IF amplifier of a super-heterodyne receiver. Thus, $s(t) + n(t)$ is the input to the experimental receiver. An analog voltage multiplier demodulates the signal plus noise using a reference coherent with $s(t)$. An integrate and dump circuit is used to average the demodulated signal plus noise $v_d(t)$. Finally, a decision circuit extracts the recovered data $d(t)$ from the integrate and dump circuit output $v_{ID}(t)$ and an error detection circuit provides BER by comparing the data $d(t)$ with the recovered data $\hat{d}(t)$.

There are no carrier or clock recovery circuits in the receiver. Receiver synchronization is obtained via hard wire from the transmitter circuit.

Subsystem building blocks are described in the following sections of this chapter. Complete circuit schematics are contained in Appendix 1B.
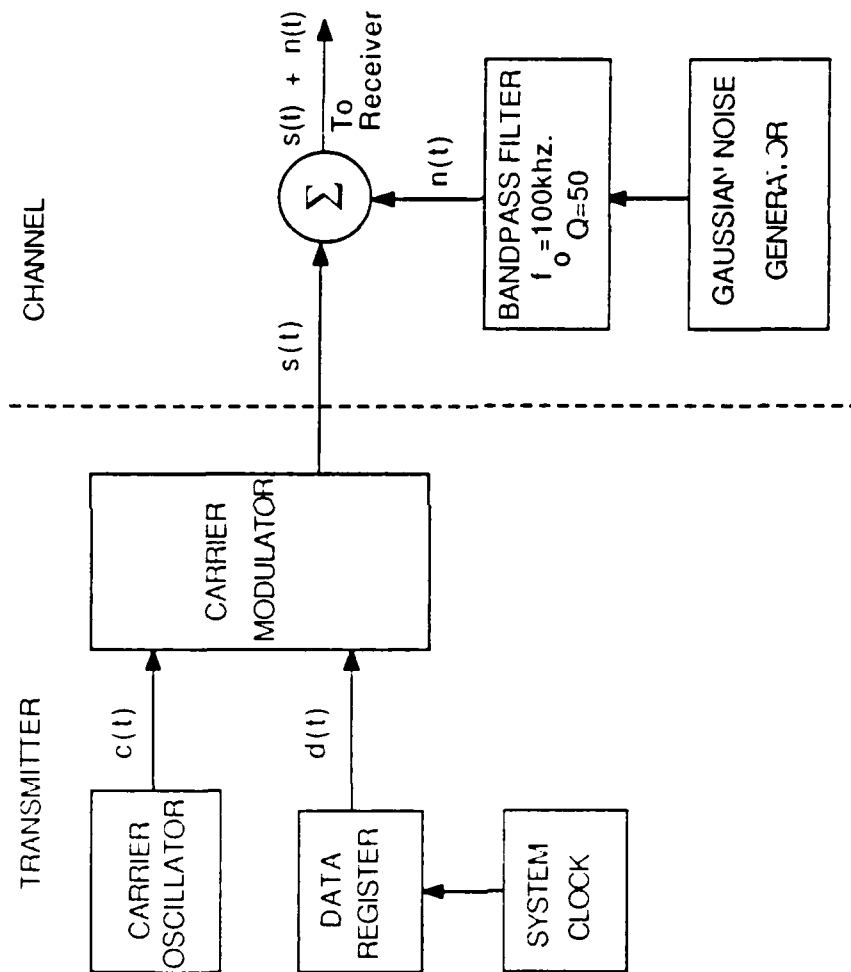
Figure 1.7

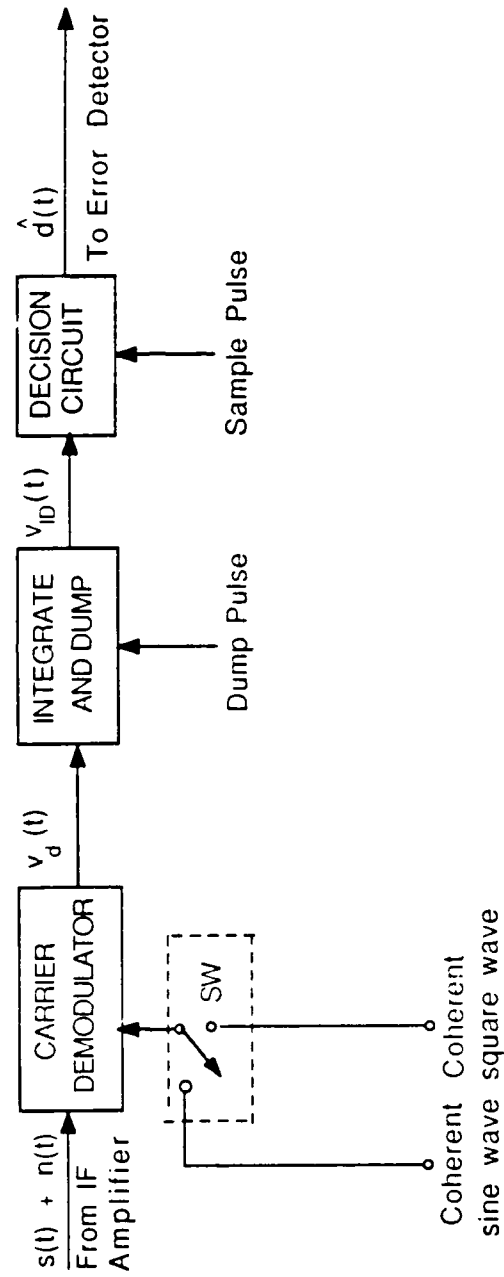**Block Diagram of the Experimental BPSK Transmitter and Channel**

Figure 1.8

Block Diagram of the Experimental BPSK Receiver

A. SUBSYSTEMS

1. Feedback Shift Register

A maximal length code, or m-sequence, is used to generate a pseudo-random bit stream d(t). This binary sequence is generated using a seven-stage feedback shift register (FSR) shown in Figure 1.9. An eight-bit shift register (74164) is used. The first seven stages, together with an EX-NOR gate (74266), constitute the important elements of the FSR. Feedback connections are made as shown in Figure 1.9, and the serial output of the seventh stage is the m-sequence of length = $2^7 - 1$ = 127 bits. All stages of the shift register are clocked synchronously so that the m-sequence is repeated.

With the EX-NOR operation, "all ones" in the shift register will terminate the sequence. The "all ones" condition does not occur normally, since the contents of the shift register is "all zeros" when voltage is initially applied to the system. However, transients and different delay times may cause the contents to be "all ones" at some time. A way to prevent the "all ones" state from persisting is to use an 8-input NAND gate (7430) connected as shown in Figure 1.10.

The NAND gate generates an "0" whenever the "all ones" condition appears in the shift register. This "0" clears the contents of the shift register and starts the m-sequence again.

The output of the shift register (74166) is TTL (0-5V), so a voltage comparator (LM311) is used to convert the TTL voltage levels to polar form (-5, +5V).
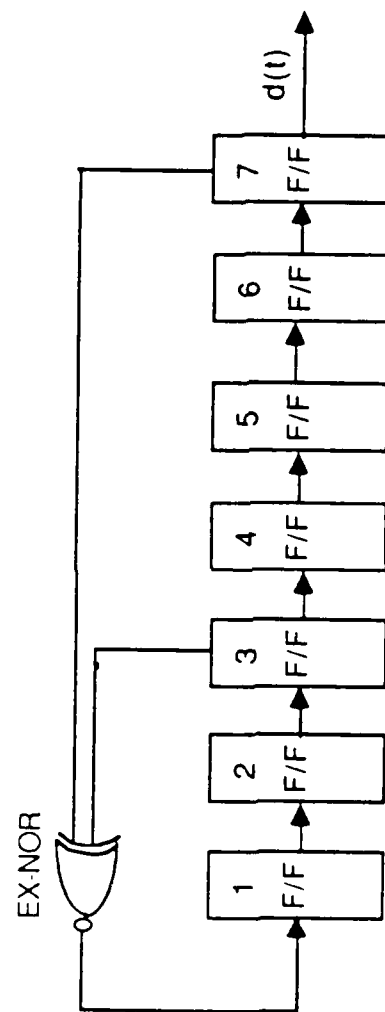
30

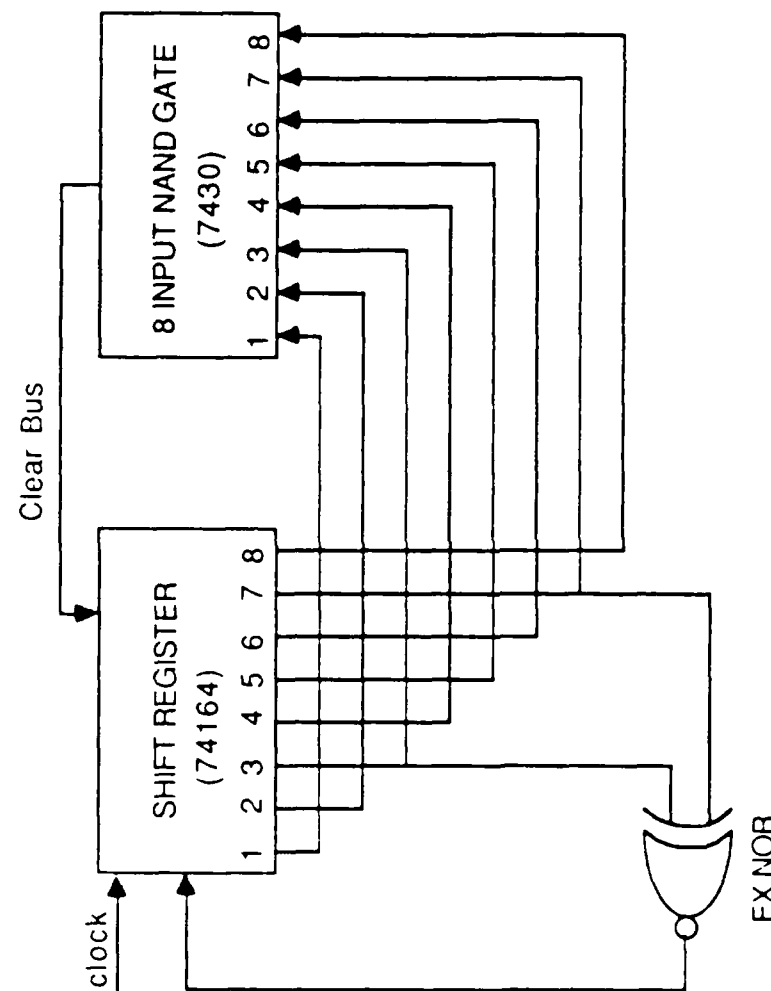Figure 1.9

Diagram of the Seven-Stage Feedback Shift Register

Figure 1.10

Diagram of the Feedback Shift Register With Protection Circuit

2. Carrier Modulator

The polar data d(t) phase modulates a sinusoidal carrier c(t) to create BPSK. This is accomplished by multiplying the polar data at 1 kHz and a 100-kHz sinusoidal carrier using an analog voltage multiplier (AVM-AD534) as shown in Figure 1.11. Since the AVM does not completely compensate for DC voltages which appear at the AVM input ports, small DC balancing voltages are used to compensate the modulated signal at the AVM output. Figure 1.12 shows the polar data and modulated carrier (6 kHz carrier in picture).

Figure 1.11

Block Diagram of the Modulator

3. Channel

The system channel can be modeled as depicted in Figure 1.13. White Gaussian noise n(t) is added to the transmitted signal s(t), so the receiver input is the sum s(t) + n(t).

33

Figure 1.12

Data (top) and Modulated Carrier (bottom) Voltages
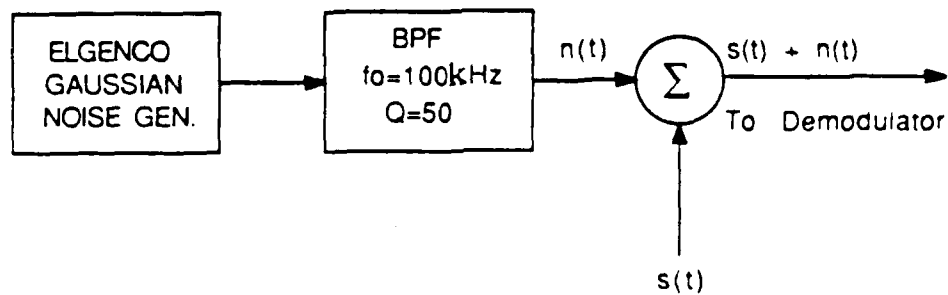
Figure 1.13

Model of the System Channel and Receiver Predetection Circuitry

34

A white Gaussian noise (WGN) generator (ELGENCO Model 603A) is used together with an active bandpass filter, centered at 100 kHz, to generate the bandpass noise. The bandpass filter simulates the characteristics of a receiver IF strip and is necessary here since the experimental system does not include a receiver IF amplifier. The bandwidth of the polar data d(t) is 1 kHz so the bandwidth of the modulated carrier is approximately 2 kHz. Ideally, the noise bandwidth should also be 2 kHz. However, with the components available, the minimum bandwidth achievable is about 2.5 kHz. A computer simulation of the bandpass filter with the MICROCAB (Analog Circuit Simulation Program) is shown in Figure 1.14. Figure 1.15 shows the actual filter response to the white noise input. Filtered signal and signal plus noise waveforms at the IF filter output are shown in Figures 1.16 and 1.17, respectively.

4. **Demodulator**

Coherent demodulation is used to recover the message from the received signal. An analog voltage multiplier (AVM AD534) is used to construct the coherent demodulator, as shown in Figure 1.18. In theory, demodulation of the received BPSK signals is equivalent to the rectification of the received signal by a coherent replica of the carrier (Local Reference Voltage). Therefore, the demodulator output is a positive full-wave rectified sine wave when a "1" is received and a negative full-wave rectified sine wave when a "0" is received. This is shown in Figure 1.19, where a sine wave reference voltage is used to rectify the received signal. For this experiment, a coherent sine-wave
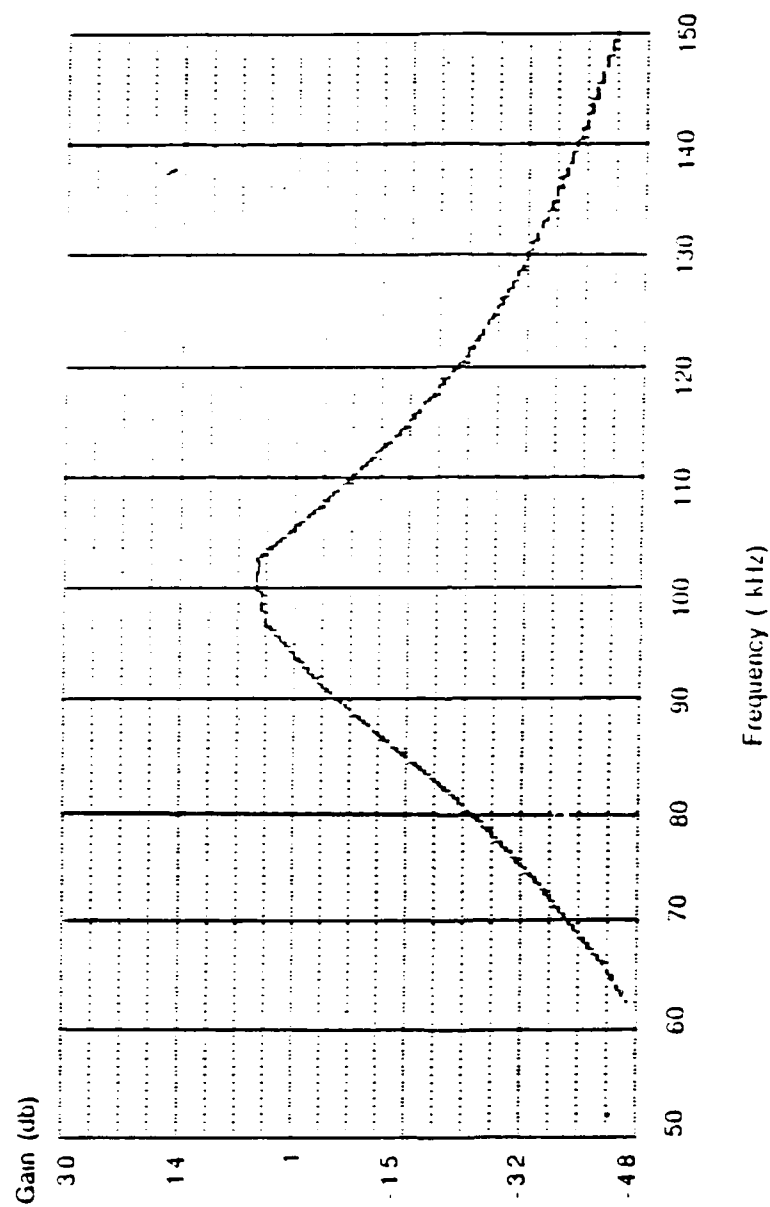
Figure 1.14

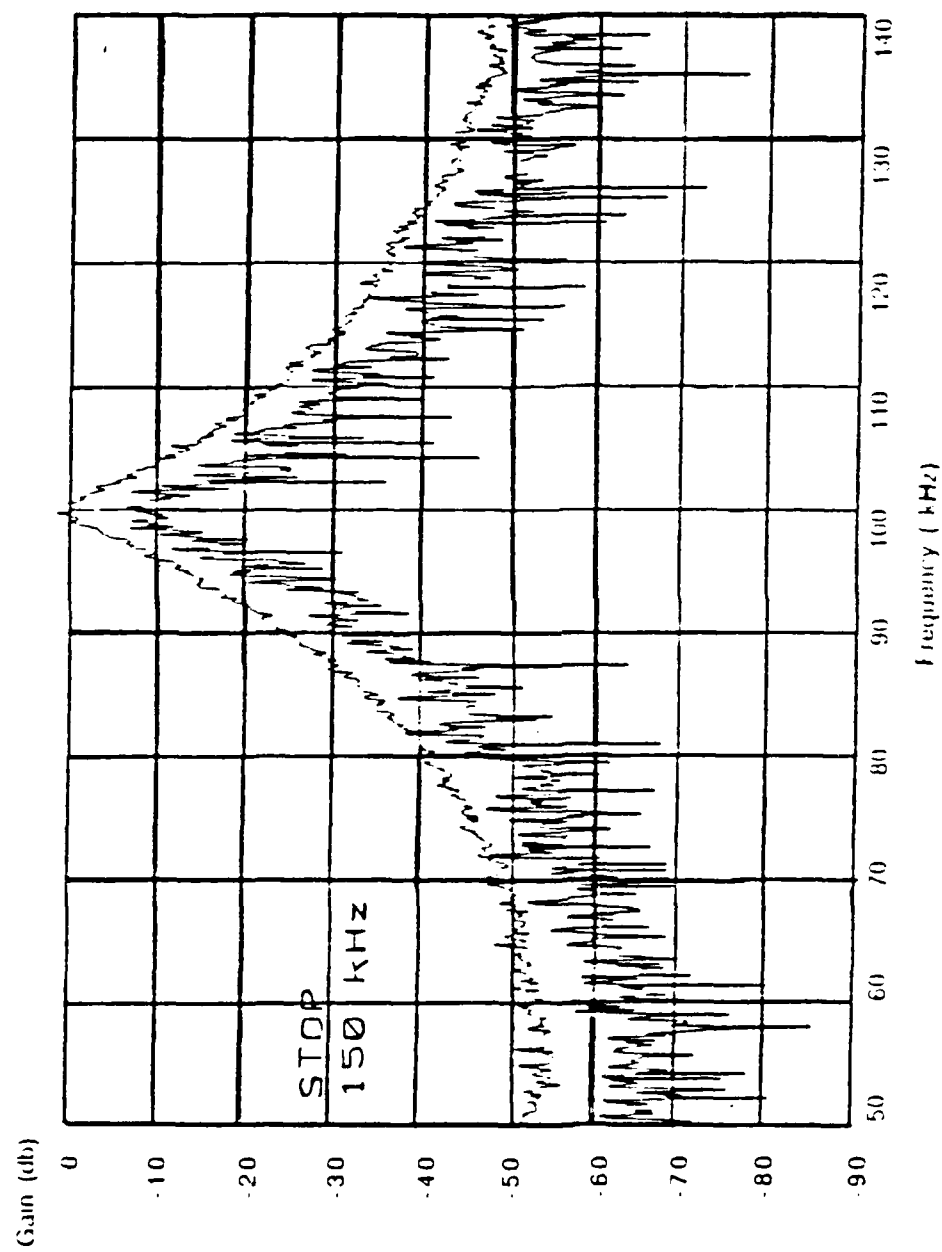Simulated Frequency Response of the Bandpass Filter

Figure 1.15

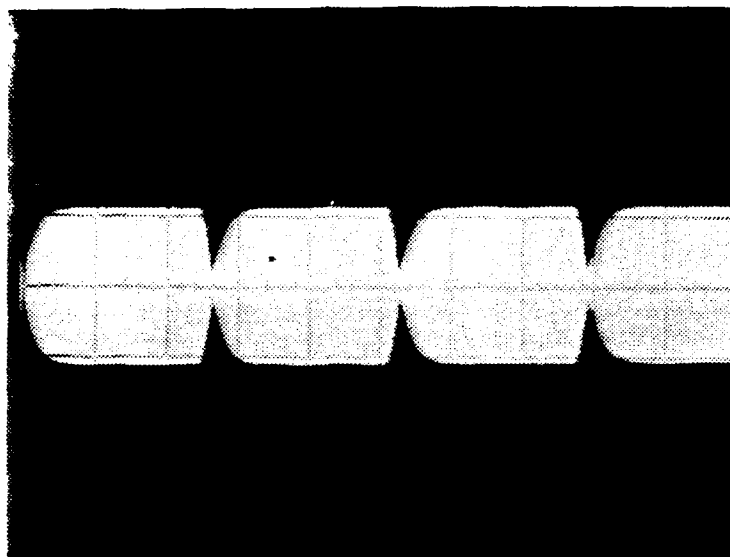Response of the Bandpas Filter to White Noise Input

Figure 1.16

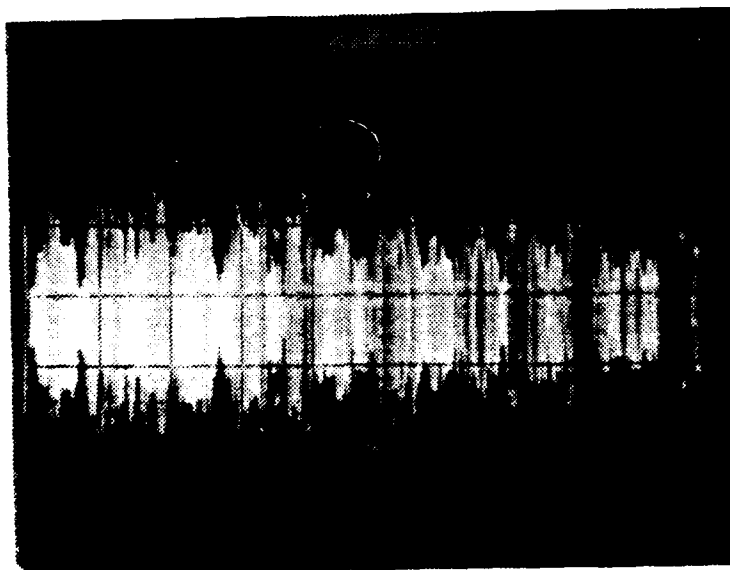**Typical BPF Output With No Noise Present**

Figure 1.17

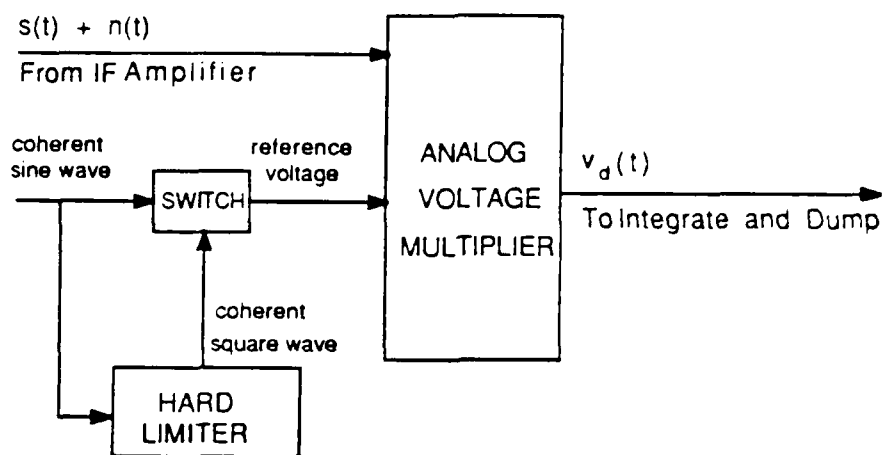**Typical BPF Output With Noise Present**

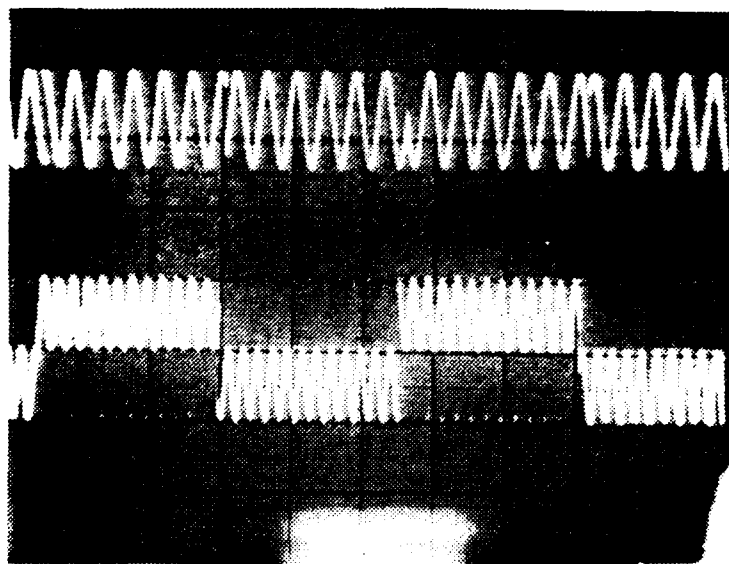38

Figure 1.18

Block Diagram of the Demodulator

Figure 1.19

**Photographs of the Input s(t) (top trace)
and Output $s_d(t)$ (bottom trace) of the Demodulator**

39

local oscillator and then a coherent square-wave local oscillator are used for demodulation. The coherent square wave is produced from the coherent sine wave reference by using a high-speed comparator (LM 319) as a hard limiter. Figure 1.20 shows the coherent sine-wave reference voltage and coherent square-wave reference voltage at the input and output of the comparator, respectively. The output of the demodulator is $\cos^2\omega_0 t$ when using a sinusoidal reference voltage and is $|\cos\omega_0 t|$ when using a square-wave reference voltage in the receiver as shown in Figure 1.21. These waveforms verify the theory given by equations 1.4 and 1.5, respectively.
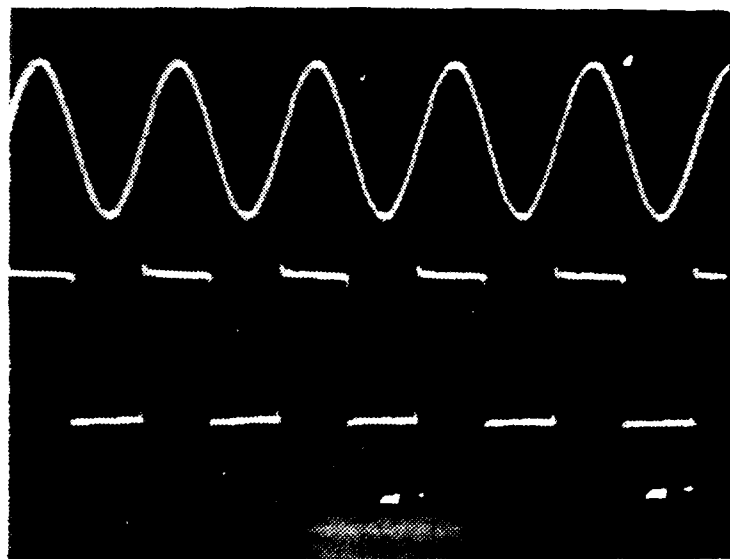
Figure 1.20
Hard Limiter Input (top trace) and Output (bottom trace)
(scales: horizontal 5μsec/div., vertical 5V/div.)
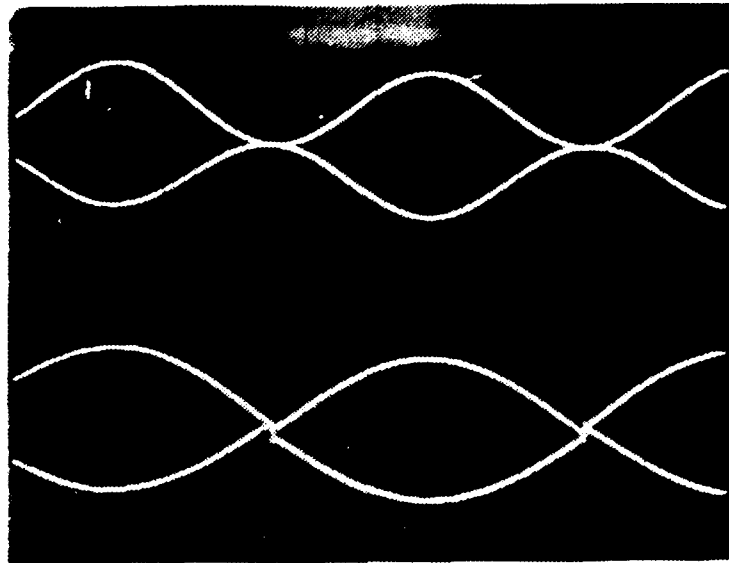
Figure 1.21
**Demodulator Outputs for a Sine-Wave Reference (top trace)
and a Square-Wave Reference (bottom trace)
With Data Modulation**

The lowpass portion of the demodulator output is the information-bearing signal $s_d(t)$ plus noise $n_d(t)$. Further processing of the demodulator output is necessary to remove the harmonics of the carrier and to recover the information (binary data).

5. Integrate and Dump Circuit

For the detection of rectangular pulses (binary data) in noise, an integrate and dump circuit is used as a matched filter implementation [Ref. 1:p. 252]. An operational amplifier (LM741) is used to construct the active integrate and dump circuit. The dump circuit is an analog switch (MC14052B) with dump synchronization coming from the dump pulse generator (one shot). This ensures that the dump

41

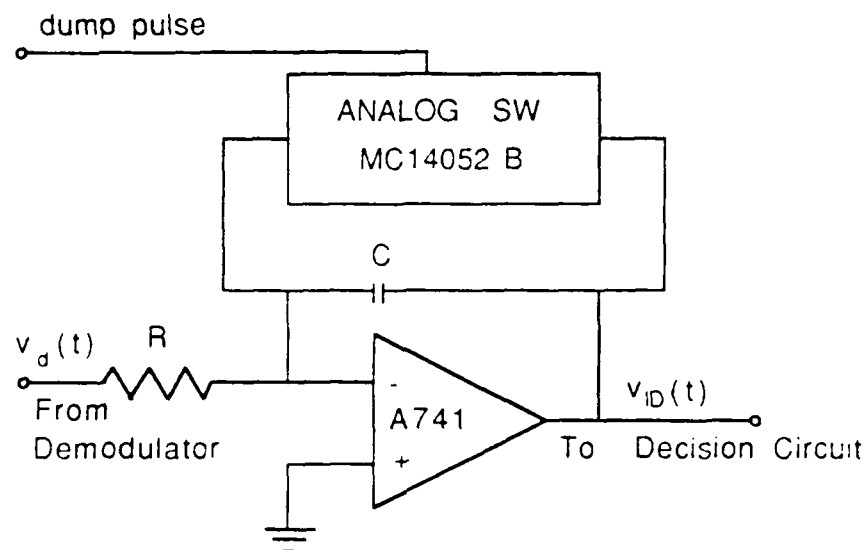occurs at the end of each data bit interval. Figure 1.22 shows the hardware realization of the integrate and dump circuit.

Figure 1.22
Diagram of the Integrate and Dump Circuit

For the data "1" with no noise present, $v_d(t)$ is applied to the integrator. The resulting output is a positive ramp of increasing voltage. For the data "0," the output is a negative ramp of decreasing voltage. When noise is present, the effect of the integrator is to average out this random variation so that net positive and negative ramps still occur for data "1" and data "0." This post-detection processing improves recovery of signals when noise is present. The integrator output is then applied to a decision circuit to recover the transmitted bit stream. Several integrator outputs are shown in Figures 1.23

through 1.30 for various received SNR when using a sinusoidal refer-
ence and square-wave reference, respectively. Inspection of Figures
1.23 and 1.24, which are for the no noise case, shows that the
integrator output voltage when using a square-wave reference is larger
in amplitude by a factor of 1.1 as compared with the output voltage
when using a sinusoidal reference. This is the experimental validation
of the theory stated in Chapter II. Also, in the presence of additive
white Gaussian noise (AWGN), Figures 1.25 through 1.30 show that the
detector output variation due to noise is larger when using a square-
wave reference which agrees with the theory developed in Chapter II.

6. Decision Circuit

The decision circuit generates the recovered data $\hat{d}(t)$ by
sampling the integrator output. This circuit also provides the neces-
sary interface between the analog and digital circuitry.

The integrator output is applied to a sample and hold circuit
(LF398), which samples the integrate and dump output at the end of
each data interval. Synchronization of the integrator and sampling
circuits must be ensured. This is achieved using synchronous sample
and dump pulses. Two one shots (mono stable multivibrator 74121)
are used to generate the sample and dump pulses from the system
clock. The first one shot fires at the leading edge of the clock and
generates the sample pulse. The output of the first one shot also
drives the second one shot, which fires at the falling edge of the sam-
ple pulse. This pulse is used to dump the integrator output. This
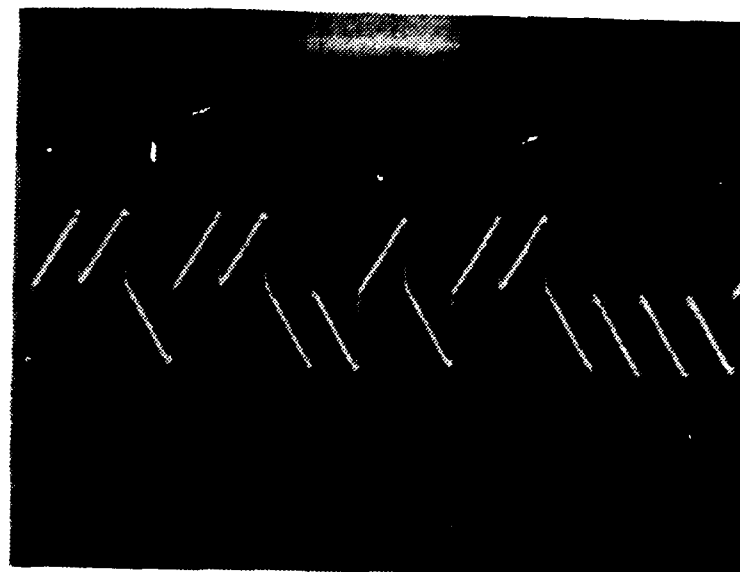ensures that sampling occurs just before the integrator is reset to

43

Figure 1.23
**Photograph of the Integrate and Dump Circuit Output
When Using Sinusoidal Reference Voltage**

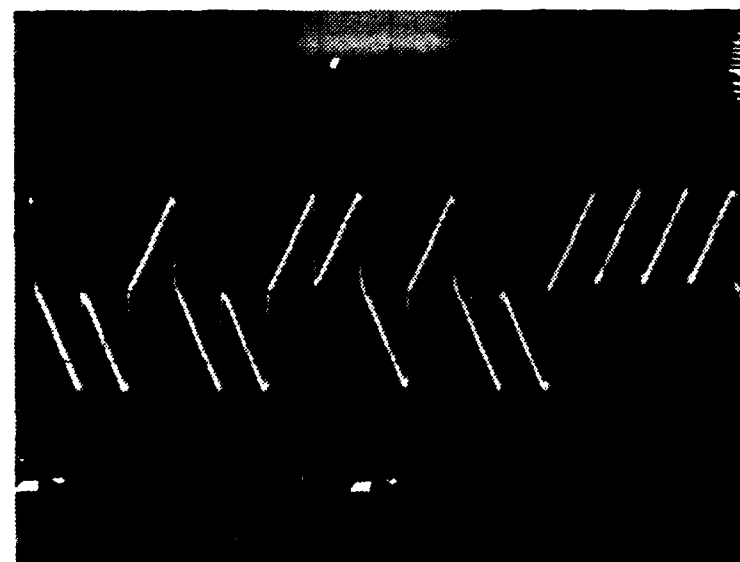(SNR = ∞; scales: Horizontal 1msec/div., vertical 1V/div.)

Figure 1.24
**Photograph of the Integrate and Dump Circuit Output
When Using Square-Wave Reference Voltage**

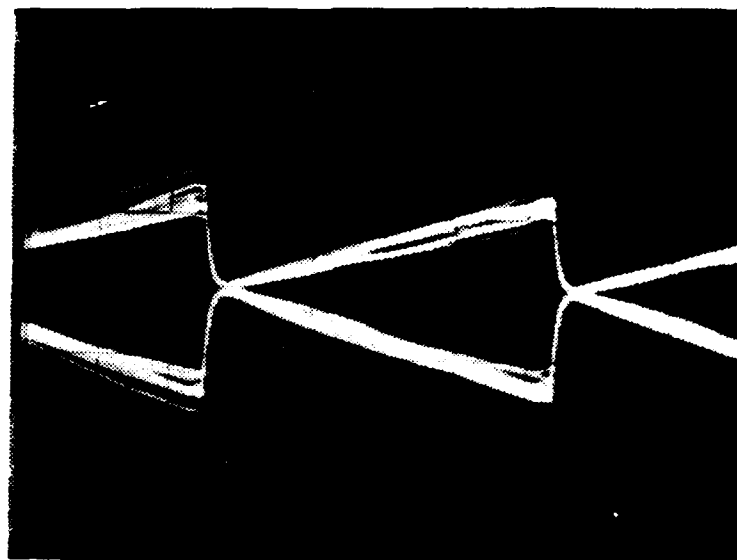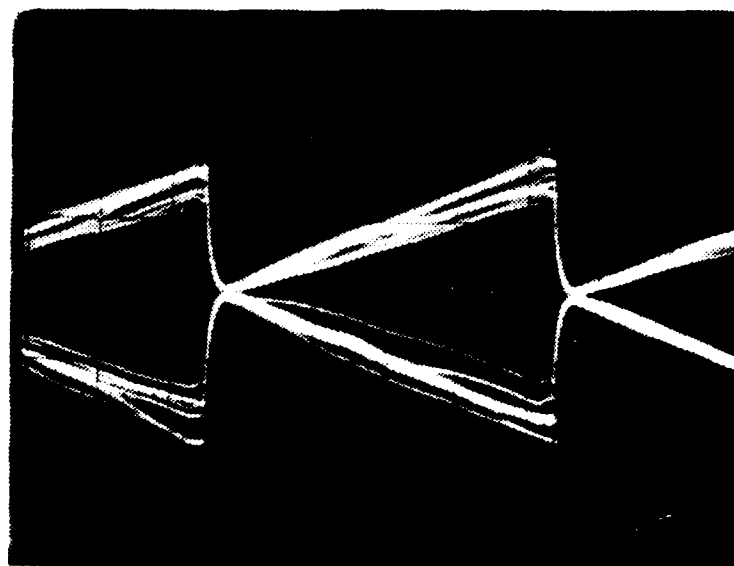(SNR = ∞; scales: Horizontal 1msec/div., vertical 1V/div.)

44

Figure 1.25
**Photograph of the Integrate and Dump Circuit Output
When Using Sinusoidal Reference Voltage**
(SNR = 10 db; scales: Horizontal 200μsec/div., vertical 1V/div.)

Figure 1.26
**Photograph of the Integrate and Dump Circuit Output
When Using Square-Wave Reference Voltage**
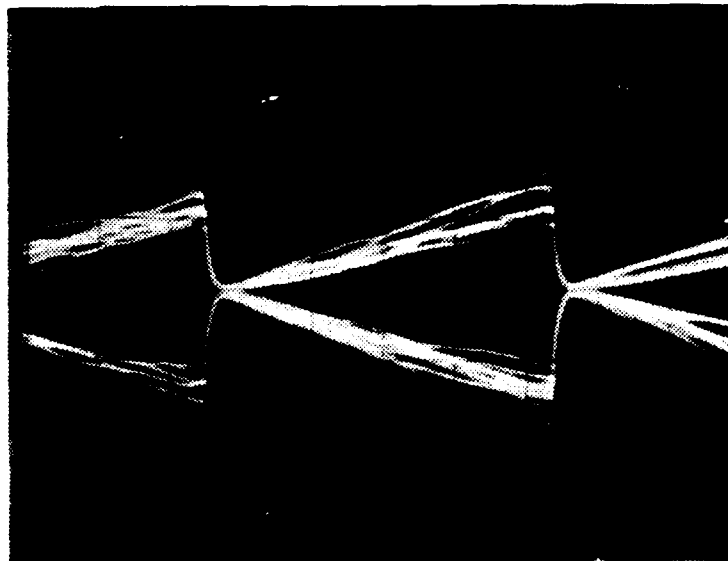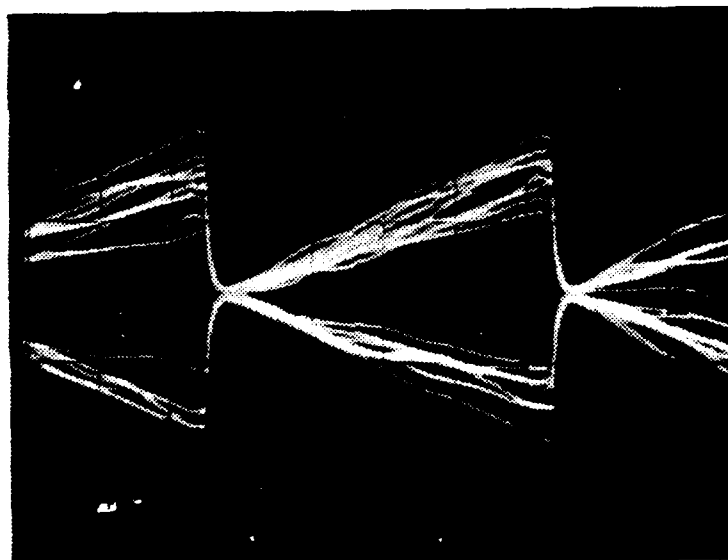(SNR = 10 db; scales: Horizontal 200μsec/div., vertical 1V/div.)

Figure 1.27

**Photograph of the Integrate and Dump Circuit Output
When Using Sinusoidal Reference Voltage**

(SNR = 5 db: scales: Horizontal 200μsec/div., vertical 1V/div.)

Figure 1.28

**Photograph of the Integrate and Dump Circuit Output
When Using Square-Wave Reference Voltage**

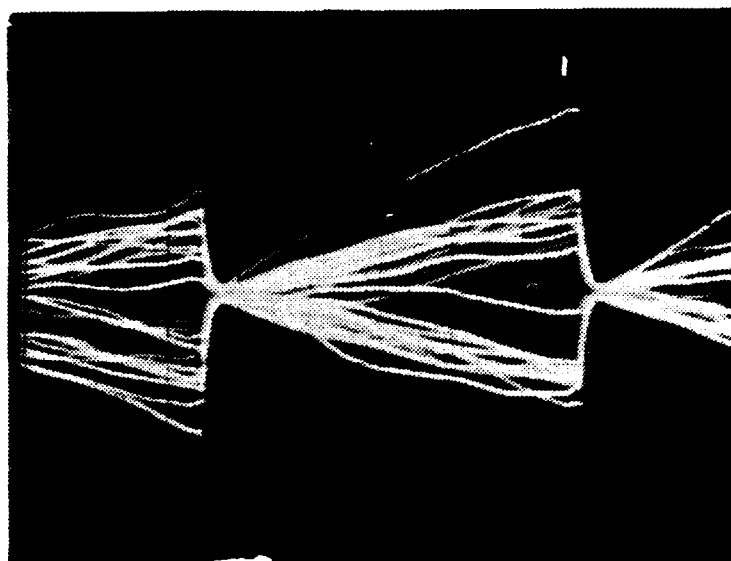(SNR = 5 db: scales: Horizontal 200μsec/div., vertical 1V/div.)

46

Figure 1.29
**Photograph of the Integrate and Dump Circuit Output
When Using Sinusoidal Reference Voltage**
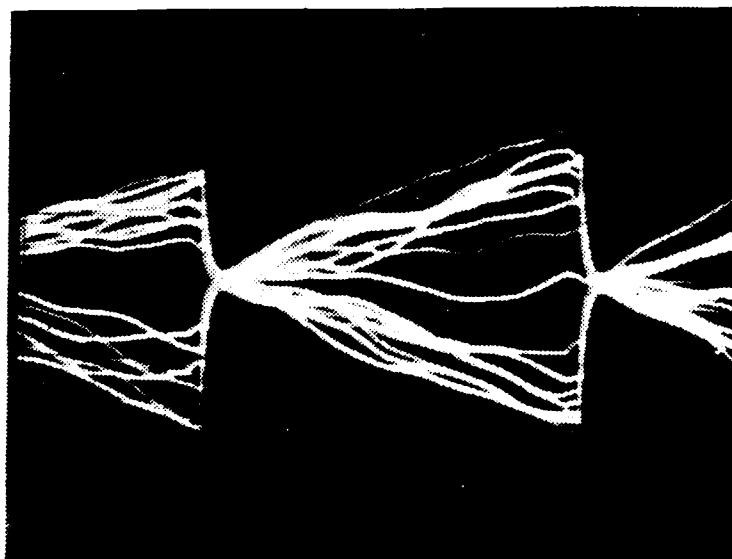(SNR = 3 db; scales: Horizontal 200μsec/div., vertical 1V/div.)

Figure 1.30
**Photograph of the Integrate and Dump Circuit Output
When Using Square-Wave Reference Voltage**
(SNR = 3 db; scales: Horizontal 200μsec/div., vertical 1V/div.)

47

zero. Figure 1.31 pictorially presents the system clock, sample pulse, and the dump pulse in the time domain.
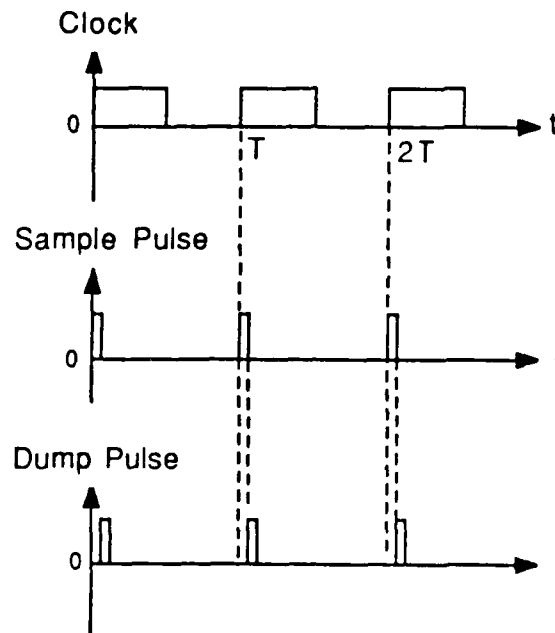

Clock

Sample Pulse

Dump Pulse

Figure 1.31

Time Domain Representation of the System Clock, Sample Pulse, and Dump Pulse

The sample and hold output $v_{SH}(t)$ is applied to a comparator (LM311) with a threshold of zero volts. This threshold implements the maximum likelihood decision rule for the assumed pdfs represented by Figure 1.5. When the bits are equiprobable, this is also the minimum probability of error decision rule which is desired [Ref. 4:p. 41-42].

The comparator output is converted to TTL voltage levels using a flip-flop (one stage of an 8-bit shift register 74164). The flip-

48

flop output is the recovered data. $\hat{d}(t)$. Figure 1.32 shows the construction of the decision and pulse generator circuits.

7. **Error Detection Circuit**

The error detection circuit provides the probability of error for various values of receiver input SNR. From these results, curves of probability of error versus SNR for each of the two reference voltages (sinusoid and square wave) are prepared.

Design of the error detection circuit is such that a single decision for each data bit is made by sampling both the original data bit and the recovered data bit and making a comparison. The sampling circuit is driven by the transmitter clock and generates a window which occurs in time just before the integrator is dumped. This window is extremely small in comparison to the duration of a data bit, and its occurrence just before the dump time maximizes the probability that the recovered data will be stable. As seen in Figure 1.33, the sampling window enables two AND gates (7408) whose other inputs are $d(t)$ and $\hat{d}(t)$, respectively. Comparison of the samples is accomplished by connecting the AND gate outputs to an EX–OR gate (7486). With EX–OR logic, a "1" output is generated only when the two inputs differ. In this case, an error is recorded. Two counters (HP5302A) record errors and the number of data bits transmitted, respectively. The data run time window is activated by a test start switch. Bit error ratio is determined by dividing the number of errors recorded by the total number of bits transmitted. This process is repeated for various values of input SNR to obtain a plot of bit error ratio versus SNR.
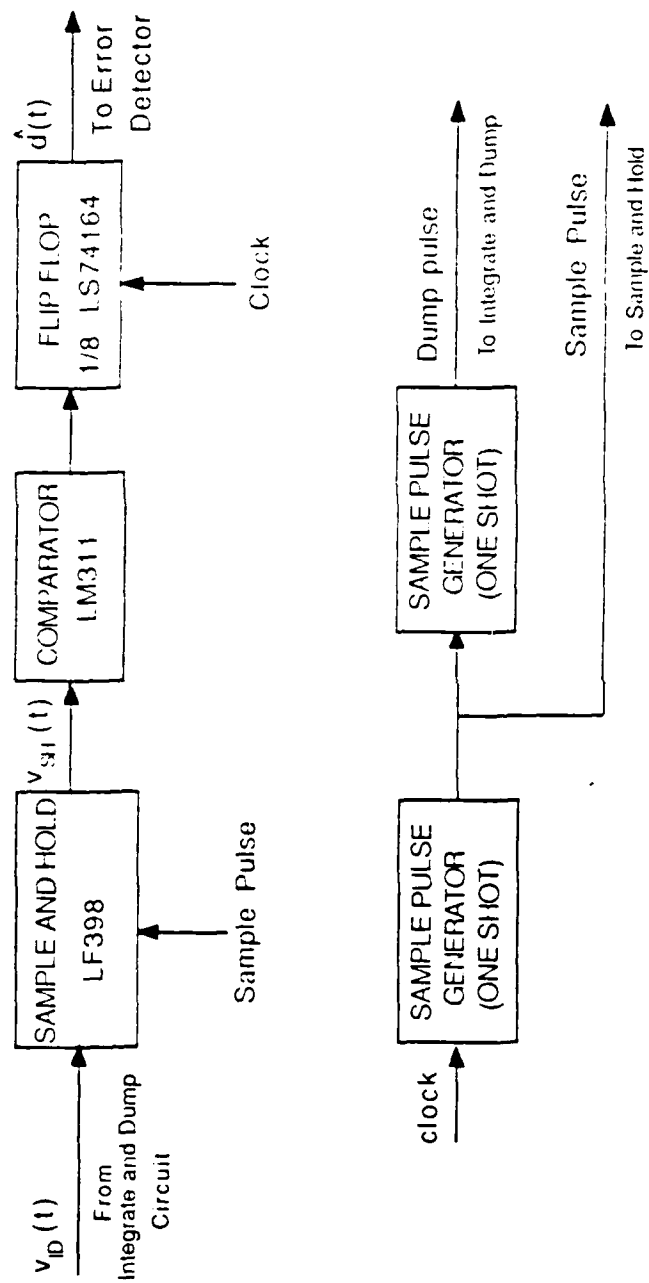
49

Figure 1.32

Block Diagram of the Bit Decision Circuit (top) and Sample and Dump Pulse Generator Circuits (bottom)
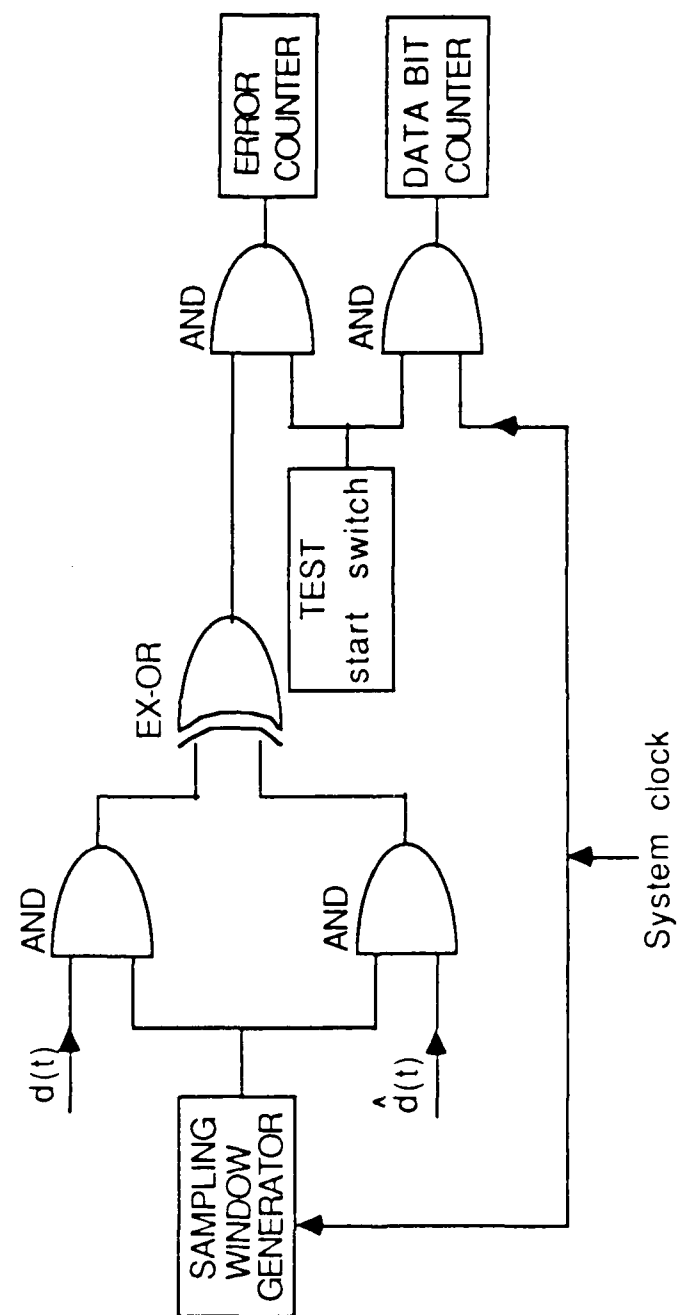
Figure 1.33

Block Diagram of the Error Detection Circuit

B. TEST PROCEDURE AND RESULTS

The final outputs of the experimental system described are the recovered data $\hat{d}(t)$ and bit error ratio (BER). BER is a measure of the degree of difference between the transmitted data $d(t)$ and recovered data $\hat{d}(t)$. A plot of BER versus receiver input SNR is a measure of system performance. A systematic approach to operation of the experimental system is desirable for accurate results.

After initial application of the supply voltages to the system, synchronization of the receiver and transmitter must be ensured. A binary switch is used to reset the contents of the feedback shift register to the "all zeros" state. Placing the switch in its opposite position ("1" position) initiates the operation of the feedback shift register.

For this experiment, a constant 2V RMS sinusoidal carrier is used in the transmitter. The AVM attenuates the input carrier wave such that the RMS voltage is 0.5 volts. Thus, the transmitted signal power is $(0.5)^2 = 0.25$ watts. Narrowband Gaussian noise $n(t)$ is added to the AVM output in an analog summer in the channel. The RMS value of the noise voltage input is varied to obtain various values of SNR of interest. In order to determine the value of SNR, the RMS voltage value of the signal at the input to the demodulator (IF amplifier output) with no noise is first measured with a true RMS voltmeter. The square of this voltage gives the signal power S. Then the same voltage is measured when there is noise. This is the RMS voltage of signal plus noise = $(s(t) + n(t))_{RMS}$. Noise power N is obtained by subtracting

the measured signal power S from $\left[(s(t) + n(t))_{RMS}\right]^2$. Since the signal power is fixed (0.25 watts), the demodulator input SNR is

$$SNR_{in} = \frac{0.25}{N}$$

or, in decibels,

$$(SNR_{in}) \, dB = 10 \log \frac{0.25}{N}$$

For the SNR of interest, BER is experimentally determined and a plot of BER versus $(SNR)_{in}$ dB is constructed when using a sinusoidal reference and when using a square-wave reference, respectively. In the case of a sinusoidal reference, this experimentally obtained curve can be compared with the theoretical curve of Figure 1.6 in Chapter II. This comparison provides a kind of calibration of the experimental system. Then a comparison between the experimental curves obtained when using a sinusoidal reference and when using a square-wave reference is made. Experimentally obtained curves are shown in Figure 1.34. BER curves are drawn to be consistent with the literature which uses E_b/N_0 instead of SNR. The relation between input SNR and E_b/N_0 is as follows.

Signal power at the output of the IF amplifier is $S = \frac{E_b}{T}$ where E_b = energy per bit and T = bit duration. The noise power at the output of the IF amplifier is $N = \frac{N_0}{2} \cdot (2B)$, where $\frac{N_0}{2}$ = power spectral density level (two-sided in watts/Hz), and 2B = IF amplifier bandwidth when B = 1/T. Therefore,
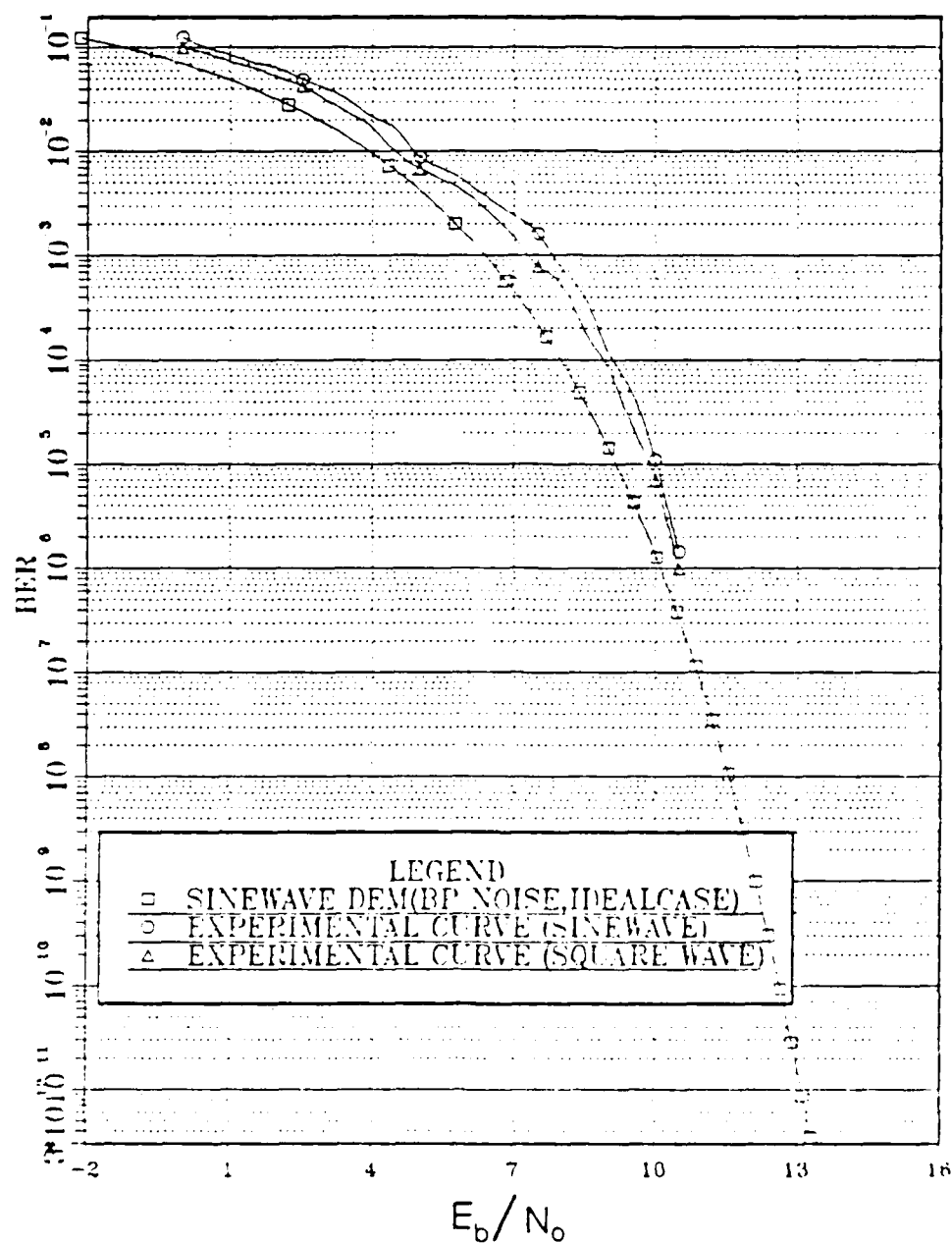
BPSK BER CURVE FOR MF DETECTION

Figure 1.34

**Experimental BER Curves for a Sinusoidal Reference
and for a Square-Wave Reference
When Considering Bandpass Noise in the Channel**

54

$$\frac{S}{N} = \text{SNR} = \frac{E_b/T}{2N_0B}$$

$$= \frac{E_b}{2N_0} \tag{1.9}$$

or

$$\frac{E_b}{N_0} = 2\ \text{SNR}$$

$$\left(\frac{E_b}{N_0}\right) dB = 3\ dB + (\text{SNR})_{dB} \tag{1.10}$$

In practice, $\frac{E_b}{N_0}$ is obtained by adding 3 dB to the measured $(\text{SNR})_{dB}$ as stated in equation 1.10.

The curves show a difference of about 1 dB in SNR for a given BER when comparing the data with theory. The analytical curve assures an ideal rectangular form for the transfer function of the predetection bandpass filter.

Figure 1.34 also shows the square-wave reference provides about 0.4 dB improvement in receiver noise performance relative to a sinusoidal reference. Theory predicts no improvement (0 dB). The theory assumes a perfect square wave and ideal voltage multiplication.

IV. CONCLUSIONS AND RECOMMENDATIONS

A square-wave reference can be used to demodulate the BPSK signals, and in practice receiver noise performance improves somewhat. Since a square wave is easy to generate, this technique may provide hardware design advantages in some applications.

A typical BPSK receiver operating with bandpass noise has about 0.4 dB better performance than predicted by that theory which assumes white noise at the demodulator input (usual published result).

APPENDIX 1A

ANALYTICAL BER ANALYSIS

This appendix contains the associated BPSK bit error rate (BER) analysis when considering a sinusoidal reference and a square-wave reference in the receiver. BER analysis is given for allpass white noise and also for bandpass noise. The system model for the analysis is shown in Figure 1A-1.
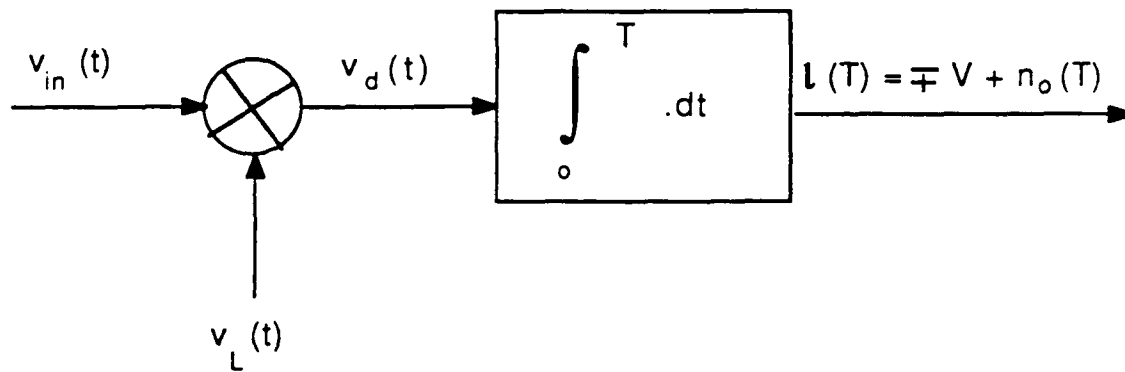

Figure 1A-1

BPSK Receiver Model for BER Analysis

where

$$v_{in}(t) = \pm A \cos 2\pi f_0 t + n(t) \tag{1A.1}$$

$$n(t) = x(t) \cos 2\pi f_0 t - y(t) \sin 2\pi f_0 t \text{ (Rice's noise model)} \tag{1A.2}$$

where x(t) and y(t) are lowpass and $N(0, \sigma^2)$ where σ^2 is the total noise power N,

$l(T)$ = output random variable

= $\pm V + n_0(T)$

where V is the signal (constant) and $n_0(T)$ is the noise (random) portion of $l(T)$, and so

$V = E[l(T)/("1" \text{ or } "0" \text{ received})]$

The mean and variance of the output random variable $l(T)$ and the output pdfs have to be determined to obtain the BERs for each case.

1. **Mean of $l(T)$**

$$E\,[l(T)] = E\left\{\left[\int_0^T v_{in}(t)\,v_L(t)\,dt\right]\right\} \tag{1A.3}$$

a. **Sine–Wave Reference**

$v_L(t) = \cos 2\pi f_0 t$ and from equation 1A.3

$$E\,[l(T)] = E\left\{\left[\int_0^T \left(\pm A \cos 2\pi f_0 t + n(t)\right) \cos 2\pi f_0 t\,dt\right]\right\}$$

$$= \pm \frac{AT}{2} \tag{1A.4}$$

b. Square–Wave Reference

Express the unit amplitude square wave as a Fourier series.

$$v_L(t) = \frac{4}{\pi} \cos 2\pi f_0 t + \frac{4}{3\pi} \cos 2\pi.3f_0 t + \frac{4}{5\pi} \cos 2\pi.5f_0 t + \ldots \qquad (1A.5)$$

Substituting equation 1A.5 in equation 1A.3 gives

$$E[l(T)] = \pm \frac{4}{\pi} \cdot \frac{AT}{2} \qquad (1A.6)$$

2. Variance of $l(T)$

$$\text{Var } [l(T)] = \sigma_0^2 = \text{output noise power}$$

$$\text{Var } [l(T)] = E\left\{ \underbrace{\left[\int_0^T (s(t) + n(t))\, v_L(t)\, dt\right]^2}_{\text{Total power}} - \underbrace{[E [l(T)]]^2}_{\text{dc power}} \right\}$$

and so,

$$\text{Var}[l(T)] = E\left\{\left[\int_0^T s(t)\, v_L(t)\, dt\right]^2 + 2\int_0^T s(t)\, n(t)\, v_L(t)\, dt + \right.$$

$$\left. \left[\int_0^T n(t)\, v_L(t)\, dt\right]^2 - [E [l(T)]]^2\right\}$$

$$= [E [l(T)]]^2 + 2\int_0^T s(t)\, E[n(t)]\, v_L(t)\, dt + E\left[\int_0^T n(t)\, v_L(t)\, dt\right]^2$$

$$- [E [l(T)]]^2$$

$$= E\left[\int_0^T n(t)\, v_L(t)\, dt\right]^2$$

59

or

$$\text{Var} \; [l(T)] = E \left\{ \left[\int_0^T \int_0^T n(t) \, n(\tau) \, v_L(t) \, v_L(\tau) \, dt \, d\tau \right] \right\} \qquad (1A.7)$$

Since the expectation is a linear operator and assuming the noise is stationary, then $E \; [n(t) \, n(\tau)] = R_n(t - \tau)$, so substituting this in equation 1A.7 gives

$$\text{Var} \; [l(T)] = \int_0^T \int_0^T R_n(t - \tau) \, v_L(t) \, v_L(\tau) \, dt \, d\tau \qquad (1A.8)$$

a. Allpass White Noise

In this case,

$$R_n(t) = \frac{N_0}{2} \delta(t) \qquad (1A.9)$$

Substituting equation 1A.9 in equation 1A.8 gives

$$\text{Var} \; [l(T)] = \sigma_0^2 = \frac{N_0}{2} \int_0^T v_L^2(t) \, dt \qquad (1A.10)$$

(1) Sine-Wave Reference

$$v_L^2(t) = A^2 \cos^2 \omega_0 t = \frac{A^2}{2} (1 + \cos \omega_0 t)$$

therefore,

$$\sigma_0^2 = \frac{N_0 T}{4} \qquad (1A.11)$$

60

(2) Square-Wave Reference

$$v_L^2(t) = 1$$

and so,

$$\sigma_0^2 = \frac{N_0 T}{2} \qquad (1A.12)$$

So the output noise power σ_0^2 is doubled when using a square-wave

reference as compared to a sinusoidal reference.

b. Bandpass White Noise

Equation 1A.8 can be written as given in equation 1A.13

by introducing a function $z(x)$ where

$$z(x) = \begin{cases} 1 & 0 < x < T \\ 0 & \text{otherwise} \end{cases}$$

Substituting this function $z(x)$ in equation 1A.8 gives

$$\sigma_0^2 = \int_{-\infty}^{\infty} \int_{-\infty}^{\infty} R_n(t - \tau) \, v_L(t) \, z(t) \, v_L(\tau) \, z(\tau) \, dt \, d\tau \qquad (1A.13)$$

Now, equation 1A.13 can be transformed to the frequency domain.
Observe that,

$$\mathcal{F}\{R_n(t - \tau)\} = e^{-j\omega\tau} \, S_n(f)$$

where $S_n(f)$ = power spectral density function of noise at the input to
the demodulator and $\mathcal{F}\{y(t)\}$ is the Fourrier transform of $y(t)$

$$S_n(f) = \frac{N_0}{2} |H(f)|^2 \qquad (1A.14)$$

and $H(f)$ is the transfer function of the IF amplifier. Also, $\frac{N_0}{2}$ is the two-sided power spectrum of the noise at the input to the IF amplifier. Therefore,

$$R_n(t - \tau) = \int_{-\infty}^{\infty} (S_n(f) \; e^{-j\omega\tau}) \; e^{j\omega t} \; df \qquad (1A.15)$$

Substituting equation 1A.14 and equation 1A.15 in equation 1A.13 gives

$$\sigma_0^2 = \int_{-\infty}^{\infty} \int_{-\infty}^{\infty} \left[\int_{-\infty}^{\infty} S_n(f) \; e^{-j\omega\tau} \; e^{j\omega t} \; df \right] v_L(t) \; z(t) \; v_L(\tau) \; z(\tau) \; dt \; d\tau$$

which can be written as

$$\sigma_0^2 = \int_{-\infty}^{\infty} S_n(f) \; df \int_{-\infty}^{\infty} v_L(\tau) \; z(\tau) \; e^{-j\omega\tau} \; d\tau \int_{-\infty}^{\infty} v_L(t) \; z(t) \; e^{j\omega t} \; dt.$$

or

$$\sigma_0^2 = \int_{-\infty}^{\infty} S_n(f) \; |V_L'(f)|^2 \; df \qquad (1A.16)$$

where

$$V_L'(f) = \mathcal{F}[v_L(x) \; z(x)]$$

(1) Cosine Reference

$$V_L'(f) = \int_{-\infty}^{\infty} \underbrace{v_L(t)\; z(t)}_{y(t)}\; e^{-j2\pi ft}\, dt$$

$$= Y(f) = V_L(f) * Z(f)$$

where * denotes convolution and where

$$Z(f) = T\; e^{-j\pi fT}\; \text{sinc}(\pi fT)$$

$$V_L(f) = \frac{1}{2}\delta(f - f_0) + \frac{1}{2}\delta(f + f_0)$$

Therefore,

$$V_L'(f) = \frac{T}{2} e^{-j\pi(f-f_0)T}\; \text{sinc}\,\pi(f - f_0)T + \frac{T}{2} e^{-j\pi(f+f_0)T}\; \text{sinc}\,\pi(f + f_0)T \quad (1A.17)$$

The resulting spectrum of the $V_L(f)$ is shown in Figure 1A.2.
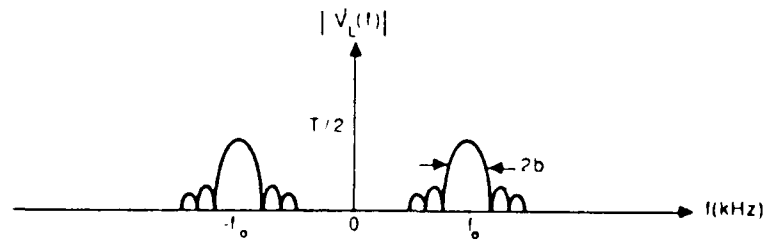
Figure 1A-2

Frequency Spectrum of $V_L(f)$

$$\left(\text{Assuming } f_0 * \frac{1}{T} \right)$$

63

Then we can write

$$\sigma_0^2 = 2 \int_0^\infty \frac{N_0}{2} |H(f)|^2 \cdot \frac{T^2}{4} \text{sinc}^2 \, \pi \, (f - f_0) \, T \, df \qquad (1A.18)$$

For an ideal bandpass filter (IF amplifier), then $H(f)$ is constant (unity) over a region about f_0 as shown in Figure 1A-3.
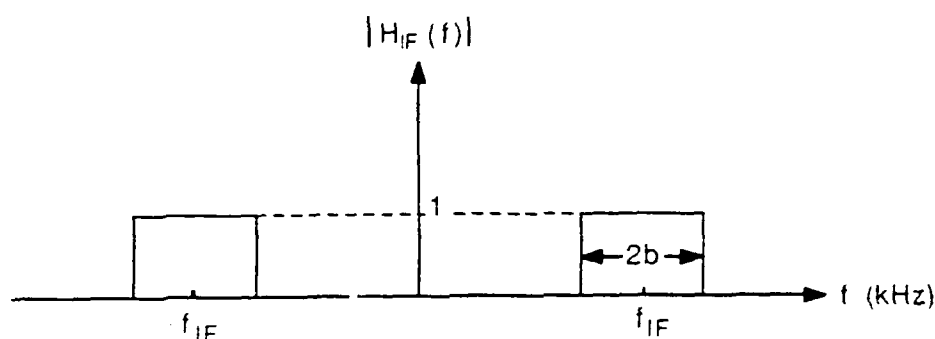
Figure 1A-3

Transfer Function of an Ideal Bandpass Filter Centered at f_0

And so, for this case we obtain

$$\sigma_0^2 = \frac{N_0 T^2}{2} \int_{f_0-b}^{f_0+b} \text{sinc} \, \pi(f-f_0) \, T \, df$$

which is equivalent to

$$\sigma_0^2 = N_0 T^2 \int_0^b \text{sinc}^2 \, \pi f \, T \, df$$

64

when $b = \frac{1}{T}$, then from numerical integration,

$$\sigma_0^2 = \frac{N_0 T}{2\pi} \, (1.4181) \qquad\qquad (1A.19)$$

(2) Square-Wave Reference. Again,

$$V'_L(f) = \mathcal{F}\{v_L(t) \, z(t)\}$$

where $v_L(t)$ is a square wave of amplitude ± 1 volt having the spectrum shown in Figure 1A.4. So, for this case,

$$V_L(f) = T \cdot \frac{4}{\pi} \frac{1}{2} \frac{\sin{(\pi(f - nf_0)T)}}{\pi(f - nf_0)T} \quad \begin{array}{l} n \neq 0 \\ n = 1,2,3,... \end{array} \qquad (1A.20)$$

and the spectrum of $V_L(f)$ is shown in Figure 1A.5 for this case. It is obvious from Figure 1A.5 that only the values of $V_L(f)$ around f_0 contribute to the output noise power σ_0^2 because of the bandpass filter. So, substituting equation 1A.20 in equation 1A.16 and using the form of $|H(f)|$ in Figure 1A.3 gives

$$\sigma_0^2 = \frac{T^2}{2} \cdot \left(\frac{4}{\pi}\right)^2 \cdot \frac{N_0}{2} \int_0^\infty \text{sinc}^2 \pi f T \, df$$

which is equivalent to

65

$$\sigma_0^2 = \frac{T^2}{2} \cdot \left(\frac{4}{\pi}\right)^2 \frac{N_0}{2} \int_0^b \text{sinc}^2 \pi fT \, df$$

$$= \left(\frac{4}{\pi}\right)^2 \frac{N_0 T}{2\pi} \cdot (1.4181) \qquad\qquad (1A.21)$$

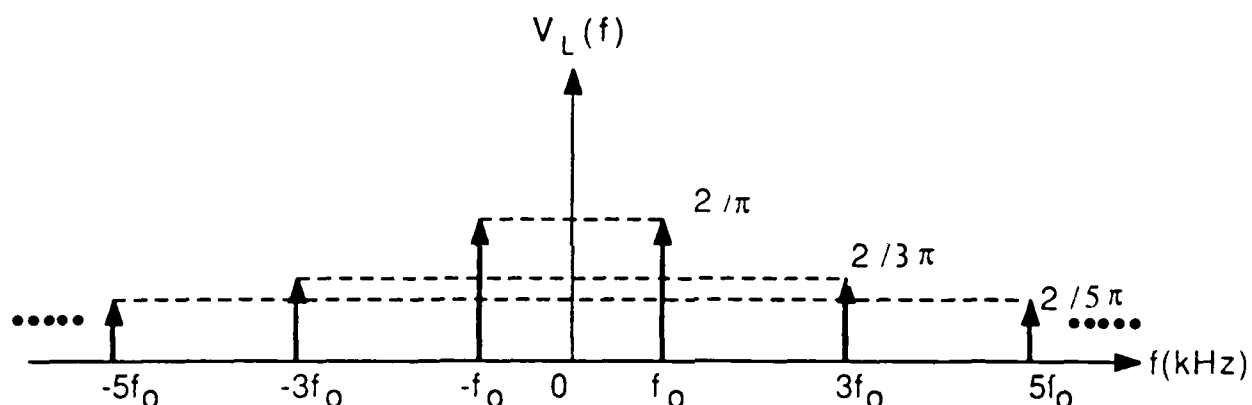Equation 1A.21 is also obtained by numerical integration.

Figure 1A–4

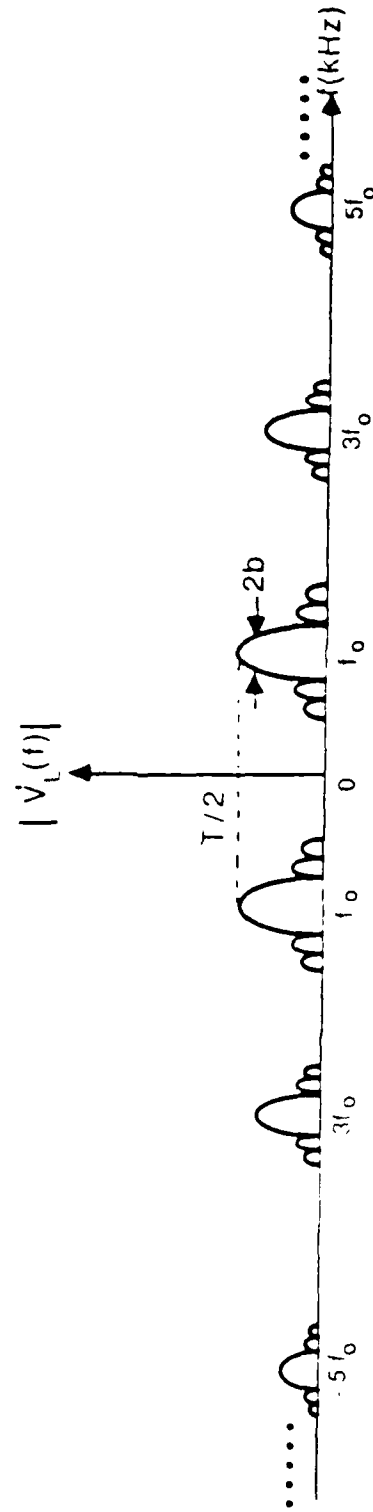**Frequency Spectrum of a Square–Wave of Amplitude ± 1 volt**

66

Figure 1A-5

Frequency Spectrum of $V_L(f)$ When Using a Square-Wave Reference Voltage

3. Output pdfs.

Use equation 1A.2, the noise model of Rice [Ref. 3:pp. 46–157].

a. Sinusoidal Reference

The lowpass noise term out of the detector is $x(t)/2$, which is $N(0, \sigma^2/4)$. Since the integrator is a linear system, then $n_0(T)$ is a sample value of a Gaussian noise and so

$$n_0(T) \rightarrow N(0, \sigma^2/4)$$

b. Square–Wave Reference

$$n_0(T) = \int_0^T n(t)\, v_L(t)\, dt \qquad (1A.22)$$

Substituting equation 1A.5 (Fourier series expansion of a square wave) in equation 1A.22 gives the lowpass noise term out of the detector as $x(t)$. Therefore, reasoning as for the sinusoidal reference gives $n_0(T)$ as $N(0, (4/\pi)^2 \sigma^2)$.

4. Associated BER Analysis

When the output random voltage variations are Gaussian, then use of Figure 1.5 gives

$$BER = erfc \left(\frac{E[l(T)]}{\sigma_0} \right) \qquad (1A.23)$$

where

$$erfc(x) = \int_{x}^{\infty} \frac{1}{\sqrt{2\pi}} e^{-\tau^2/2} \, d\tau$$

a. Sinusoidal Reference and Allpass Noise n(t)

Substituting equation 1A.4 and equation 1A.11 in equation 1A.23 gives

$$BER = erfc\left(\frac{AT/2}{\sqrt{\frac{N_0 T}{4}}}\right)$$

$$= erfc\left(\sqrt{4\ SNR}\right)$$

or, as stated in equation 1.10,

$$BER = erfc\left(\sqrt{\frac{2\ E_b}{N_0}}\right)$$

b. Sinusoidal Reference and Bandpass Noise n(t)

Substituting equation 1A.4 and equation 1A.19 in equation 1A.23 gives

$$BER = erfc\left(\sqrt{\frac{2\ E_b}{N_0} 1.1}\right)$$

c. Square–Wave Reference and Allpass Noise n(t)

Substituting equation 1A.6 and equation 1A.12 in equation 1A.23 gives

$$BER = erfc\left(\sqrt{\frac{2\ E_b}{N_0} 0.81}\right)$$

69

d. Square–Wave Reference and Bandpass Noise n(t)

Substituting equation 1A.6 and equation 1A.21 in equation 1A.23 gives

$$BER = erfc\left(\sqrt{\frac{2\,Eb}{N_0}\,1.1}\right)$$

APPENDIX 1B

CIRCUIT SCHEMATICS

This appendix contains schematic diagrams for all of the circuits used in the experimental system. The components used to implement the various circuits include TTL gates (EX-OR, EX-NOR, NAND, AND NOT gates), mono stable multivibrators, shift registers, counters, digital switches, analog voltage multipliers, operational amplifiers, voltage comparator, and analog switches. The operating characteristics of each component can be found in references 5 through 7.

The various circuit diagrams are presented in Figures 1B-1 through 1B-8 in the following order:

Figure 1B-1   FSR With Protection Circuit

Figure 1B-2   Carrier Modulator

Figure 1B-3   Bandpass Filter

Figure 1B-4   Carrier Demodulator and Hard Limiter

Figure 1B-5   Sample and Dump Pulse Generators

Figure 1B-6   Integrate and Dump Circuit

Figure 1B-7   Decision Circuit

Figure 1B-8   Error Detection Circuit

The values of all capacitors are in microfarads unless otherwise indicated.

Figure 1B-1 shows the FSR with protection circuit. The clock is set at 1 kHz and is provided by a Wavetek signal generator. One 8-bit
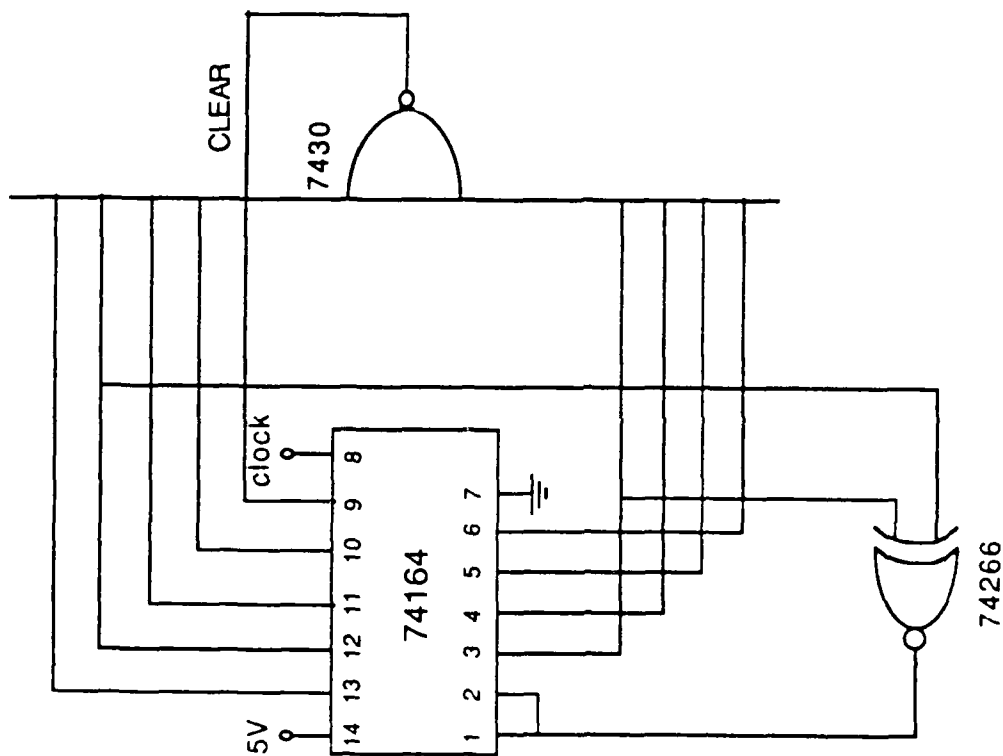
Figure 1B-1

Schematic of the FSR With Protection Circuit

shift register (74164) is used to obtain the seven-stage FSR. This shift register (74164) is a serial in, parallel out type so that they may be easily cascaded. The outputs of the third and seventh stages formed by cascading the registers are tapped and fed back through an EX-NOR gate (74266) whose output is serially loaded into the first input of the register. Synchronous clocking of the stages, together with the serial feedback, generates a repeating m-sequence having 127 bits per period. If the "all ones" condition occurs in the shift register contents, the NAND gate (7430) generates an "0" which clears the shift register contents, thus starting the m-sequence again.

The AVM (AD534) is used for carrier modulation as shown in Figure 1B-2. A Wavetek function generator (model 142) is used to generate the sinusoidal carrier. The variable DC voltage which is added to one of the input ports of the AVM ensures that no dc offset will occur at the AVM output.

A third-order multiple feedback bandpass filter with Q-multiplier is chosen to meet the design specifications for the experimental system. Figure 1B-3 shows the filter schematic. This filter is centered at 100 kHz, the carrier frequency, and the design 3 db bandwidth is 2 kHz. Designed band stop attenuation is -25 db at 100 kHz ± 4 kHz. Q-multiplication used with the basic multiple feedback configuration achieves the design Q of 50. With the available components, the minimum bandwidth achievable is about 2.5 kHz. Therefore, the actual filter transfer function (see Figure 1.15) differs from the ideal transfer function (see Figure 1.14) by a small amount. Reference 8
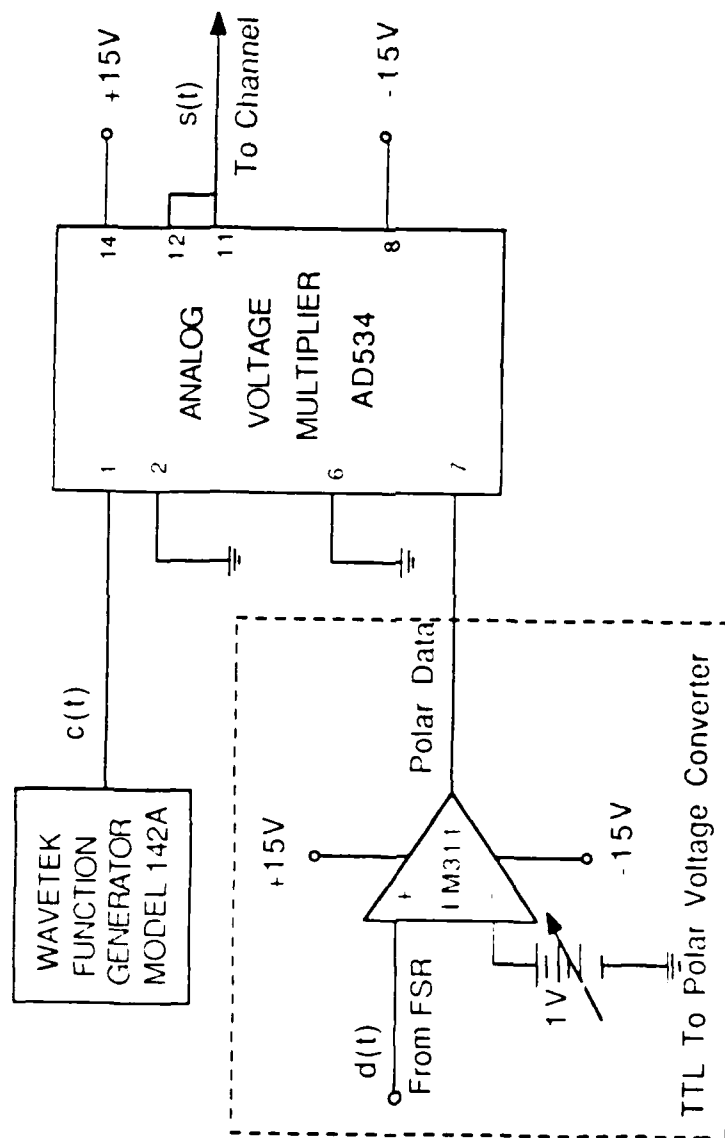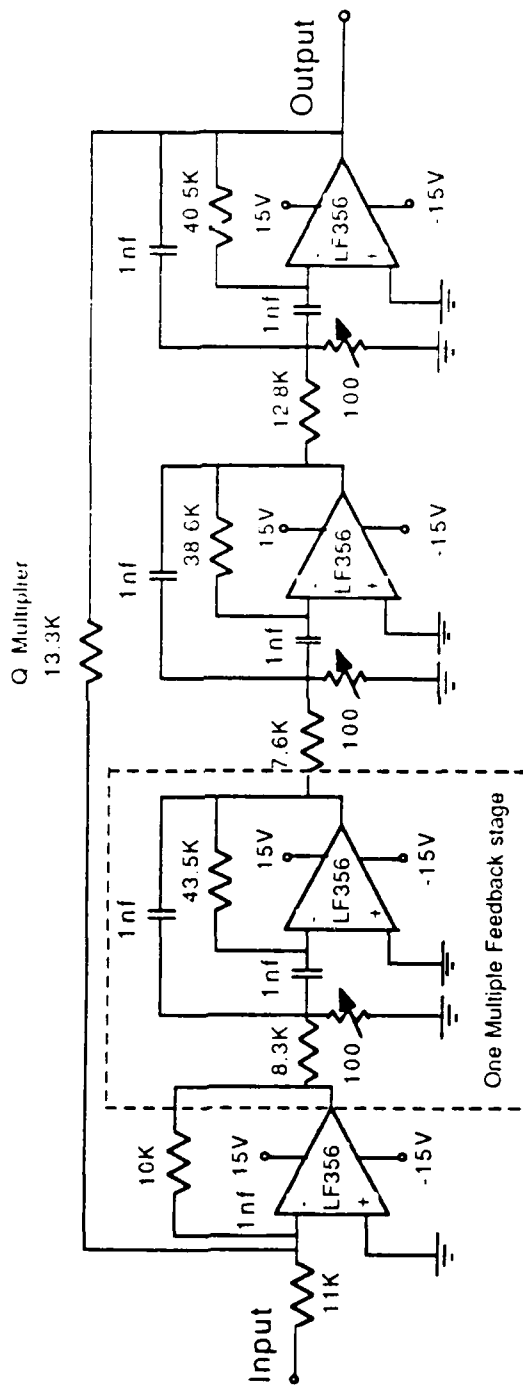
Figure 1B-2

Schematic of the Carrier Modulator

Figure 1B-3

Schematic of the Bandpass Filter

outlines the procedure for the design of this filter. Following these procedures, the circuit in Figure 1B-3 evolves. Four high-speed FET operational amplifiers (LF356) are needed for the construction of this filter. Three LF356 operational amplifiers are connected with the capacitor and resistor feedback connections shown to realize the third-order multiple feedback filter. The fourth LF356 operational amplifier and filter output-to-input feedback resistor is added for Q-multiplication.

The input to the bandpass filter is from an ELGENCO white Gaussian noise generator (model 603A). Its output is added to the carrier modulator output in an analog summer. A high-speed operational amplifier (LF356) is used to construct the analog summer circuit shown in Figure 1B-4.

Schematics for the demodulator and the coherent square-wave generator are shown also in Figure 1B-4. The demodulator is constructed using an AVM (AD534). Inputs to the demodulator are the signal plus noise (from BPF output) and the local oscillator voltage, either a sinusoidal reference voltage or a square-wave reference voltage.

The square wave is generated using a high-speed comparator (LM319) having the coherent sinusoidal reference as input. The comparator saturates at the zero crossing of the sinusoidal reference voltage and produces a ±5 volts, 100 kHz coherent reference. An analog switch is used to connect the sinusoidal or square-wave reference voltage to the AVM input port.
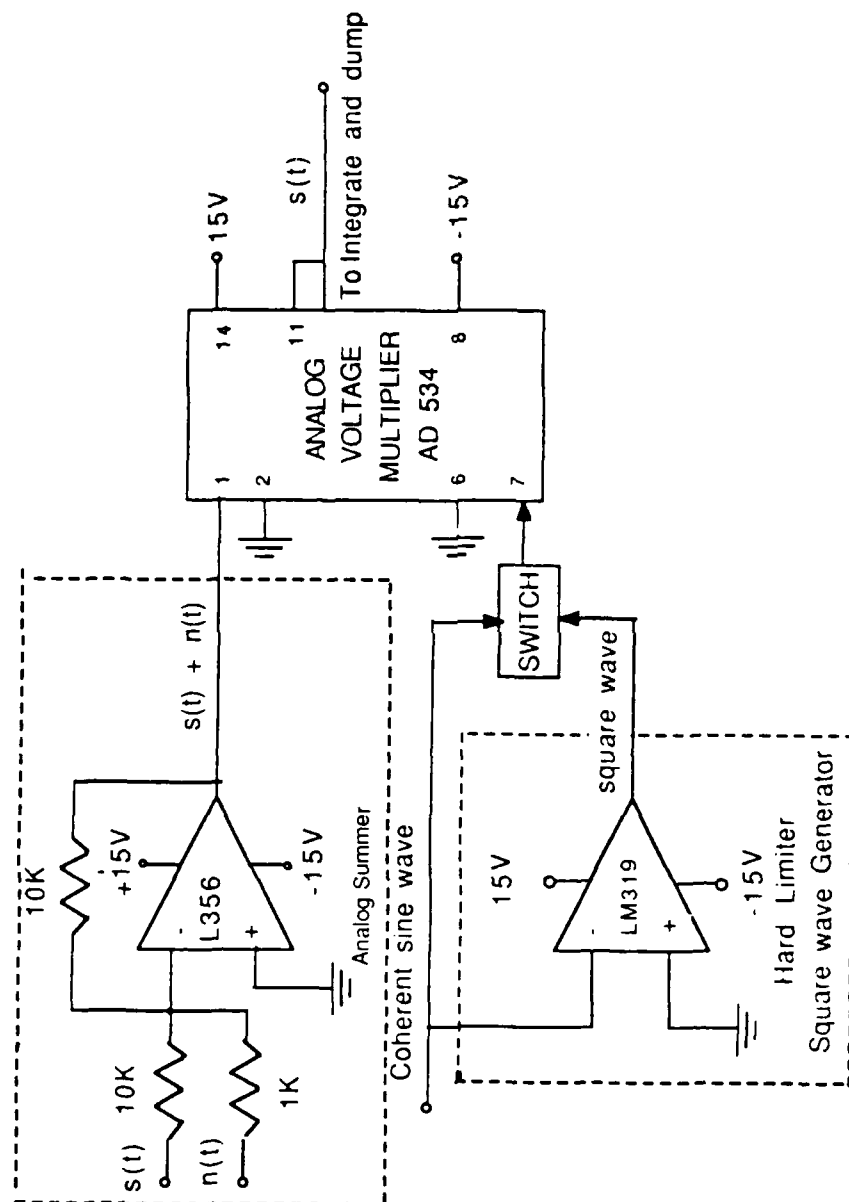
Figure 1B-4

Schematic of the Analog Summer and Carrier Demodulator

Figure 1B-5 is the integrate and dump circuit schematic. The input to the integrate and dump circuit is the AVM output. The integrator consists of an operational amplifier (LM741) and an analog switch (MC14051B), connected as shown. The dump pulse is obtained from the dump generator circuit shown in Figure 1B-6. The output of the integrator is amplified and inverted through use of an LM741 operational amplifier. Inversion of the integrator output is necessary since the integrator is an inverting circuit.

Synchronization of the receiver is provided by sample and dump pulse generators as shown in Figure 1B-6. Two cascaded one shots (monostable multivibrator 74121) generate the synchronous sample and dump pulses, respectively.

The integrate and dump output is applied to the decision circuit. A sample and hold (LF398), a comparator (LM311), and a flip-flop (one stage of an 8-bit shift register, 74164) are the major parts of the decision circuit as depicted in Figure 1B-7. A sample pulse triggers the sampling circuit and a sample is taken from the integrator output slightly before the integrator is reset to zero by the dump pulse. This sample voltage is held for a bit interval (1 msec) and applied to the comparator (LM311). The comparator generates a ±5 volt pulse, depending on the polarity of the sample voltage at the input. The comparator threshold voltage is set to zero volts. A flip-flop (one stage of a 74164 shift register) provides the interface between the analog circuitry and the digital circuitry.
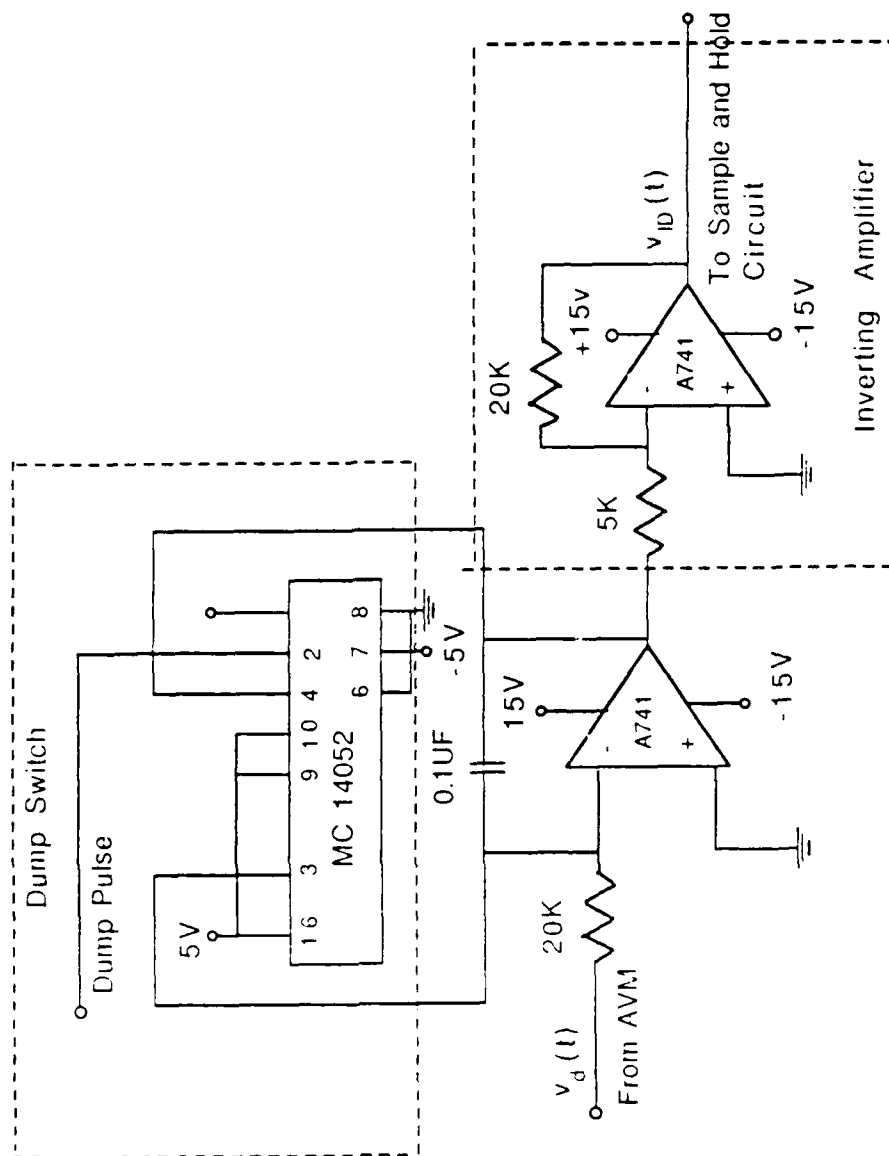
Figure 1B-5

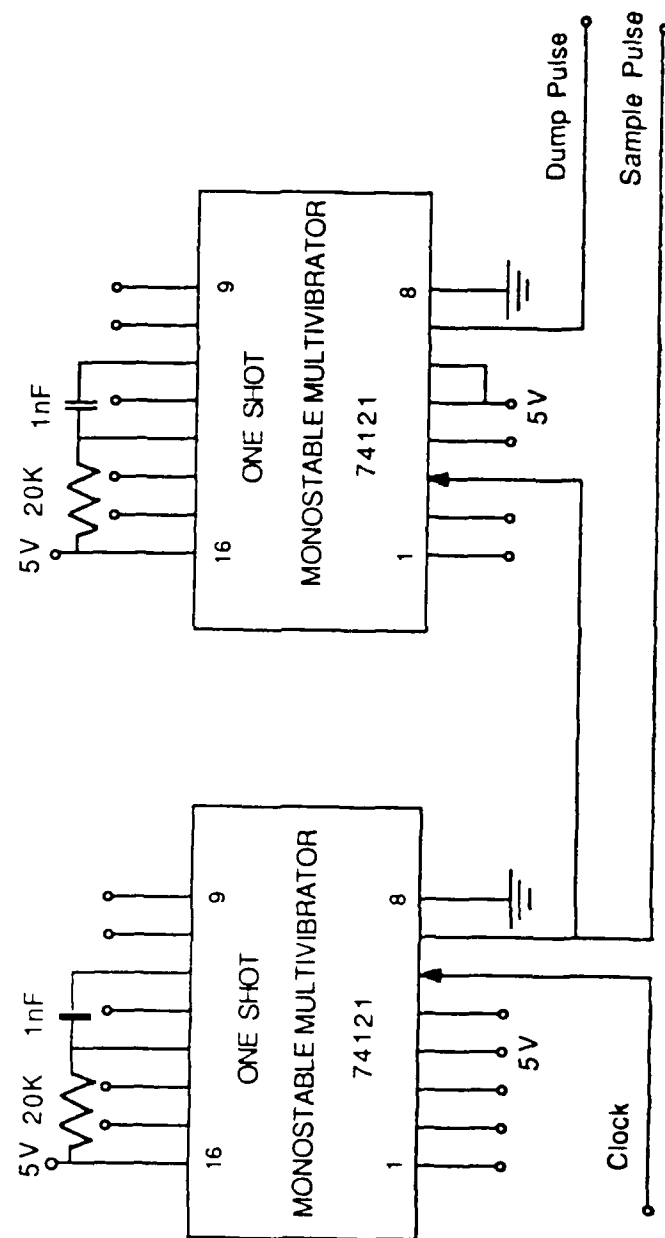Schematic of the Integrate and Dump Circuit

79

Figure 1B-6

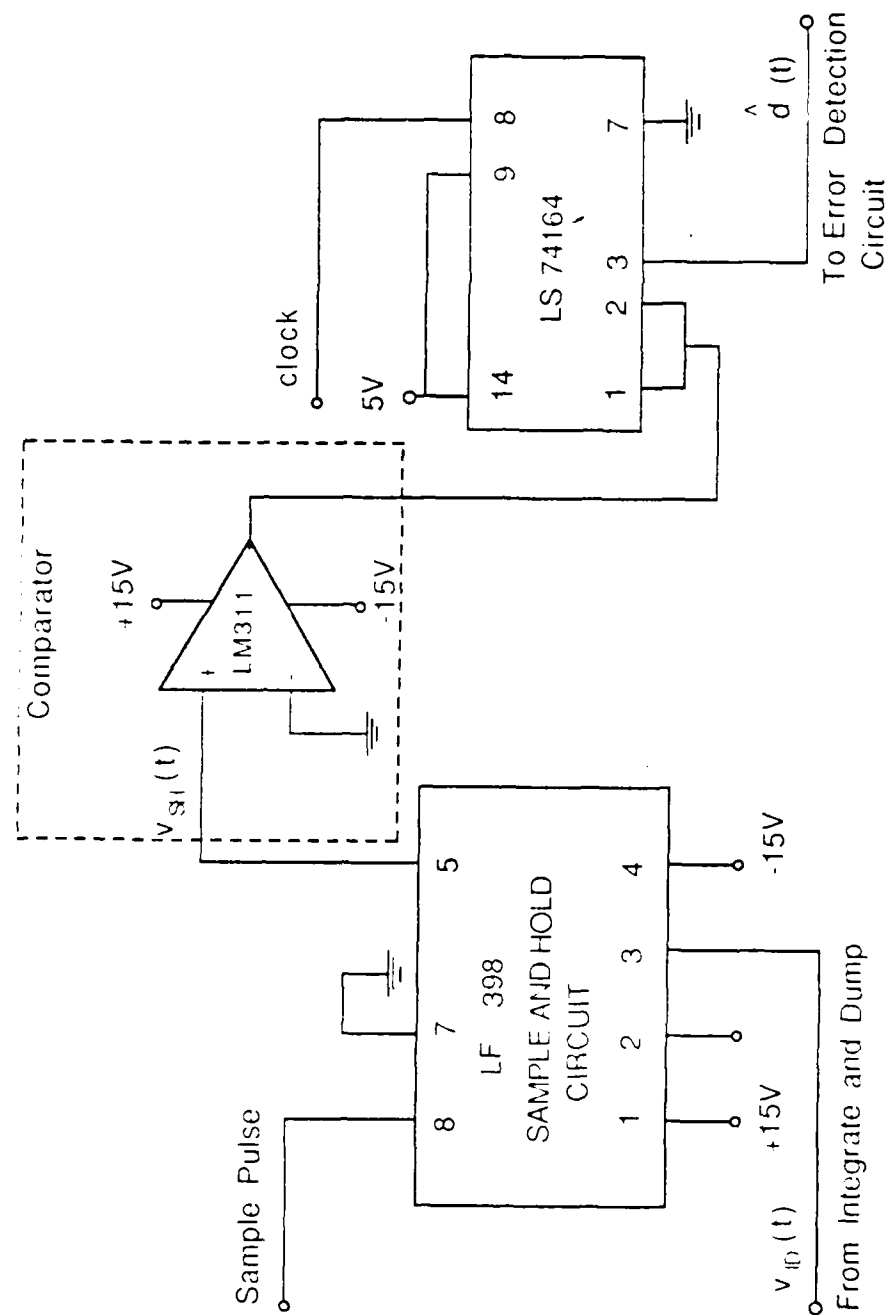Schematic of the Dump and Sample Pulse Generators

Figure 1B-7

Schematic of the Decision Circuit

81

The error detection circuit is depicted in Figure 1B-8. Two monostable multivibrators (74121) and two AND gates (7408) are connected to sample the transmitted data and the recovered data simultaneously. A parity check between the samples is made by an EX-OR gate (7486). When the samples differ in polarity, the EX-OR gate output is "1." When the samples are the same, the EX-OR gate output is "0." Two counters (HP5302A) are enabled by a binary switch and two AND gates (7408). One of the counters counts the number of errors (corresponding to the EX-OR gate "1" output). The other counter counts the total number of data bits transmitted. BER is the ratio of the two counts.
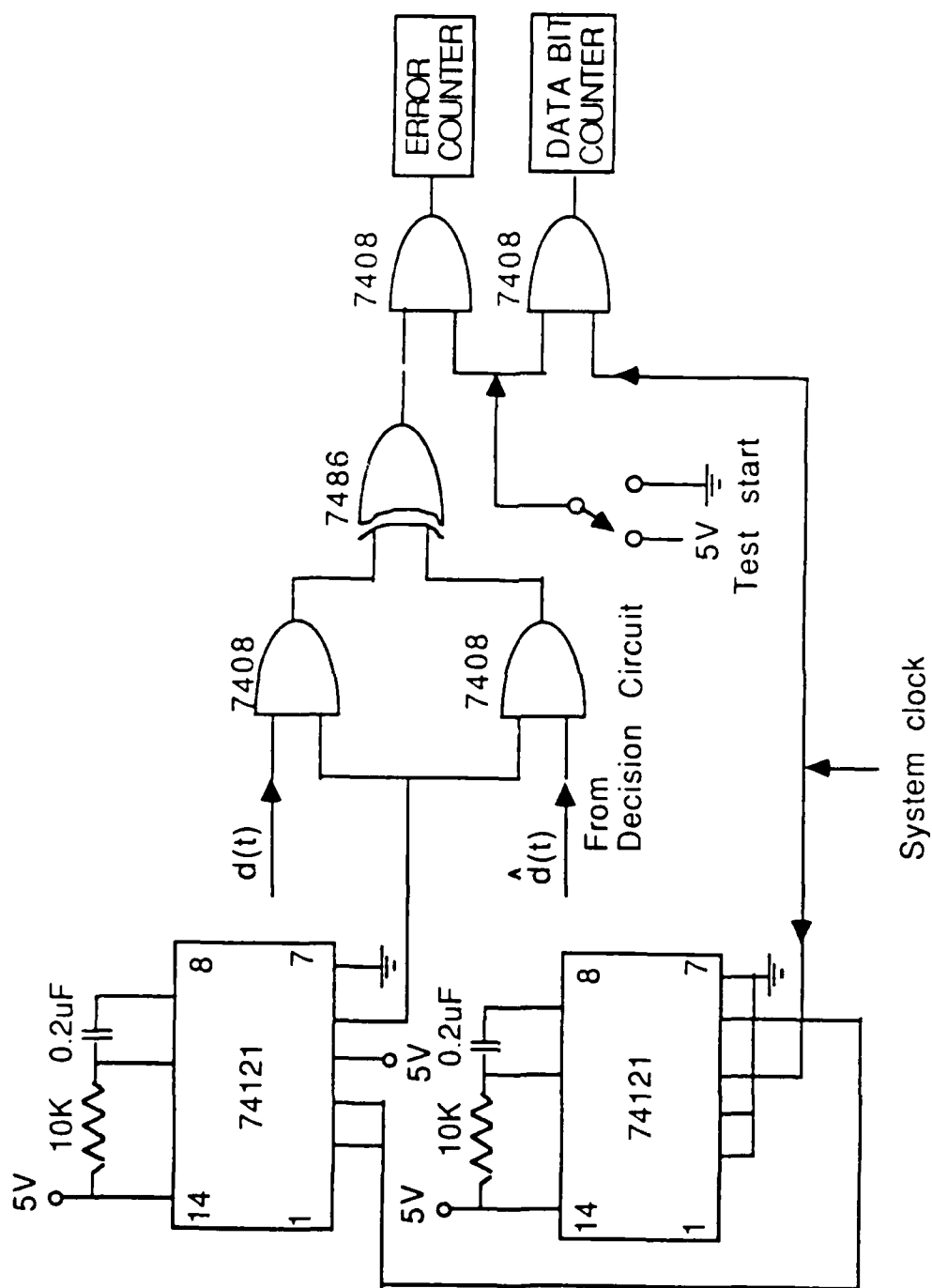
Figure IB 8

Schematic of the Error Detection Circuit

PART 2
I. INTRODUCTION AND BACKGROUND

This research considers a visual indication of the quality of quadrature phase shift keyed (QPSK) signals. QPSK is a popular form of digital data transmission in which two bits are sent simultaneously. This doubles the rate at which bits are transmitted without increasing the switching rate (bandwidth) of the carrier.

In a QPSK receiver, there are two independent channels, in-phase I and quadrature Q. Applying the demodulated I-channel and Q-channel voltages on an x-y oscilloscope creates a two-dimensional signal space. This signal space diagram reveals the transitions between the four possible symbols transmitted and gives valuable information about the quality (probability of error, input signal-to-noise ratio, multipath fading, carrier phase, etc.) of the received QPSK signal. In this research, QPSK receiver performance is assessed by observing (photographing) the x-y oscilloscope display for various values of input SNR, channel mismatch, and multipath fading, respectively. Experimental results show that the oscilloscope display gives a useful indication of the quality of received QPSK signals and can be used to diagnose system operation.

Chapter II presents the motivation for this research and discusses research objectives in detail. The experimental system, test procedures, and results are presented in Chapter III. Chapter IV contains conclusions and recommendations. The experimental system circuit schematics are shown in Appendix 2.

84

II. DESCRIPTION OF THE RESEARCH

A. OBJECTIVE

The objective of this research is to observe the demodulated I-channel and Q-channel voltages in a QPSK receiver using an x-y oscilloscope to determine the system performance for various input signal-to-noise ratios (SNR) under the following conditions:

1. Additive Gaussian noise (AGN) environment

2. Significant intersymbol interference (ISI) caused by channel and data rate mismatch

3. Multipath fading

Single sample decision (lowpass filtering) is used to process the coherently demodulated I-channel and Q-channel voltages, which are then applied to the x and y parts of an oscilloscope to create a two-dimensional display (signal space diagram or constellation diagram). From this display, any impairments (channel, ISI, multipath fading, carrier phase, etc.) can be diagnosed.

B. SYSTEM DISCUSSION

A QPSK transmitter and receiver was designed, built, and then tested under a variety of conditions. In ordinary QPSK systems, the modulated signal has four distinct phase states. These states are generated by a unique mapping scheme of consecutive pairs of bits into symbols, as shown in Figure 2.1. The corresponding phase states are maintained during the symbol interval T_s. This interval has a two-bit duration (i.e., $T_s = 2T$ where T is the bit interval). The four possible symbols

85

are frequently assigned using a Gray code (i.e., adjacent symbols differ by only one bit), as shown in Figure 2.1.
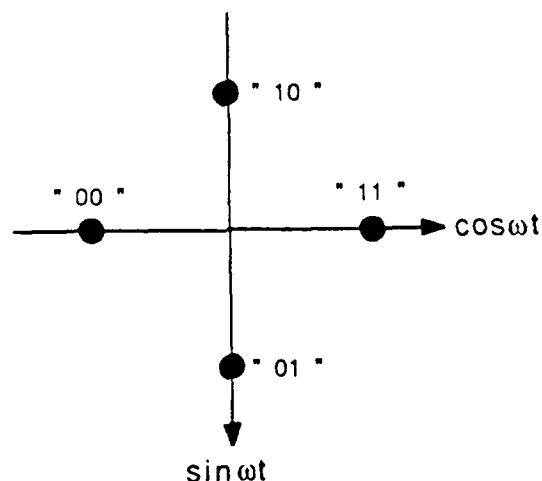

Figure 2.1

Constellation Diagram for Received QPSK Signals

The four Gray coded signalling states may be described as follows:

$s_{11}(t) = A \cos 2\pi f_0 t$

$s_{01}(t) = A \sin 2\pi f_0 t$

$s_{00}(t) = -A \cos 2\pi f_0 t$

$s_{10}(t) = -A \sin 2\pi f_0 t$ (2.1)

In these equations, the subscript represents the bit pairs.

A block diagram of a typical QPSK transmitter is shown in Figure 2.2. Two separate data streams, $d_1(t)$ and $d_2(t)$, control the selective inputs of an analog multiplexer (MC 14051B). Four distinct phase carriers (stated in equation 2.1) are inputs to the analog multiplexer.

86
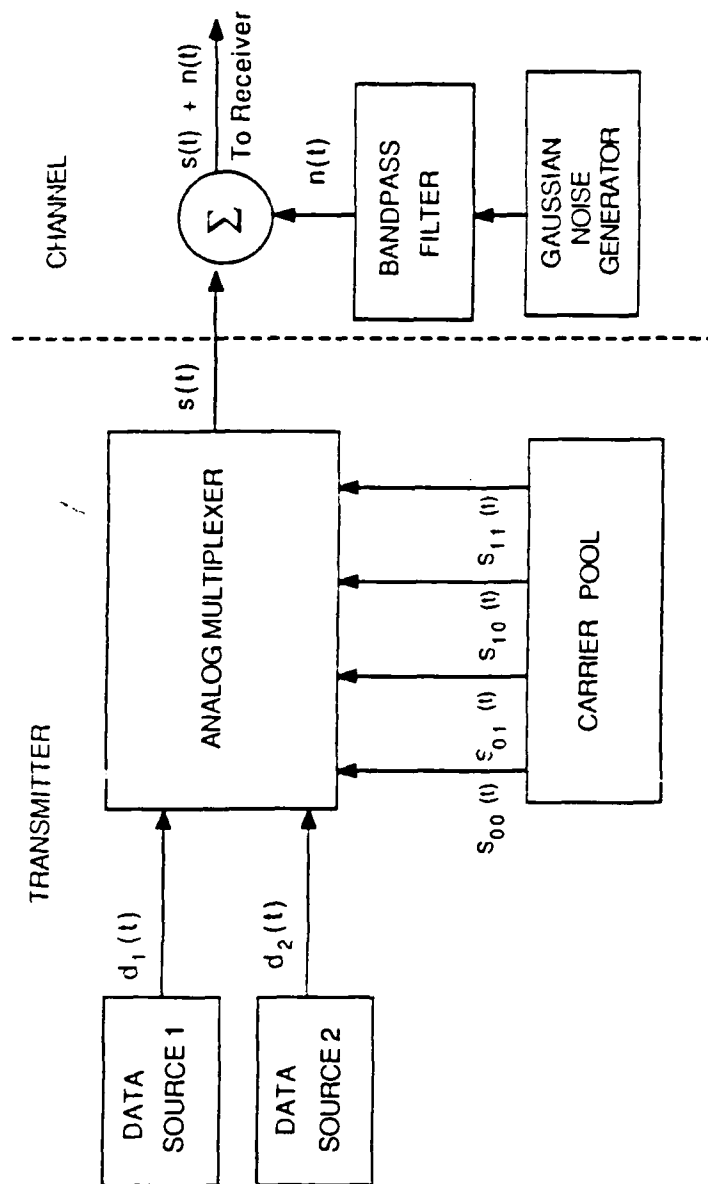
Figure 2.2

Block Diagram of the 9PSK Transmitter and Channel

The multiplexer transmits one of the carriers, depending on the selective input values (i.e., "00," "10," "11," "01"). The result is QPSK transmission of the digital data. Data streams $d_1(t)$ and $d_2(t)$ may be from two independent sources or from a single bit stream.

The QPSK signal s(t) at the multiplexer output is normally filtered to limit the radiated spectrum, and amplified and transmitted over the channel. Noise n(t) is added to the signal s(t) prior to demodulation in the receiver. We can consider the receiver input as s(t) + n(t). The model of this additive noise is also shown in Figure 2.2.

The two–channel receiver shown in Figure 2.3 is able to demodulate the received QPSK signals. The orthogonal channels recover the transmitted data $d_1(t)$ and $d_2(t)$ independently of each other. The I-channel and Q-channel demodulator outputs can be processed by either using integrate and dump circuit (optimum post–detection system) or using lowpass filters (single sample decision detection system). In this project, lowpass filters are used to recover the transmitted data.

C. CONSTELLATION DIAGRAMS

In the absence of system impairments (additive noise, channel mismatch, multipath fading, etc.), the constellation of the received phase modulated signals consists of four well–defined points (see Figure 2.1) and no data errors will occur. Figure 2.1 is an ideal display for the received QPSK signals.
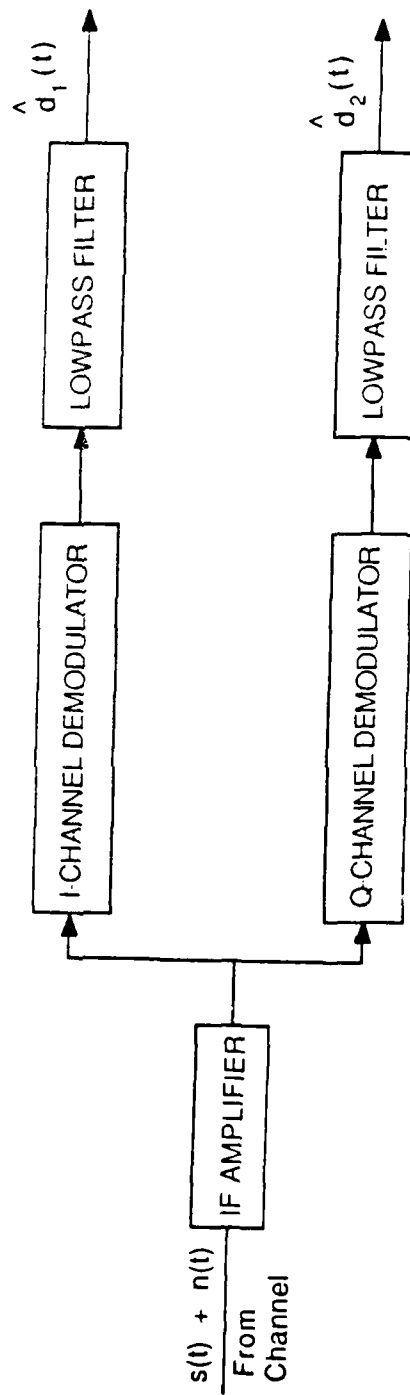
88

Figure 2.3

Block Diagram of a QPSK Receiver

89

In a practical system, various impairments may exist which can result in data errors. Therefore, the actual signal space diagram differs from the ideal case due to the following impairments.

1. Attenuation and Delay Distortion. This is caused by the non-ideal frequency response of cabling, filters, and equalizers in the circuit. The adaptive equalizer in the modem will remove these distortions, so they do not normally affect the constellations.

2. Signal-to-Noise Ratio. Noise can be received from background sources, crosstalk from other circuits, or quantization effects arise from circuit amplifiers, etc. Noise causes the received constellation points to become clouds rather than well-defined points (see Figure 2.4).
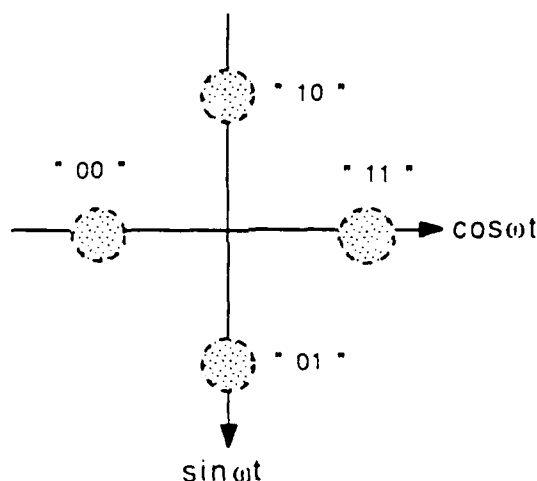
Figure 2.4

Noise Effects on the Constellation Diagram
of the Received QPSK Signals

3. Frequency Offset. An offset between the transmitter carrier frequency and the receiver carrier frequency may exist because of Doppler. This can be removed by a phase-locked loop in the

90

receiver, and so will not be observed on the received constellation [Ref. 9].

4. Phase Jitter. Phase jitter is the variation in the phase of the received carrier due to AM to PM conversion effects of amplifiers and filters.

5. Gain Hits. These are sudden changes in signal power and may be caused by switching to standby facilities or carrier supplies. Fading or route changes in microwave facilities may also cause gain hits. The gain may return its original level in a short time or remain at the new level.

6. Multipath in the Communication Link. Multipath fading can affect the constellation diagram significantly. This effect appears as the rotation of the constellation diagram axes (x–y axes). Figure 2.5 shows the multipath effects on the constellation diagram of received QPSK signals.

"10"

"00"

cos ωt

"11'

"01"

sin ωt
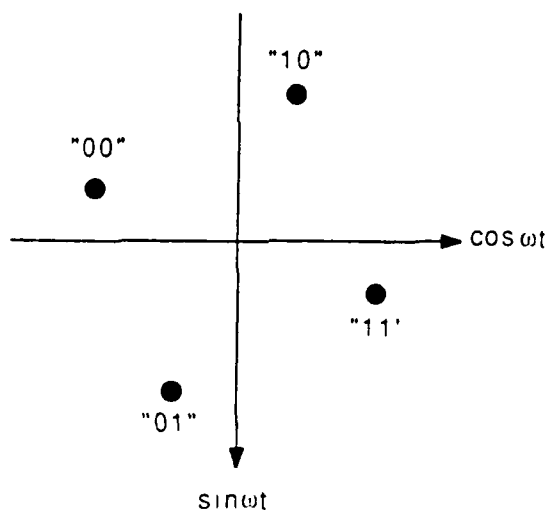
Figure 2.5

Multipath Fading Effects on the Constellation Diagram
of the Received QPSK Signals

7. Channel Data Rate Mismatch. Channel and data rate mismatch occurs when the data rate is increased for a fixed IF bandwidth. This appears as intersymbol interference in the receiver.

91

For simplicity, in this project only the following impairments are considered.

1. Additive Gaussian noise

2. Channel mismatch due to a large value of data rate

3. Multipath fading in the communications link.

Each case is considered individually. The corresponding constellation diagrams are observed and the receiver performance is evaluated. A detailed discussion of these phenomena follows.

1. <u>Additive Gaussian Noise Effects on the Signal Space Diagram</u>

The presence of additive Gaussian noise causes the received constellation points to become clouds rather than well–defined points, and the transition lines between any pair of symbols is not a straight line. Assuming $s_{11}(t)$ is sent, then the received signal $s_r(t)$ is

$$s_r(t) = s_{11}(t) + n(t)$$

where we assign

$$s_{11}(t) = A \cos 2\pi f_0 t$$

and using the noise model of Rice [Ref. 3:pp. 46–157],

$$n(t) = x(t) \cos 2\pi f_0 t - y(t) \sin 2\pi f_0 t$$

where $x(t)$ and $y(t)$ are uncorrelated lowpass noise voltages. Therefore,

92

$$s_r(t) = [A + x(t)] \cos 2\pi f_0 t - y(t) \sin 2\pi f_0 t \qquad (2.2)$$

After demodulation and lowpass filtering, the I–channel and Q–channel output voltages are

$$v_I = \text{lowpass part of } \Big[[(A + x(t)) \cos \omega_0 t - y(t) \sin \omega_0 t] \cos \omega_0 t\Big]$$

$$= \frac{A + x(t)}{2} \text{ volts} \qquad (2.3)$$

$$v_Q = \text{lowpass part of } \Big[[(A + x(t)) \cos \omega_0 t - y(t) \sin \omega_0 t] \sin \omega_0 t\Big]$$

$$= -\frac{y(t)}{2} \text{ volts} \qquad (2.4)$$

Note that, in the absence of noise, the I–channel and Q–channel output voltages are

$$v_I = \frac{A}{2} \text{ volts} = \text{constant}$$

$$v_Q = 0 \text{ volts} \qquad (2.5)$$

These I–channel and Q–channel voltages are the coordinates of the symbol point on the two–dimensional constellation of Figure 2.1. From equation 2.4, in the presence of noise the coordinates are random. Transition lines between symbols become skewed since the symbol points are not stationary. As the noise power increases, the clouds around the symbol points become larger. This is a condition associated with errors in the receiver. A simulation of this problem on

the computer (Hewlett-Packard I-Q tutor program) is shown in Figure 2.6.
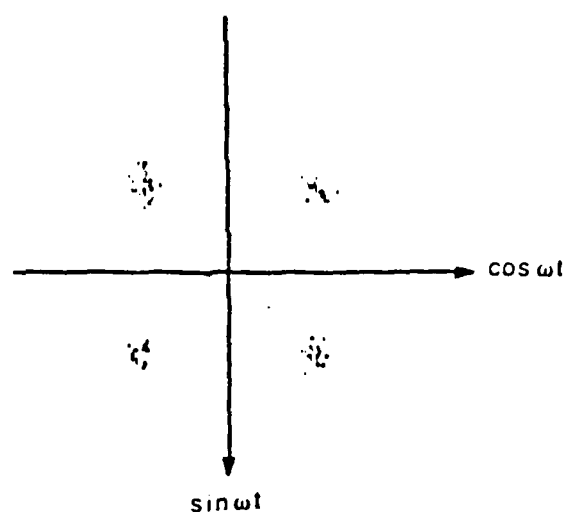
Figure 2.6

Noise Effects of the Constellation Diagram

2. <u>Effect of Channel Mismatch Due to Improper Data Rates on the Constellation Diagram</u>

In digital communications, for a fixed IF bandwidth, increasing the data rate eventually results in distortion. The demodulated pulses lose their rectangular shape and are stretched in width. So, pulses corresponding to any one bit will smear into adjacent bit intervals. This condition may cause errors in the recovered bits. This effect of improper filtering causing bit errors is called intersymbol interference (ISI) [Ref. 2:p. 164]. A simulation of this phenomenon using a digital computer is shown in Figure 2.7.

94
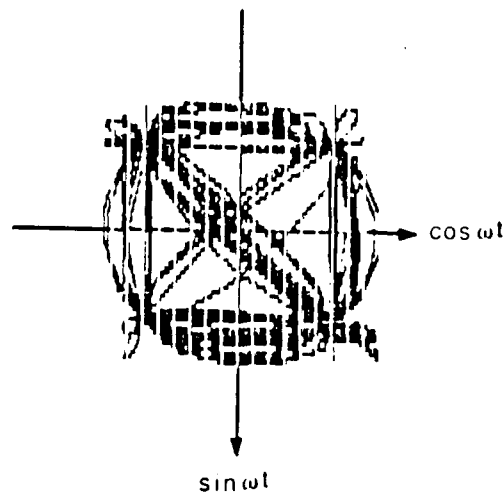
Figure 2.7

Channel Mismatch on the Constellation Diagram

3. Multipath Effects on the Signal Space Diagram

Multipath fading results from two or more of the same trans-
mitted signals reaching the receiver after traveling different paths.
This may result from the signal reflection or from the signal bending
through the atmosphere due to Fresnel Refraction. The resulting sig-
nal consists of the sum of all these signals, each having different prop-
agation delay. Figure 2.8 shows a simple model for multipath propa-
gation. The delay means that the phase and data information of the
reflected signal are different from the primary path signal. This leads
to intersymbol interference (ISI) and increased errors in the received
signal. A more subtle consequence occurs when a reflected signal is
phase shifted 180 degrees with respect to the primary path signal.
This results in a cancellation or nulling of the received signal.
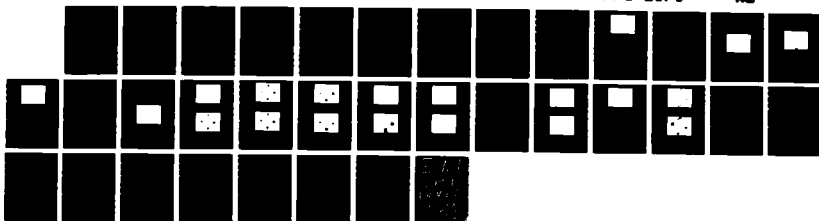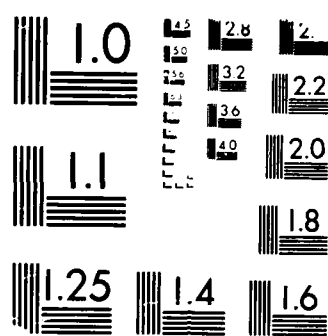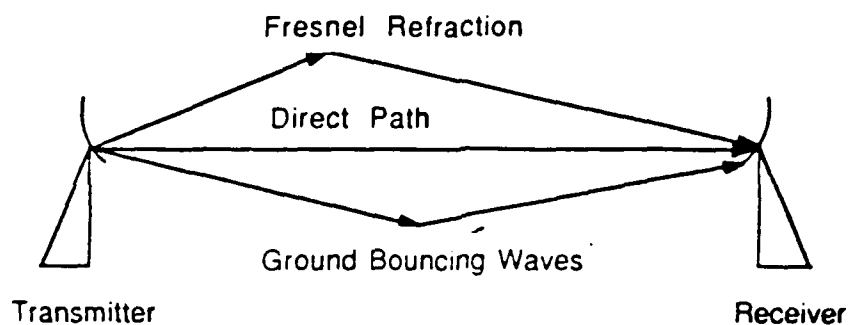
MICROCOPY RESOLUTION TEST CHART

Figure 2.8

A Simple Multipath Model

Consider the case of a single reflection (or refraction) without attenuation. Then the received signal in the absence of noise is taken here to be

$$s_r(t) = A \cos 2\pi f_0 t + A \cos 2\pi f_0(t + \tau) \tag{2.6}$$

When $s_{11}(t)$ is sent, then the demodulated and lowpass filtered I-channel and Q-channel voltages become

$$v_I = \text{lowpass part of } [(A \cos 2\pi f_0 t + A \cos 2\pi f_0(t + \tau)) \cos 2\pi f_0 t]$$

$$= \frac{1}{2} (A + A \cos 2\pi f_0 \tau) \text{ volts} \tag{2.7}$$

$$v_Q = \text{lowpass part of } [(A \cos 2\pi f_0 t + A \cos 2\pi f_0(t + \tau)) \sin 2\pi f_0 t]$$

$$= -\frac{1}{2} (A \sin 2\pi f_0 \tau)$$

These values are the coordinates of the symbol "11" on the signal diagram. In polar form, these coordinates are at an angle θ where

$$\theta = \arctan\left(-\frac{\sin 2\pi f_0 \tau}{1 + \cos 2\pi f_0 \tau}\right) \text{ in degrees} \tag{2.8}$$

and have length L where

$$L = \sqrt{v_I^2 + v_Q^2}$$

$$= \sqrt{\frac{A^2}{4}(1 + \cos 2\pi f_0 \tau)^2 + \frac{A^2}{4}\sin^2 2\pi f_0 \tau}$$

$$= \frac{A}{2}\sqrt{1 + 2\cos 2\pi f_0 \tau} \tag{2.9}$$

So, the effect of multipath is to move the points off the axes, as shown in Figure 2.5.

III. **EXPERIMENTAL SYSTEM**

In this project, a QPSK transmitter and receiver were designed, built, and then tested for various values of input SNR. A block diagram of the transmitter is shown in Figure 2.9. Digital data $d_1(t)$ and $d_2(t)$ are generated by two feedback shift registers (FSR). These data control the selective inputs of an analog multiplexer (MC 14051B). The multiplexer selects one of the distinct phase carrier signals which are connected to the input terminals. A carrier pool which consists of several phase shifters and inverting amplifiers provides the four distinct phase carriers. Gaussian noise is added to the signal in the system channel, as shown in Figure 2.9. The noise is band-limited to simulate the amount of noise which would be passed through the tuned IF amplifier of a superheterodyne receiver. Thus, the signal plus noise, $s(t) + n(t)$, is the input to the receiver. A block diagram of the receiver is shown in Figure 2.10. Two analog voltage multipliers (AVM AD534) demodulate the I-channel and Q-channel of the received QPSK carrier. Demodulated I-channel and Q-channel voltages are lowpass filtered to remove the carrier harmonics and the high-frequency noise. Finally, the lowpass filter outputs, which represent the recovered data $\hat{d}_1(t)$ and $\hat{d}_2(t)$, are applied to the x- and y-channel inputs of an oscilloscope. This creates the constellation diagram on the oscilloscope screen. The experimental system is discussed in detail in the following sections.
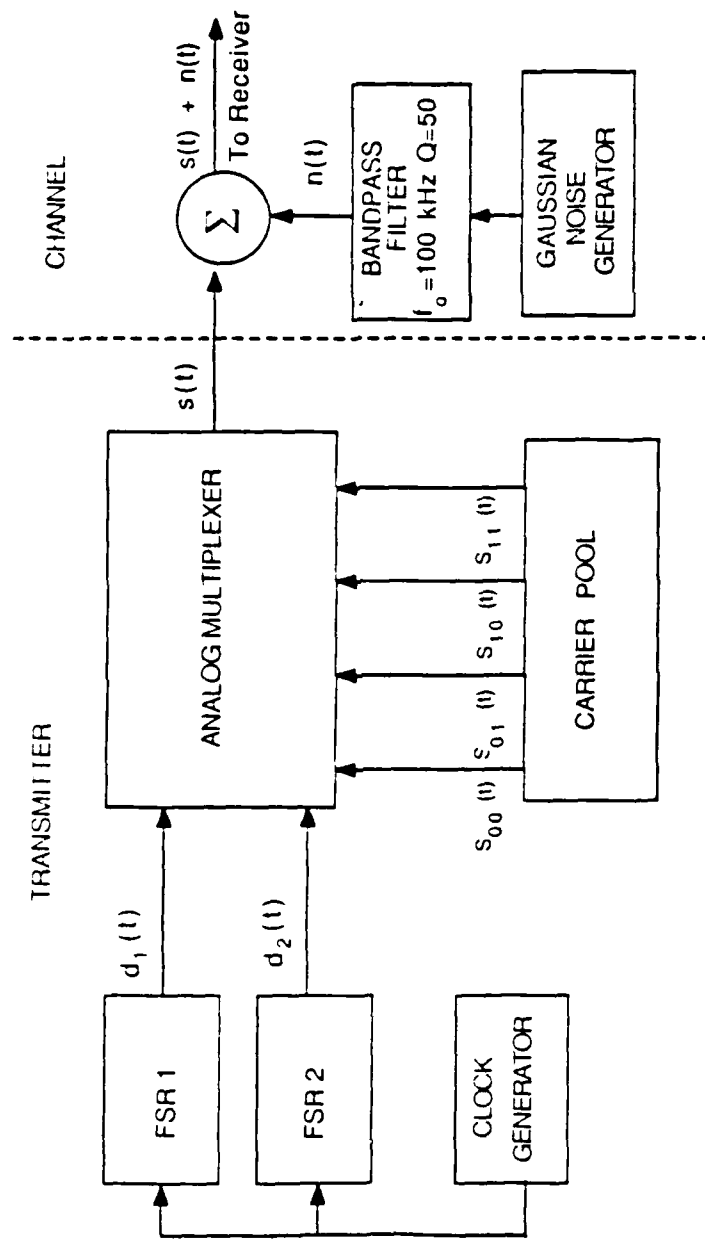
98

Figure 2.9

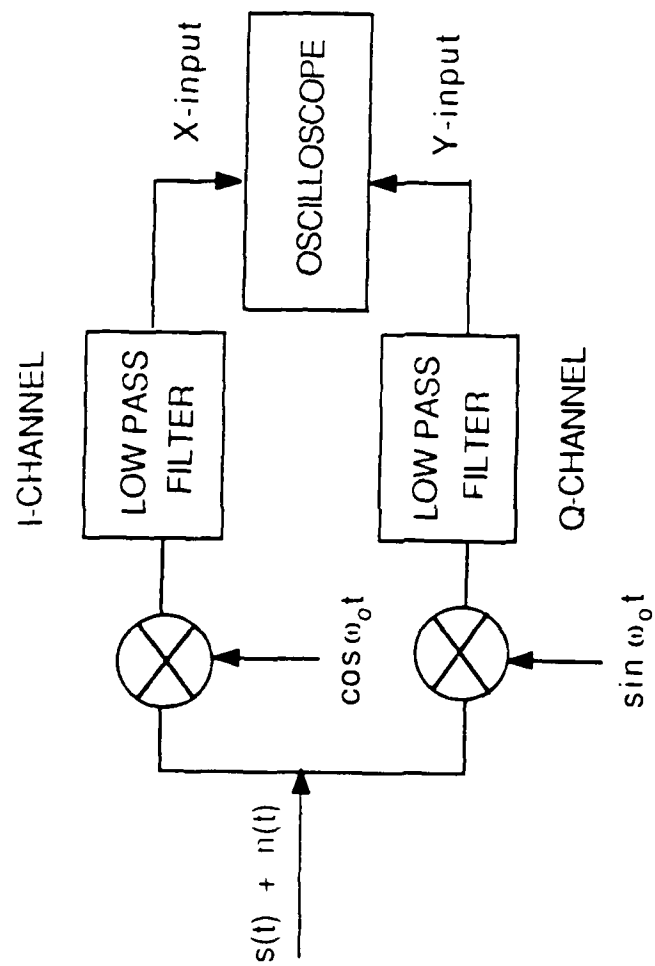Block Diagram of the Experimental QPSK Transmitter and Channel

99

Figure 2.10

Block Diagram of the QPSK Receiver

A. SUBSYSTEMS

1. Feedback Shift Registers

A detailed discussion of the feedback shift registers is given in part 1, Chapter III of this report. For this experiment, two different FSR connections, (7,3) and (7,2), are used to simulate the random data. The FSRs are clocked by a WAVETEK (model 142A) signal generator at a rate of 1 kHz. Since the transmitter transmits two data bits at a time, the effective transmitted data rate is 2 kHz. The two FSR outputs, $d_1(t)$ and $d_2(t)$ are applied to the selective input terminals of an analog multiplexer.

2. Carrier Pool

The QPSK transmitter transmits one of four distinct carriers at any time. A carrier pool, shown in Figure 2.11, generates the carriers. The key element of this carrier pool is a high-frequency, multiple feedback, bandpass phase shifter. This phase shifter is constructed using high-speed operational amplifiers (LF356). The input to the phase shifter is a sinusoid of frequency equal to 100 kHz. This signal is provided by a WAVETEK (model 142A) signal generator. The phase shifter shifts the phase of the input signal approximately 90°, and so the output is a 100 kHz cosine wave. The remaining phase-modulated carriers, $-\sin\omega_0 t$ and $-\cos\omega_0 t$, are obtained using two high-speed inverting operational amplifiers. The four phase-modulated carriers are connected to the input terminals of an analog multiplexer (MC 14051B). Use of the multiplexer as a carrier modulator is convenient in the laboratory.
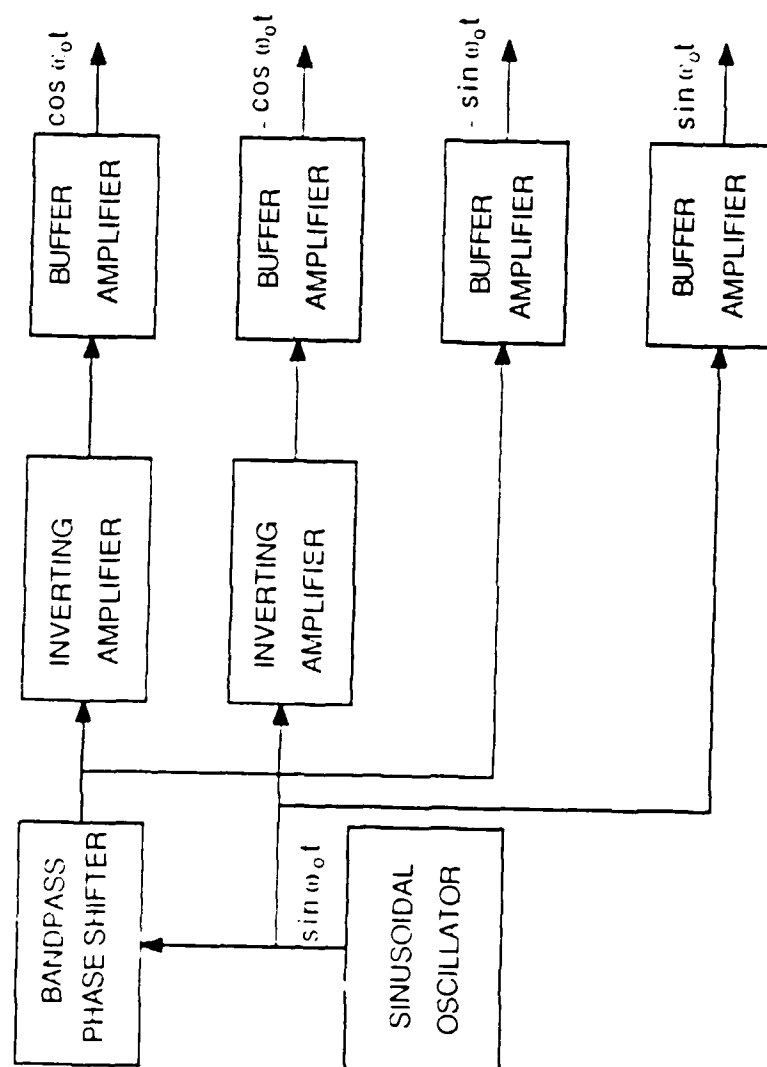
101

Figure 2.11

Block Diagram of the Carrier Pool

3. Multiplexer

An analog multiplexer (MC 14051B) is used to select the appropriate carrier. The multiplexer selective inputs (1, 2) are controlled by the input data. $d_1(t)$ and $d_2(t)$, respectively. Depending on the voltage of the selective inputs, the multiplexer selects one of the four sinusoids for transmission. At a 1 kHz switching rate, the multiplexer transmits the signals with no discernible time delay or distortion. Figure 2.12 is the schematic of the multiplexer, and Figure 2.13 shows the multiplexer output for a 1 kHz switching rate. The four outputs are equal-amplitude sinusoids as desired.

selective in 1
From FSR 1

selective in 2
From FSR 2

ANALOG MULTIPLEXER

MC 14051B

$s(t)$

To Channel

$\cos \omega_0 t$ $-\cos \omega_0 t$ $\sin \omega_0 t$ $-\sin \omega_0 t$
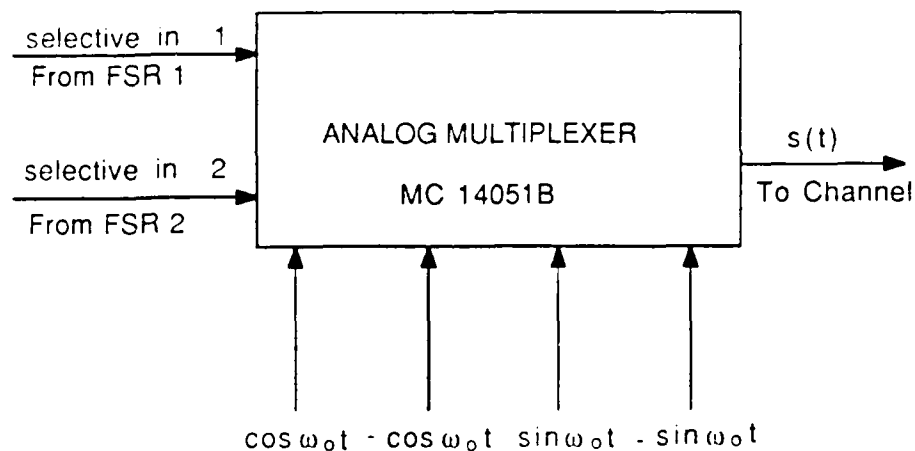
Figure 2.12

Schematics of the Multiplexer

4. Channel

The system channel model is shown in Figure 2.9. Gaussian noise is added to the transmitted signal in the transmission channel so that the receiver input is the sum $s(t) + n(t)$.
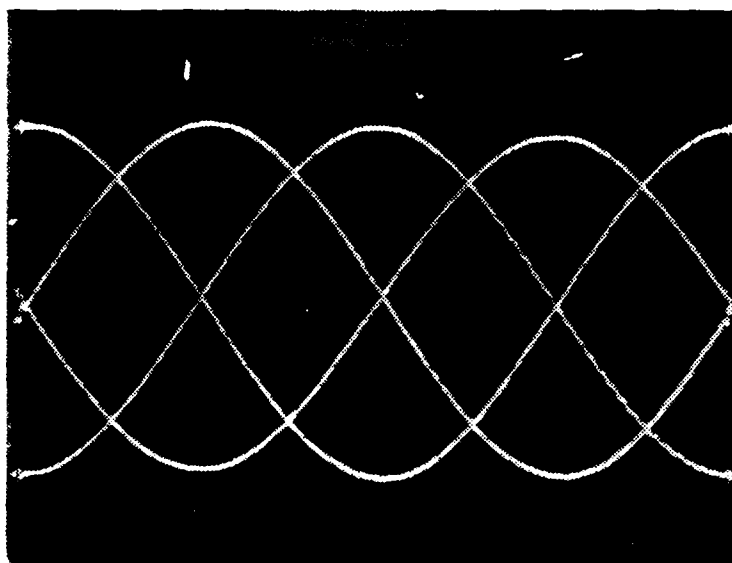
103

Figure 2.13
An Example of Multiplexer Output
at a Rate of 1 kHz Carrier Switching

The channel used in the first part of this thesis (BPSK channel) is used for this QPSK system also. This is achieved by adjusting the data rate appropriately. In this case, the data rate is 2 kbps and the carrier frequency is 100 kHz, so that the resulting QPSK bandwidth is ± 1 kHz centered at 100 kHz. The required RF bandwidth is half of the data rate for QPSK modulation. Therefore, a bandpass filter used in the first part of this thesis (centered at 100 kHz with 2 kHz 3 dB bandwidth) is used to simulate the actual IF amplifier of a QPSK system. A detailed discussion of the BPF is presented in Part 1, Chapter III of this thesis.

5. **Demodulators and Lowpass Filters**

Figure 2.14 shows the block diagram of the I-channel and Q-channel demodulators. Analog voltage multipliers (AVM–AD534) are

104
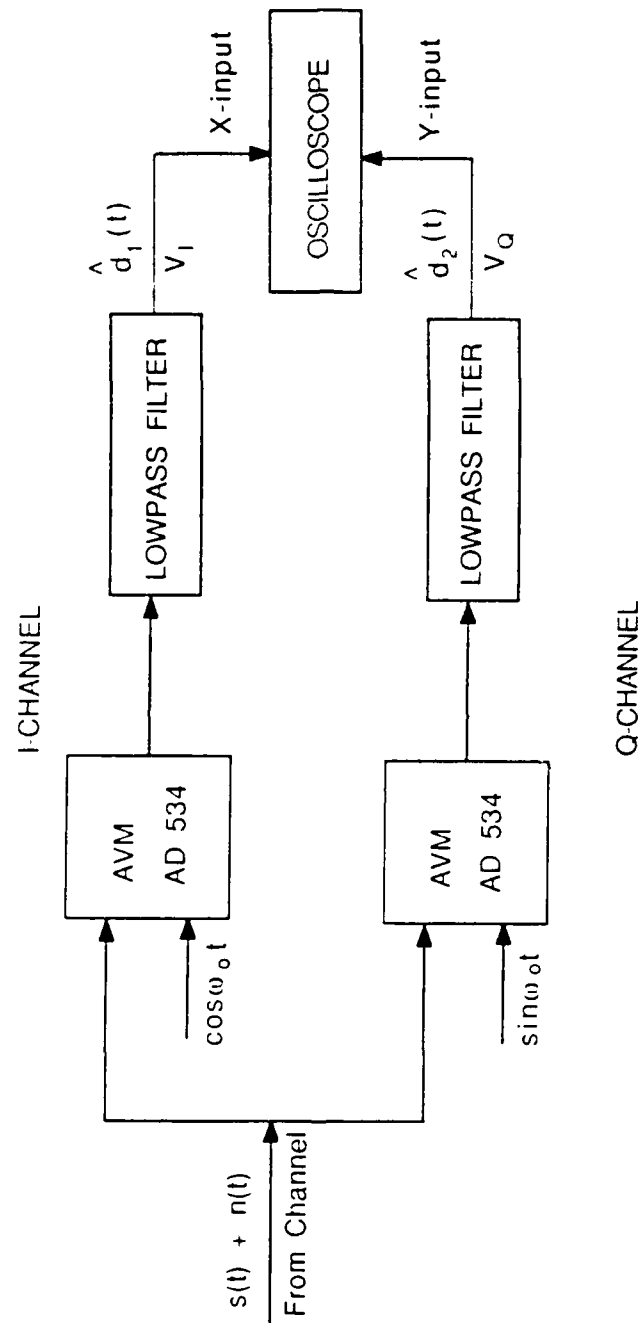
Figure 2.14

Block Diagram of the Experimental I-Channel and Q-Channel Demodulators

used to construct the demodulators. Signal plus noise is multiplied by a coherent cosine wave and a coherent sine wave in the I-channel and Q-channel demodulators, respectively. The result is rectification of the signals. Figure 2.15 shows the I-channel and Q-channel demodulator outputs, respectively. Shown in Figure 2.15 are the positively and negatively rectified waveforms and the sum frequency created as the product of coherent sinusoids.
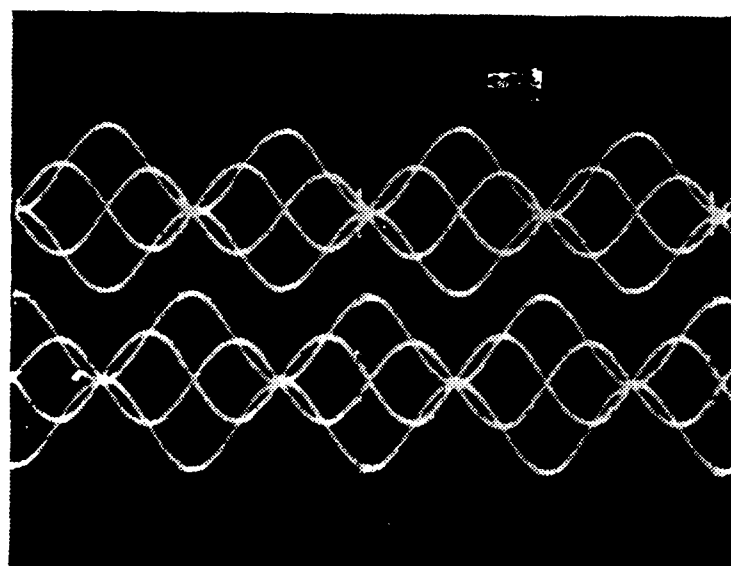
Figure 2.15
Photograph of the I–Channel and
Q–Channel Demodulator Outputs
(Top: I-channel; Bottom: Q-channel)

Lowpass filters are used to recover the transmitted data. For this experiment, two KHRONITE (model 3202A) lowpass filters are used. The performance of this receiver is 3 dB worse than a receiver using optimum detection technique (integrate and dump) [Ref. 2:pp.

180-187]. Figure 2.16 shows the lowpass filter outputs. The polar waveforms $\hat{d}_1(t)$ and $\hat{d}_2(t)$ are applied to the x and y channels of an oscilloscope (COS 6001A). This creates on the oscilloscope screen the constellation diagram. The result is shown in Figure 2.17 when there are no system impairments.
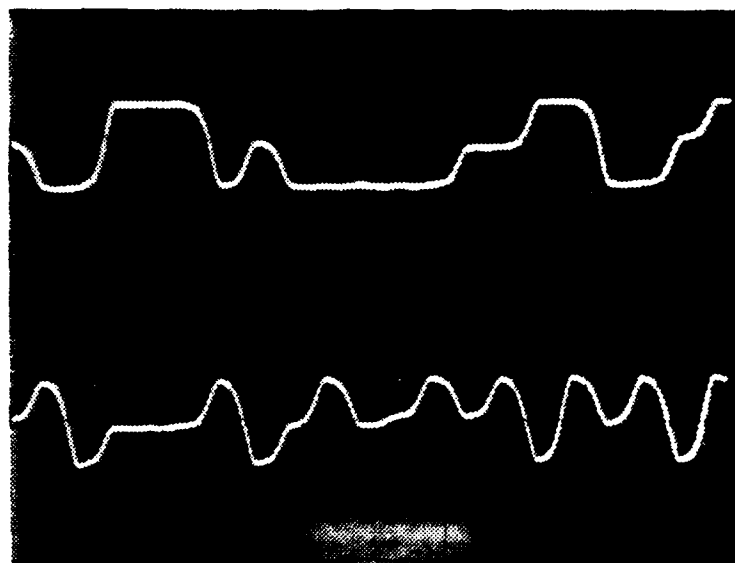

Figure 2.16
Photographs of the Lowpass Filter Outputs
(Top: I-channel; Bottom: Q-channel)

6. Multipath Simulator

A delay line is designed to simulate multipath effects of a transmission channel. The model for multipath simulation is shown in Figure 2.18. Basically, a direct path and a delayed path signal are added in an analog summer prior to demodulation. The resulting signal is demodulated and lowpass filtered by I-channel and Q-channel circuitry. The delay line is constructed using high-speed operational
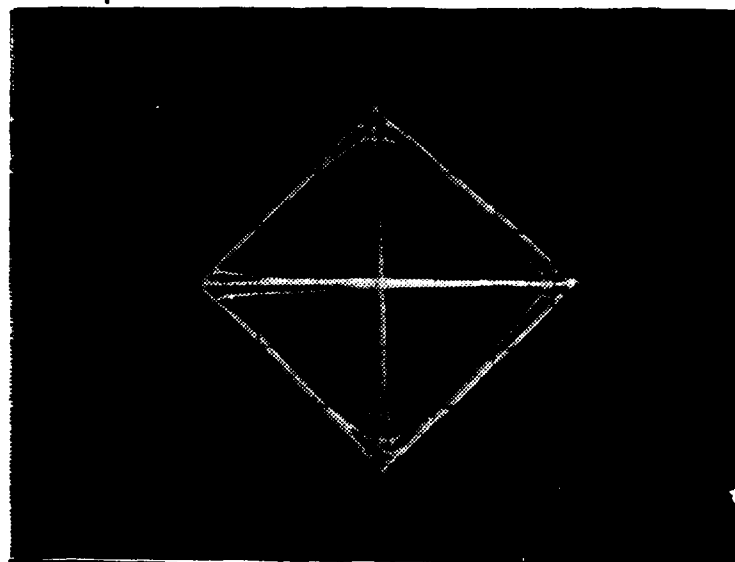
107

Figure 2.17
Photograph of the Constellation Diagram for QPSK Signals
(SNR = ∞, symbol rate = 1000 symbols/sec,
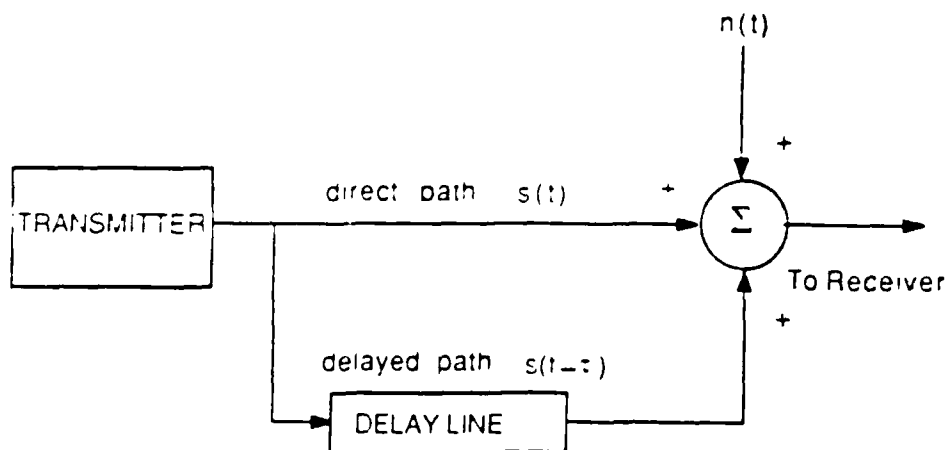LPF cut-off frequency = 1100 Hz)

Figure 2.18
Multipath Simulator Model

amplifiers (LF 356) configured as a multiple feedback bandpass phase shifter and is capable of producing time delays up to 2.5 microseconds. The bandpass section ensures that the output signal of the delay line is a 100 kHz sinusoid.

B. TEST PROCEDURES AND RESULTS

After initial applications of the supply voltages to the system, synchronization of the transmitter and receiver must be ensured. Since the experimental system does not include the carrier and clock recovery circuits, synchronization of the transmitter and receiver is provided via hard wire from the transmitter. Feedback shift registers are reset to "all zero" state and data streams $d_1(t)$ and $d_2(t)$ drive the multiplexer selective inputs.

The experimental system data rate is set to 2000 bps (1000 bps for each channel). To recover the transmitted data from the demodulated signals, the lowpass filter cutoff frequencies are set to 1100 Hz.

For this experiment, a 1 volt RMS sinusoidal carrier is used. Therefore, signal power at the IF output is (1 V RMS)^2 = 1 watt relative to 1 ohm load. The desired signal-to-noise ratio (SNR) is obtained by appropriately changing the noise power out of the noise generator. Constellation diagrams were obtained for the following effects for various values of SNR at the input to the demodulator.

1. Gaussian noise effects;

2. Channel mismatch effects due to improper data rate;

3. Multipath fading effects.

1. Gaussian Noise Effects on the Constellation Diagram (experimental results)

In the absence of any impairments, the constellation diagram for QPSK signals consists of well-defined coordinates as shown in Figure 2.17. The transitions between symbols are straight lines. As stated in Chapter II, the presence of noise causes these points to become clouds. This effect is shown in Figure 2.19 and 2.20 for SNR = 15 dB and SNR = 12 dB, respectively. As the noise power increases, the clouds increase in size and the probability of error of the data bits increases. Examples are shown in Figures 2.21 through 2.29.

Figure 2.19

An Example of the Constellation Diagram for
Received QPSK Signals
(When SNR = 15 dB, symbol rate = 1000 symbols/sec,
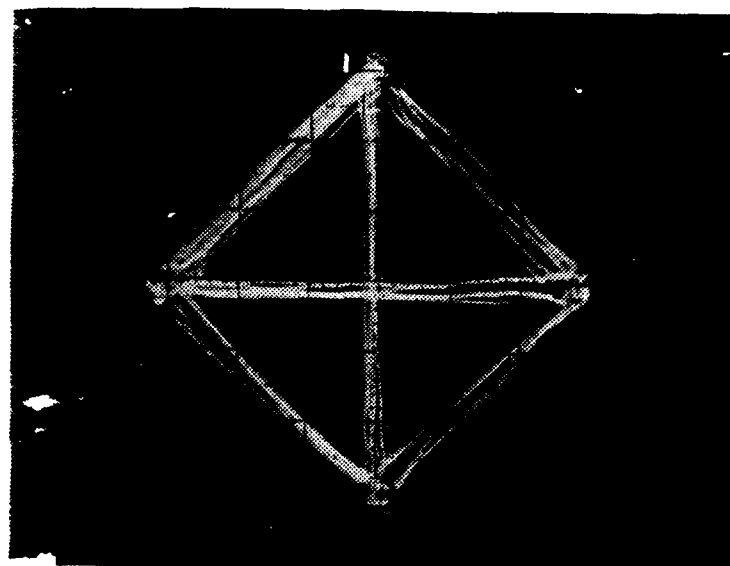LPF cut-off frequency = 1100 Hz)

Figure 2.20

An Example of the Constellation Diagram for
Received QPSK Signals

(When SNR = 12 dB, symbol rate = 1000 symbols/sec,
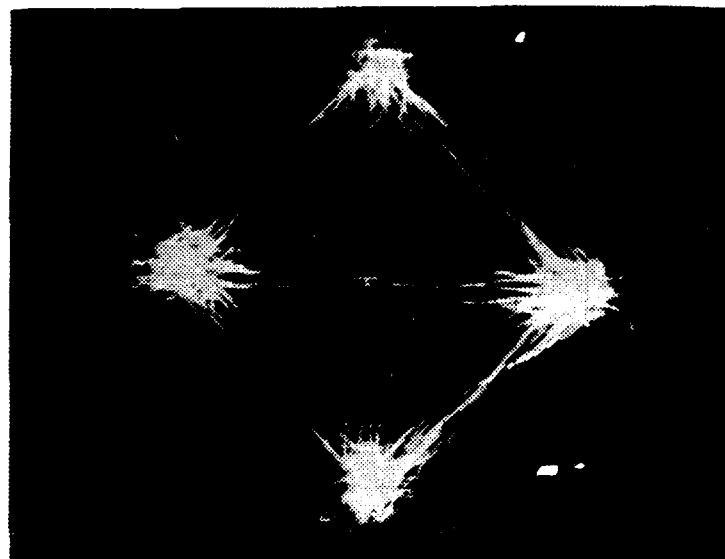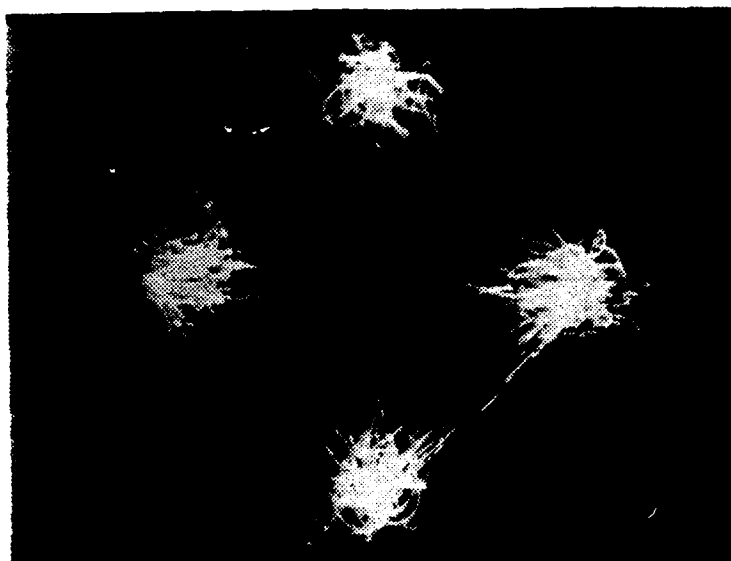LPF cut-off frequency = 1100 Hz)
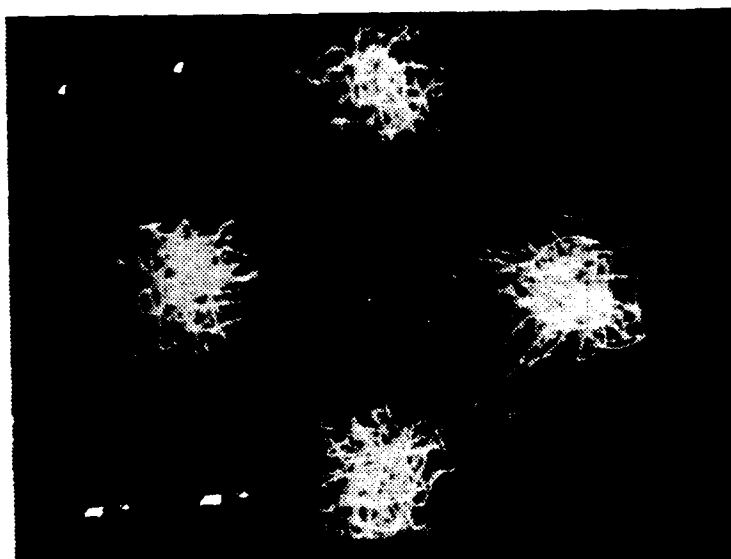

Figure 2.21

An Example of the Constellation Diagram for
Received QPSK Signals

(When SNR = 10 dB, symbol rate = 1000 symbols/sec,
LPF cut-off frequency = 1100 Hz)

111

Figure 2.22

An Example of the Constellation Diagram for
Received QPSK Signals

(When SNR = 9 dB, symbol rate = 1000 symbols/sec,
LPF cut-off frequency = 1100 Hz)

Figure 2.23

An Example of the Constellation Diagram for
Received QPSK Signals

(When SNR = 7 dB, symbol rate = 1000 symbols/sec,
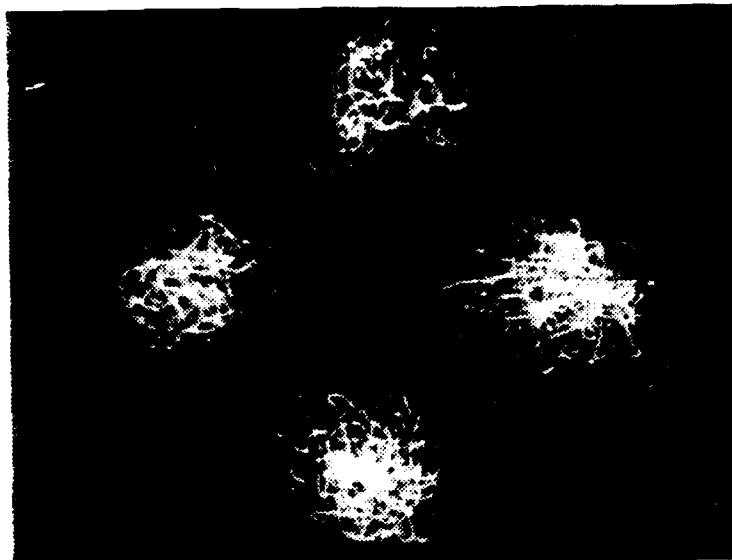LPF cut-off frequency = 1100 Hz)

112

Figure 2.24

An Example of the Constellation Diagram for

Received QPSK Signals

(When SNR = 5.5 dB, symbol rate = 1000 symbols/sec.
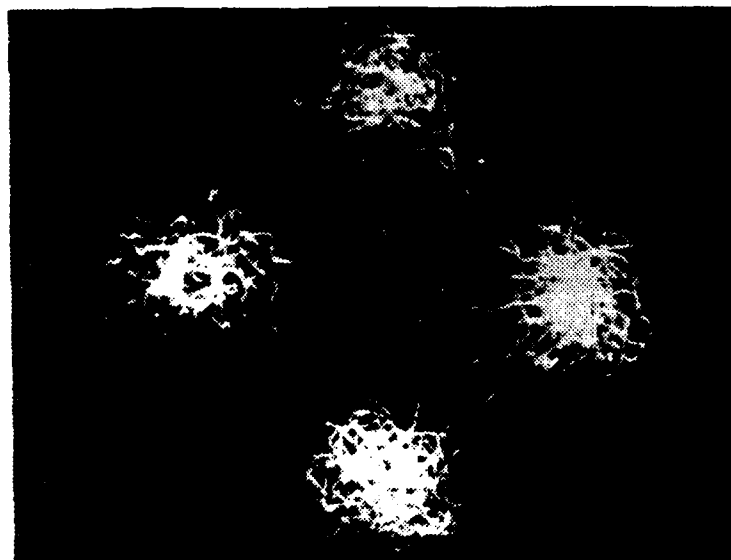LPF cut-off frequency = 1100 Hz)

Figure 2.25

An Example of the Constellation Diagram for

Received QPSK Signals

(When SNR = 4.5 dB, symbol rate = 1000 symbols/sec.
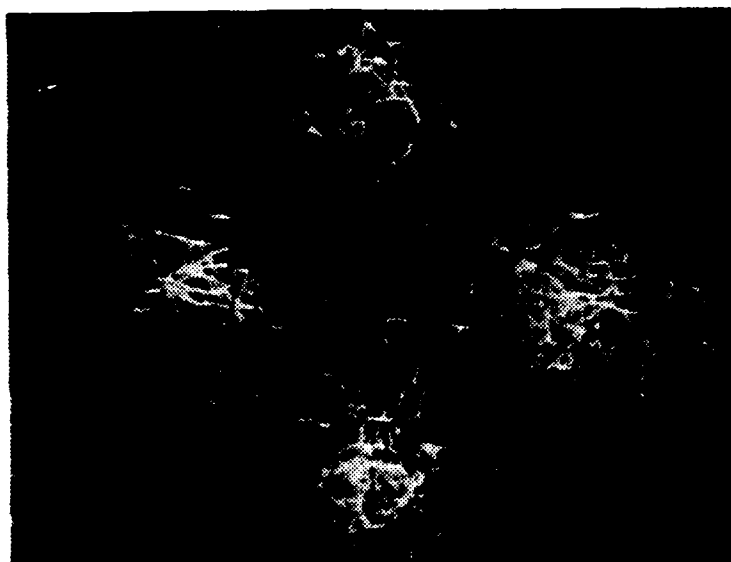LPF cut-off frequency = 1100 Hz)

113

Figure 2.26

An Example of the Constellation Diagram for Received QPSK Signals

(When SNR = 3 dB, symbol rate = 1000 symbols/sec, LPF cut-off frequency = 1100 Hz)

Figure 2.27

An Example of the Constellation Diagram for Received QPSK Signals

(When SNR = 2 dB, symbol rate = 1000 symbols/sec, LPF cut-off frequency = 1100 Hz)

114

Figure 2.28

An Example of the Constellation Diagram for Received QPSK Signals

(When SNR = 1 dB, symbol rate = 1000 symbols/sec, LPF cut-off frequency = 1100 Hz)

Figure 2.29

An Example of the Constellation Diagram for Received QPSK Signals

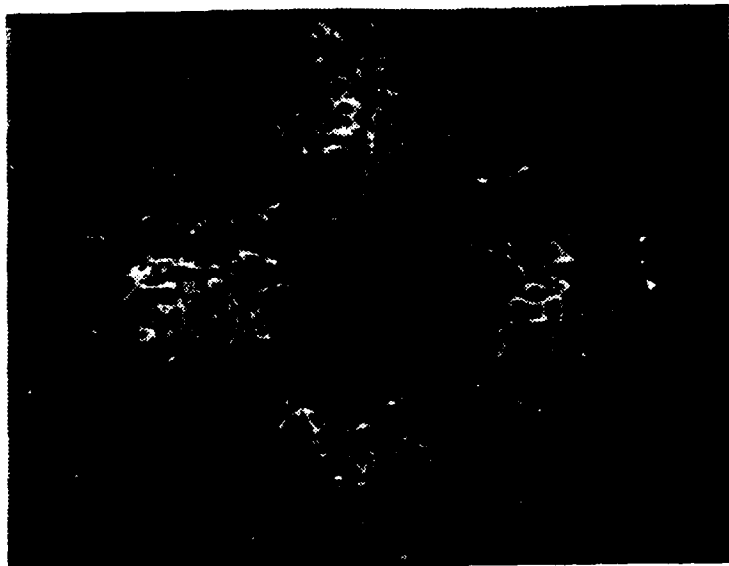(When SNR = 0 dB, symbol rate = 1000 symbols/sec, LPF cut-off frequency = 1100 Hz)

115

2. Channel Mismatch Effects on the Constellation Diagram (due to improper data rate)

As stated in Chapter II, a data rate which is too large for the system causes ISI in the received signals. For QPSK, the RF bandwidth is commonly considered to be half the data rate. For a fixed data rate of 2 kbps, the required RF bandwidth is 2 kHz. This is the matched channel case. Even with a matched channel, a very small amount of ISI occurs, as seen in Figure 2.17. With ISI, transitions on the diagram become curves instead of lines. Channel mismatch degrades system performance because the signal voltage out of the demodulator is reduced. In this experiment, ISI is observed by changing the data rate for fixed IF and lowpass filter bandwidths. Three cases are considered.

a. The Data Rate is 1500 bps

The IF bandwidth = 2 kHz. The LPF cut-off frequency = 1100 Hz. The resulting constellation diagram is shown in Figure 2.30. Little ISI is observed, as expected.

b. The Data Rate is 2500 bps

The IF bandwidth = 2 kHz. The LPF cut-off frequency = 1100 Hz. The resulting constellation diagram is shown in Figure 2.31. This figure clearly shows the ISI.

c. The Data Rate is 3000 bps

The IF bandwidth = 2 kHz. The LPF cut-off frequency = 1100 Hz. The resulting constellation diagram is shown in Figure 2.32.
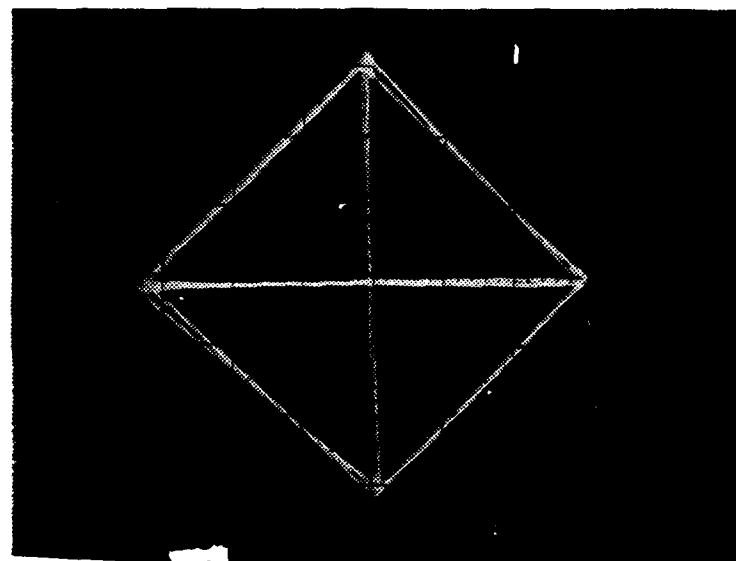
116

Figure 2.30

An Example of the Constellation Diagram for

Received QPSK Signals

(When SNR = ∞, data rate = 1500 bps,
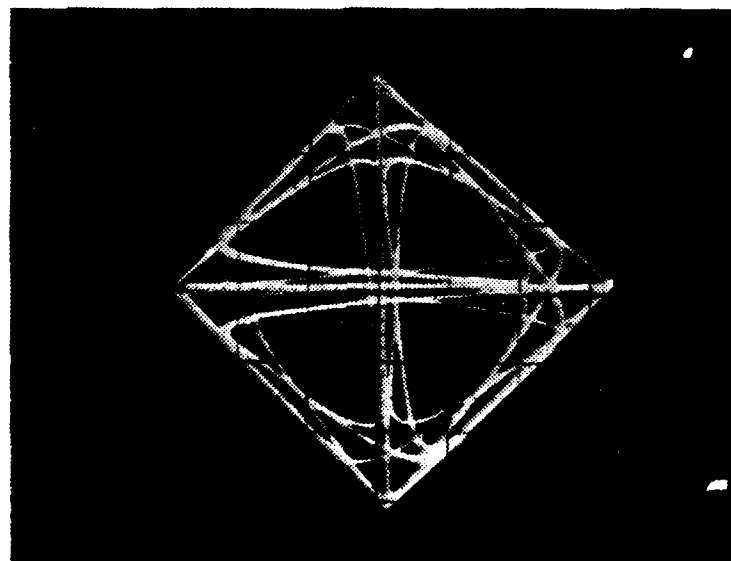IF bandwidth = 2 kHz, LPF cut-off frequency = 1100 Hz)

Figure 2.31

An Example of the Constellation Diagram for

Received QPSK Signals

(When SNR = ∞, data rate = 2500 bps,
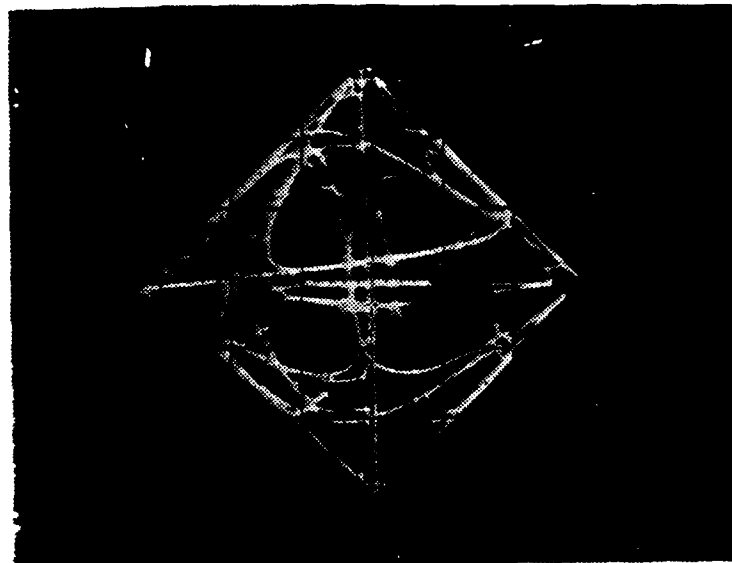IF bandwidth = 2 kHz, LPF cut-off frequency = 1100 Hz)

117

Figure 2.32

An Example of the Constellation Diagram for
Received QPSK Signals
(When SNR = ∞, data rate = 3000 bps,
IF bandwidth = 2 kHz, LPF cut-off frequency = 1100 Hz)

3. Multipath Fading Effects

Multipath is simulated using the system model shown in Figure 2.18. As stated in Chapter II (part 2), multipath causes the reference axes of the two-dimensional constellation diagram to rotate with respect to the horizontal and vertical axes of the oscilloscope. The delay line is capable of producing time delays less than 2.5 microseconds. Figures 2.33 and 2.34 show the constellation diagrams for a delay time of 0.5 microseconds when SNR = ∞ and SNR = 8 dB, respectively.

Figure 2.33

An Example of the Constellation Diagram for
Received QPSK Signals With Multipath Fading
(When SNR = ∞, delay time = 0.5 microseconds)
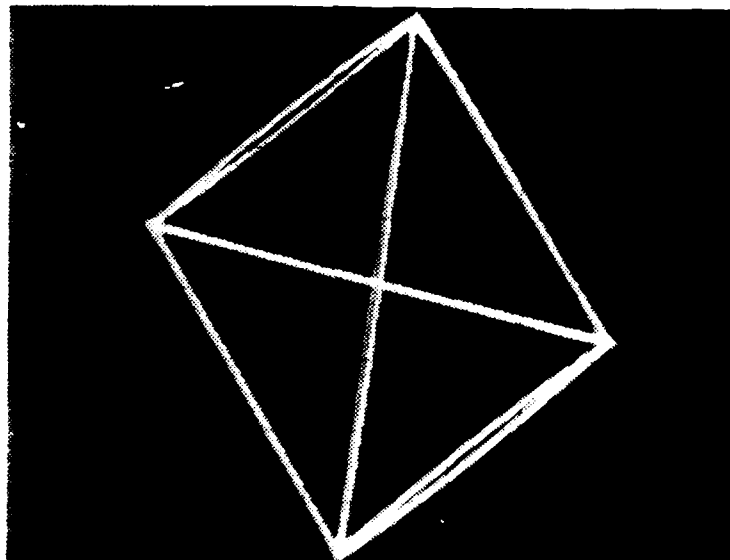

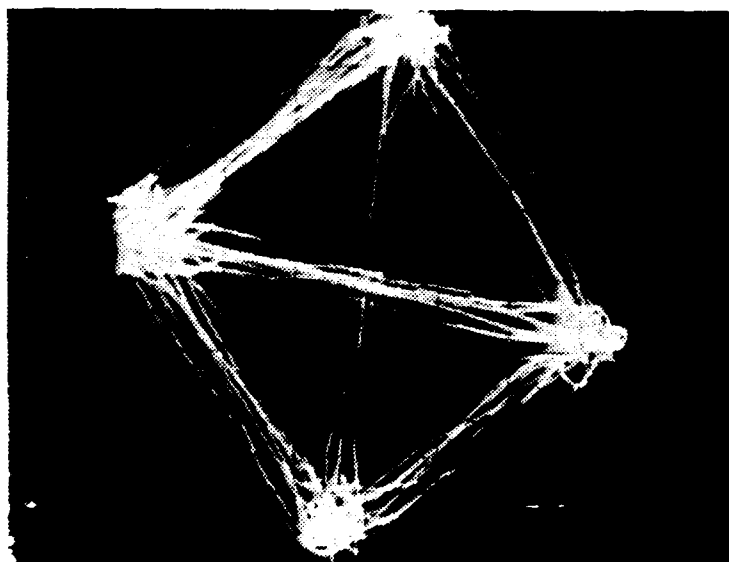Figure 2.34

An Example of the Constellation Diagram for
Received QPSK Signals With Multipath Fading
(When SNR = 8 dB, delay time = 0.5 microseconds)

IV. CONCLUSIONS AND RECOMMENDATIONS

The experimental results show that visual display is a useful indication of the quality of received QPSK signals. Further, the display can be used to determine demodulator input SNR, to identify multipath conditions, and to assess the degree of channel mismatch. With experience, this visual presentation can be used to assess BER under a variety of operating conditions.

APPENDIX 2

CIRCUIT SCHEMATICS FOR PART 2

This appendix contains the schematic diagrams of all the circuits used in part 2 of this research. The components used to implement the various circuits include shift registers, analog voltage multipliers, operational amplifiers, analog switches, and TTL gates (EX-NOR). Operating characteristics of each component can be found in References 6, 7, and 8, respectively.

The various circuit diagrams are presented in Figures 2A-1 through 2A-4 in the following order:

Figure 2A-1   Carrier Pool

Figure 2A-2   Multiplexer

Figure 2A-3   Demodulators and LPFs

Figure 2A-4   Bandpass Delay Line

In this appendix, the circuit diagrams, including FSR, bandpass filter, and analog summer are not presented, since they are given in Appendix 1A.

Figure 2A-1 shows the carrier pool. This circuit contains the necessary subcircuits to generate four distinct phase-modulated carriers. Subcircuits consist of a bandpass multiple feedback phase shifter, three inverting amplifiers, and four voltage followers. The input to the phase shifter is a 100 kHz sinusoidal carrier and the output is a 100 kHz cosine wave. Reference 9 outlines the construction of this phase
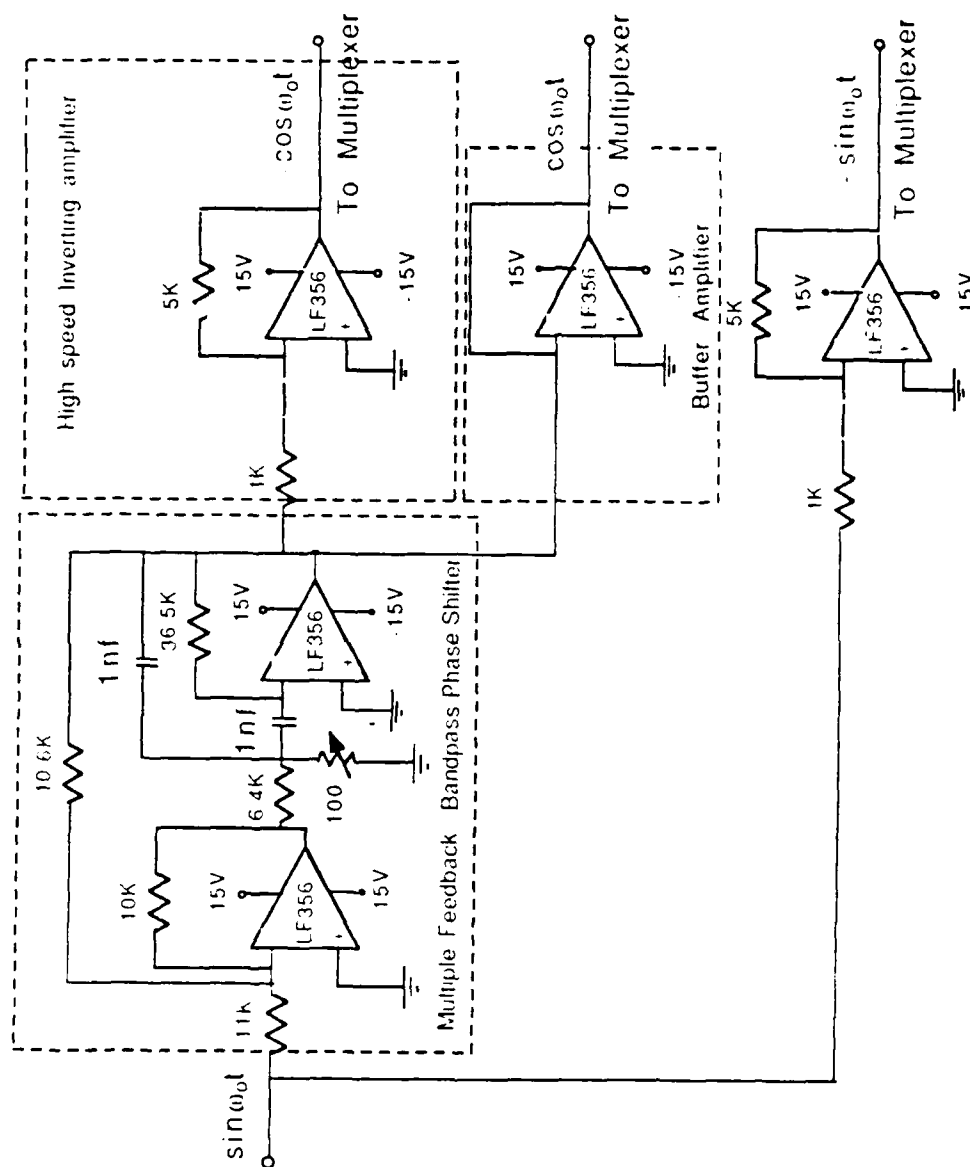
121

Figure 2A-1

Schematic of the Carrier Pool Circuit

shifter. Inverting amplifiers are used to generate –sine wave carrier and –cosine wave carrier, respectively. High–speed voltage followers (LF 356) buffer the critical points of the carrier pool circuitry. The four carrier pool output signals are hardwired to the input terminals of an analog multiplexer (MC 14051B).

The multiplexer circuit diagram is shown in Figure 2A-2. An analog multiplexer (MC 14051B) selects and transmits one of the hardwired carriers according to the selective input voltages from the two FSRs (not shown).

Gaussian noise is added in the transmission channel (Figure 1A-3). Signal plus noise is demodulated in a two–channel receiver.

Figure 2A-3 shows the demodulator circuit diagrams. Two analog voltage multipliers (AVM–AD534) are used to construct the I-channel and Q-channel demodulators. Demodulated signals are lowpass filtered by two KHRONITE (model 3202A) lowpass filters. Lowpass filter cut–off frequencies are set to 1100 Hz for a 2 kHz data rate. Lowpass filter outputs are the recovered data, $\hat{d}_1(t)$ and $\hat{d}_2(t)$, respectively. The data $\hat{d}_1(t)$ and $\hat{d}_2(t)$ drive the deflection coils of an oscilloscope (COS 6001A) to construct the constellation diagrams of received QPSK signals.

A multiple feedback bandpass phase shifter is used to simulate the delay line necessary for multipath fading in the transmission channel. Reference 9 outlines the necessary steps to design this phase shifter. Figure 2A–4 is the schematic of this phase shifter.
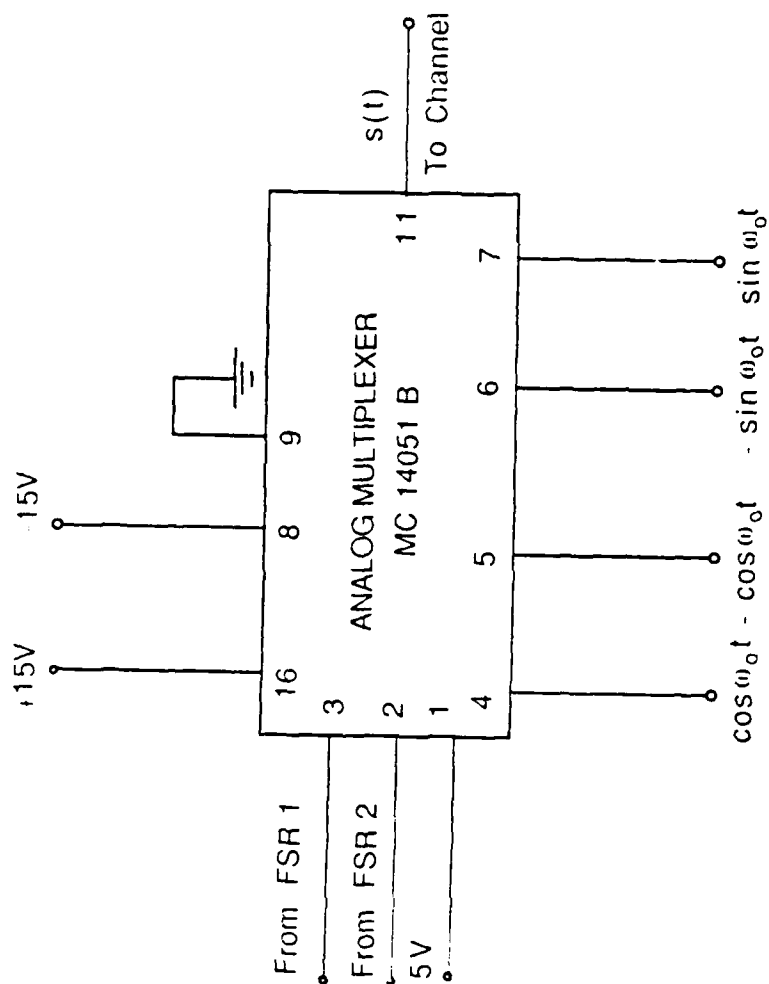
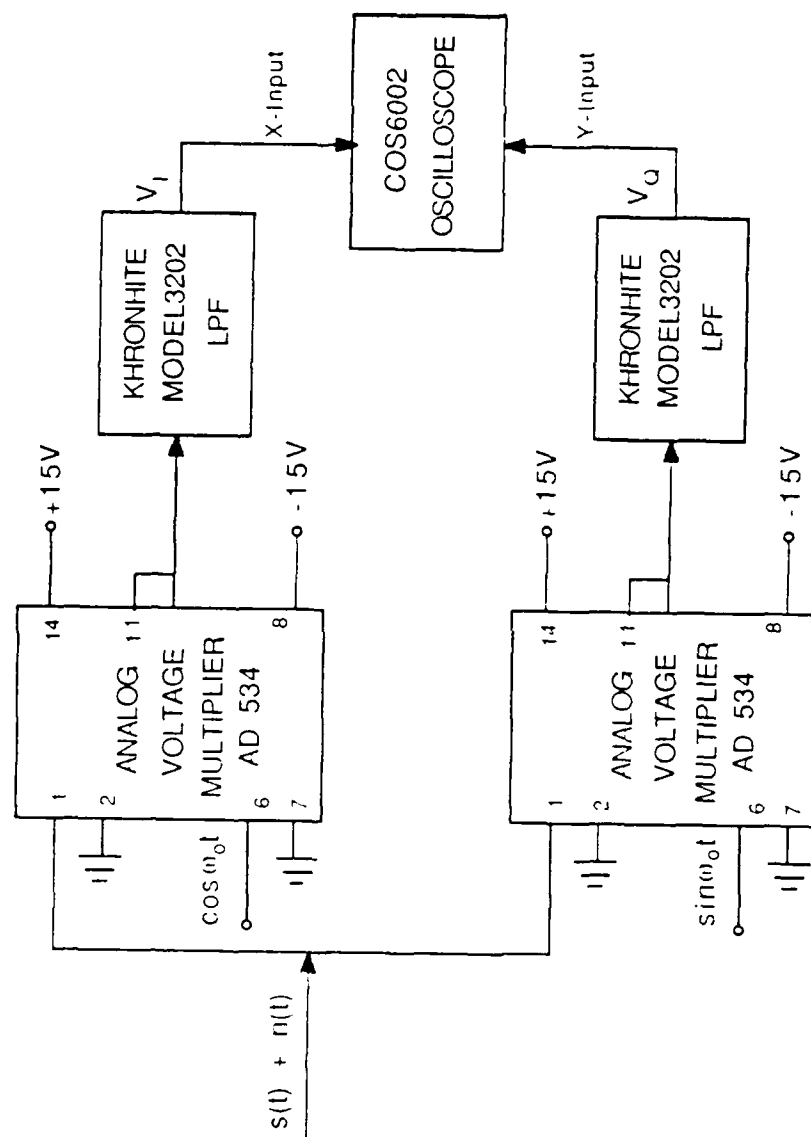Figure 2A-2

Multiplexer Circuit Diagram

124

Figure 2A-3
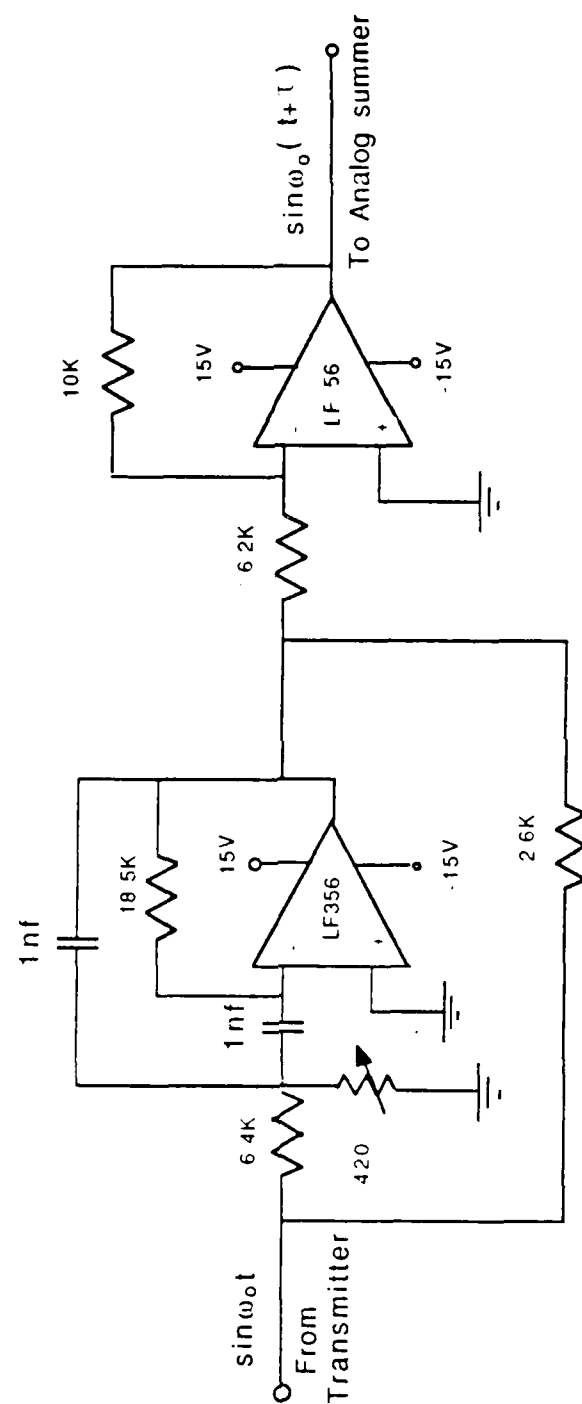
Schematic of the Demodulators and Lowpass Filters

Figure 2A-4

Schematics of the Bandpass Multipath Phase Shifter

126

INITIAL DISTRIBUTION LIST

		No. Copies
1.	Defense Technical Information Center Cameron Station Alexandria, VA 22304-6145	2
2.	Library, Code 0142 Naval Postgraduate School Monterey, CA 93943-5002	2
3.	Department Chairman, Code 62 Department of Electrical and Computer Engineering Naval Postgraduate School Monterey, CA 93943-5000	1
4.	Professor Glen Myers, Code 62Mv Department of Electrical and Computer Engineering Naval Postgraduate School Monterey, CA 93943-5000	5
5.	Professor Daniel Bukofzer, Code 62Bh Department of Electrical and Computer Engineering Naval Postgraduate School Monterey, CA 93943-5000	1
6.	Dz. K. K. Personel Egitim Daire Bsk. Bakanliklar Ankara, TURKEY	3
7.	ARGE Golcuk Tershanesi Komutanligi Golcuk, Kocaeli, TURKEY	1
8.	M. Sevki Sekerefeli Kiziltoprak mah. Taskopru cad. No: 22/8 Eskisehir, TURKEY	1

9. O.D.T.U. Kutuphanesi   1
    Orta Dogu Teknik Universitesi
    Ankara, TURKEY

10. I.T.U. Kutuphanesi   1
    Istanbul Teknik Universitesi
    Beyazit, Istanbul, TURKEY

11. Deniz Harpokulu Kutuphanesi   1
    Deniz Harpokulu Komutanligi
    Tuzla, Istanbul, TURKEY

12. Kubilay Tok   4
    Ziverbey Hilmibey sok.
    Alboyoglu apt. No: 8/8
    Kadikoy
    Istanbul, TURKEY

13. Professor Ralph Hippenstiel, Code 62Hi   1
    Naval Postgraduate School
    Monterey, CA   93943-5000

14. Professor John P. Powers, Code 62Po   2
    Naval Postgraduate School
    Monterey, CA   93943-5000

15. Commander   1
    Space and Naval Warfare
    Systems Command
    Washington, D.C. 20363-5100
    Attn: Capt. Stacy V. Holmes

16. Chris B. Bartone   1
    Naval Air Test Center
    Mail Code SY-81
    Patuxent River, MD   20670

END

DATE
FILMED

8-88

DTIC